

A HUBBLE SPACE TELESCOPE STUDY OF LYMAN LIMIT SYSTEMS: CENSUS AND EVOLUTION¹

JOSEPH RIBAUDO, NICOLAS LEHNER, J. CHRISTOPHER HOWK
Department of Physics, University of Notre Dame, Notre Dame, IN 46556
Accepted for publication in ApJ

ABSTRACT

We present a survey for optically thick Lyman limit absorbers at $z < 2.6$ using archival *Hubble Space Telescope* observations with the Faint Object Spectrograph and Space Telescope Imaging Spectrograph. We identify 206 Lyman limit systems (LLSs) increasing the number of catalogued LLSs at $z < 2.6$ by a factor of ~ 10 . We compile a statistical sample of 50 $\tau_{\text{LLS}} \geq 2$ LLSs drawn from 249 QSO sight lines that avoid known targeting biases. The incidence of such LLSs per unit redshift, $l(z) = dn/dz$, at these redshifts is well described by a single power law, $l(z) \propto (1+z)^\gamma$, with $\gamma = 1.33 \pm 0.61$ at $z < 2.6$, or with $\gamma = 1.83 \pm 0.21$ over the redshift range $0.2 \leq z \leq 4.9$. The incidence of LLSs per absorption distance, $l(X)$, decreases by a factor of ~ 1.5 over the ~ 0.6 Gyr from $z = 4.9$ to 3.5; $l(X)$ evolves much more slowly at low redshifts, decreasing by a similar factor over the ~ 8 Gyr from $z = 2.6$ to 0.25. We show that the column density distribution function, $f(N_{\text{HI}})$, at low redshift is not well fitted by a single power law index ($f(N_{\text{HI}}) \propto N_{\text{HI}}^{-\beta}$) over the column density range $13 \leq \log N_{\text{HI}} \leq 22$ or $\log N_{\text{HI}} \geq 17.2$. While low and high redshift $f(N_{\text{HI}})$ distributions are consistent for $\log N_{\text{HI}} > 19.0$, there is some evidence that $f(N_{\text{HI}})$ evolves with z for $\log N_{\text{HI}} \lesssim 17.7$, possibly due to the evolution of the UV background and galactic feedback. Assuming LLSs are associated with individual galaxies, we show that the physical cross section of the optically thick envelopes of galaxies decreased by a factor of ~ 9 from $z \sim 5$ to 2 and has remained relatively constant since that time. We argue that a significant fraction of the observed population of LLSs arises in the circumgalactic gas of sub- L_* galaxies.

Subject headings: Inter Galactic Medium — Galaxies: Quasars: Absorption lines

1. INTRODUCTION

The absorption features seen in the spectra of QSOs provide a unique opportunity to probe the intergalactic and galactic regions which intersect the lines of sight. In particular, H I absorption studies have allowed us to examine the distribution of gas associated with galaxies, the intergalactic medium (IGM), and the extended gaseous regions of galaxies which serve as an interface to the IGM, over the majority of cosmic time. Often these H I absorbers are placed in three general categories dependent on the H I column density (N_{HI}) of the absorber. The low column density Lyman- α forest absorbers ($N_{\text{HI}} < 10^{16} \text{ cm}^{-2}$) are associated with the diffuse IGM (see review by Rauch 1998). These systems probe low-density, highly ionized gas and are thought to trace the dark matter distribution throughout the IGM (Jena et al. 2005) as well as contain the bulk of the baryons at high redshift (Miralda-Escudé et al. 1996) and a significant amount of the baryons even today (e.g., Penton et al. 2004; Lehner et al. 2007; Danforth & Shull 2008). At the other end, the high column density damped Lyman- α absorbers (DLAs, $N_{\text{HI}} > 10^{20.3} \text{ cm}^{-2}$) appear associated with the main bodies of galaxies (see review by Wolfe (2005), although see Rauch et al. (2009)). These high-density, predominantly neutral systems serve as neutral gas reservoirs for high redshift star formation (Prochaska & Wolfe 2009).

The intermediate column density systems mark the transition from the optically thin Lyman- α forest to the optically thick absorbers found in and around the extended regions of galaxies. Typically these absorbers are easy to identify in QSO spectra due to the characteristic attenuation of QSO flux by the Lyman limit at $\sim 912 \text{ \AA}$ in the rest frame. These intermediate column density systems are segmented into three additional categories. The low column density absorbers ($10^{16} \text{ cm}^{-2} \leq N_{\text{HI}} < 10^{17.2} \text{ cm}^{-2}$) are known as partial Lyman limit systems (PLLSs), the intermediate column density absorbers ($10^{17.2} \text{ cm}^{-2} \leq N_{\text{HI}} < 10^{19} \text{ cm}^{-2}$) are known simply as Lyman limit systems (LLSs, Tytler 1982), and the high column density absorbers ($10^{19} \text{ cm}^{-2} \leq N_{\text{HI}} < 10^{20.3} \text{ cm}^{-2}$) are known as super Lyman limit systems (SLLSs, a.k.a. sub-DLAs; O’Meara et al. 2007; Péroux et al. 2002; Kulkarni et al. 2007). These absorbers are the least well-studied and physically understood class of absorbers, especially at $z \lesssim 2.6$, i.e. over the past ~ 10 Gyr of cosmic time. The reason for that is because at redshifts $z \lesssim 2.6$, the Lyman limit is shifted into the UV, requiring the need for space-based UV observations to observe the Lyman break in spectra.

To date, the majority of spectra used in LLS surveys have been taken from ground-based observations, providing an adequate statistical description of the high redshift ($z \gtrsim 3.0$) absorbers, most recently by Prochaska et al. (2010) and Songaila & Cowie (2010). Previous and recent surveys that partially probe the $z < 2.6$ regime (Tytler 1982; Sargent et al. 1989; Lanzetta 1991; Storrie-Lombardi et al. 1994; Stengler-Larrea et al. 1995; Songaila & Cowie 2010)

¹ Based on observations made with the NASA/ESA Hubble Space Telescope, obtained at the Space Telescope Science Institute, which is operated by the Association of Universities for Research in Astronomy, Inc. under NASA contract No. NAS5-26555.

have produced samples of tens of LLSs spanning the redshift range $0 \lesssim z \lesssim 4$. These surveys studied the statistical nature of LLSs, with some conflicting conclusions as to the evolution of these absorbers over cosmic time. A complete understanding of these optically thick absorbers is crucial as these systems in part determine the strength and shape of the ionizing ultraviolet background (UVB, Shull et al. 1999; Haardt & Madau 1996; Zuo & Phinney 1993). Due to the position of LLS column density with respect to Lyman- α forest systems and DLAs, a priori it is natural to view LLSs as tracing the IGM/galaxy interface. Thus they may provide a potentially unique probe of material moving in and out of galaxies over time. It is for these reasons that the incidence of optically thick absorbers as a function of redshift and the frequency distribution of absorbers as a function of N_{HI} serve as a critical parameter in modern cosmological simulations (Rauch 1998; Kereš et al. 2005, 2009; Kereš & Hernquist 2009; Nagamine et al. 2010).

Observations have linked LLSs to the extended regions of galaxies, including their gaseous halos, winds, and the interactions of these with the IGM (e.g., Simcoe et al. 2006; Prochaska et al. 2004, 2006a; Lehner et al. 2009a; Stocke et al. 2010). Simulations have also shown a physical connection between LLSs and galaxies of a wide range of masses at $z \sim 2$ to 4 (Gardner et al. 2001; Kohler & Gnedin 2007). In addition, surveys of Mg II and C IV absorbers have shown connections to extended galactic environments and indicate the metal absorbers trace similar physical regions as LLSs (e.g., Chen et al. 2001, 2010; Churchill et al. 2000, 2005; Charlton & Churchill 1998; Steidel & Sargent 1992). Mg II absorbers have been studied extensively in optical surveys where the absorbers are observed over the redshift range $0.3 \leq z \leq 2.2$ and led the way in connecting QSO absorption features with galactic environments (e.g., Tytler 1987; Petitjean & Bergeron 1990; Nestor et al. 2005). Due to the nature of the Mg II absorption lines, which are strong and easily saturated, measurements of the Mg II column density are often impossible. This limits the information available as to their origin, metallicity, and physical properties. LLSs provide a complementary approach in understanding the gas around galaxies and provide a reliable estimate of N_{HI} for $\tau_{\text{LLS}} \leq 2.5$ (from the Lyman limit) and $\tau_{\text{LLS}} \geq 50$ (from the Lyman- α line) absorbers. For example, measurements of N_{HI} allow an examination of the frequency distribution with column density, which provides additional insight into the evolution of the strength and shape of the UVB over cosmic time.

In this work we analyze the population of LLSs at low redshift using a new sample of spectra from archival *Hubble Space Telescope* (*HST*) observations with the Faint Object Spectrograph (FOS) and the Space Telescope Imaging Spectrograph (STIS). We present the most complete survey to date of LLSs at $z \leq 2.6$. We catalogue 206 LLSs at $z < 2.6$ and examine a redshift path $\Delta z = 96$ from a statistical sample of 249 QSO spectra to search for $\tau_{\text{LLS}} \geq 2$ LLSs. We compare our results with previous surveys, including the recent high redshift survey of Prochaska et al. (2010), probing the evolution of LLSs over redshifts $0 \lesssim z \lesssim 5$. We connect the observational quantities to physical properties assuming the 737 Λ CDM cosmology with $t_0 = 13.47$ Gyr, $H_0 = 70$

km s⁻¹ Mpc⁻¹, $\Omega_m = 0.3$, and $\Omega_\Lambda = 0.7$ (consistent with WMAP result, Komatsu et al. 2009).

This paper is organized as follows. After a brief description of the properties of LLSs in § 2, we give an overview of the data and the process of assembling the survey sample in § 3. In § 4 we describe the process used to identify LLSs and characterize their properties, while the analysis of these properties, in particular $l(X)$ and $f(N_{\text{HI}})$, is given in § 5. We conclude with a discussion of the connection between galaxies and LLSs in § 6 and a summary of our principal results in § 7.

2. DESCRIPTION OF LYMAN LIMIT SYSTEMS

The Lyman limit of neutral hydrogen is located at ~ 912 Å in the rest frame of the absorber. For a background source with intrinsic flux F_{QSO} and observed flux F_{OBS} , the observed optical depth blueward of the limit is

$$\tau(\lambda \leq \lambda_{\text{LLS}}) = \ln \frac{F_{\text{QSO}}}{F_{\text{OBS}}(\lambda \leq \lambda_{\text{LLS}})}, \quad (1)$$

where λ_{LLS} is the assigned wavelength of the break in the LLS spectrum. The H I column density of the absorber can then be related to the optical depth using

$$N_{\text{HI}} = \sigma_{\text{HI}}^{-1} \tau_{\text{LLS}} \quad (2)$$

where τ_{LLS} is the optical depth at the Lyman limit of the absorption system and $\sigma_{\text{HI}} = 6.30 \times 10^{-18}$ cm² is the approximate absorption cross section of a hydrogen atom at the Lyman limit (Spitzer 1978).

It should be noted that while we refer to the absorption systems in this survey as LLSs, a more accurate description would be optically thick absorbers. Since we identify all systems above a minimum τ_{LLS} , we limit our sensitivity to accurately measure large H I column densities. Strong absorbers depress the absorbed flux so low that it cannot be measured. In these cases we have only lower limits for the H I column densities. As a result, some of the absorbers in the sample are likely DLAs or SLLSs, but the lack of coverage of the Lyman- α line prevents us from definitively categorizing these absorbers. Also, the frequency distribution of DLAs and SLLSs is much lower than for standard LLSs, suggesting the strong absorbers comprise a small portion of our sample (see § 5.4).

Due to the different selection criteria in past LLS surveys, we have created two statistical samples of our LLSs. The first sample, R1, defines a LLS as an absorber where $\tau_{\text{LLS}} \geq 1$, i.e., $N_{\text{HI}} \geq 10^{17.2}$ cm⁻². The majority of the surveys done through the 1990s were completed using this criterion, although these previous studies were not always rigorous about this restriction. The second sample, R2, defines a standard LLS as an absorber where $\tau_{\text{LLS}} \geq 2$, i.e., $N_{\text{HI}} \geq 10^{17.5}$ cm⁻². This second definition is adopted for comparison with the recent high redshift survey by Prochaska et al. (2010).

Although not directly included in our statistical analyses, we have identified many PLLSs with $\tau_{\text{LLS}} < 1$, i.e., $N_{\text{HI}} < 10^{17.2}$ cm⁻². These absorbers require a more refined assessment of their selection, and the present sample is incomplete. As a result, we warn against the use of such systems from our sample in statistical analyses. This incompleteness manifests itself in our analysis of the $f(N_{\text{HI}})$ distribution for LLSs (see § 5.4).

Lastly, in dealing with QSO absorption lines, it is common to exclude absorbers located within an established distance of the background source to eliminate any potential influence the source may have on the number density and ionization state of the systems. We identify these proximate-LLSs as absorbers within 3000 km s^{-1} of the background QSO and exclude them from our statistical analyses.

3. THE DATA: FOS AND STIS

In this work we make use of archival observations from both the STIS and FOS instruments on board the *HST*. The STIS sample incorporates data from a variety of projects which used the G140L and G230L gratings. These gratings are capable of a resolving power of $R \sim 1000$, and wavelength coverages of $1150 - 1700 \text{ \AA}$ for the G140L and $1600 - 3100 \text{ \AA}$ for the G230L. All the data were retrieved from the MAST archive and were processed with CALSTIS v2.22 prior to retrieval. Data for objects observed more than once were combined into a single spectrum weighted by the exposure time of the individual spectra. For objects observed with both the G140L and G230L gratings, these data were combined into a single spectrum. Table 1 summarizes the observations used in this work, giving the grating used for an observation, the total exposure time of the observation, and the proposal ID of the observation. Our final analysis of LLS statistics requires careful culling of the data to minimize biases and some of these observations were not included in our final sample; we discuss the criteria used to exclude an observation in § 3.1.

The FOS data can be separated into two distinct portions. First, we use the Bechtold et al. (2002) reductions of observations taken with the G130H, G190H, and G270H gratings.² We will refer to this subsample as FOS-H. Data taken with these gratings have a resolving power $R \sim 1300$, and wavelength coverages of $1140 - 1600 \text{ \AA}$ for the G130H, $1575 - 2330 \text{ \AA}$ for the G190H, and $2220 - 3300 \text{ \AA}$ for the G270H. We also make use of FOS data using the G160L grating, and we will refer to this subsample as FOS-L. These data have a resolving power $R \sim 250$ and a wavelength coverage of $1140 - 2500 \text{ \AA}$. We treated these data in a manner consistent with the STIS data, with multiple exposures combined to form a single spectrum. Table 2 lists the observations examined for this work, giving the total exposure time of the observation as well as the proposal ID.

For a small number of objects observed with FOS, observations were taken with both the low resolution G160L grating and a combination of the high resolution gratings. In these cases, it is possible to detect a shift in the wavelength array of the G160L spectra relative to the high resolution spectra. For objects where a shift was evident, the G160L spectra were shifted in wavelength space to align with the high resolution data. There were 20 objects where a shift in the wavelength array was detectable, of which the mean shift in spectrum was 4 \AA .

The FOS spectra all suffered from background subtraction uncertainties of $\sim 30\%$ (Keyes et al. 1995) due to the crude nature of the background determination

and lack of scattered light correction in FOS. The error vectors produced by CALFOS do not account for this background uncertainty. For regions strongly absorbed by LLSs, the background uncertainties can dominate the error budget. To estimate this uncertainty, we calculated the background flux as the product of the inverse sensitivity function and the count rate for each grating. Taking $\sim 30\%$ of this quantity allowed us to account for the error in the initial background subtraction.

3.1. Selection of a Statistical Sample of Absorbers

The initial sample of observations taken from the STIS and FOS archives contained ~ 700 QSOs with redshifts $0 \lesssim z_{\text{em}} \lesssim 3$ (Tables 1,2; Bechtold et al. 2002). However, not all of these QSOs can be used for LLS studies because the data suffer from a variety of pitfalls (i.e., poor quality or lack of coverage of 912 \AA and below in the QSO rest frame) or the selection of the QSO for the STIS or FOS observation is biased in favor or against the presence of a LLS.

To construct a sample of QSO sightlines appropriate for studying LLS statistics we used the following approach. We assigned the redshift of the QSO, z_{em} , determined through emission features of the spectrum, using the results from Bechtold et al. (2002) when available and the Veron-Cetty & Veron (2010) QSO database for the remaining objects. We removed from our sample all QSOs with no coverage below 912 \AA in the rest frame of the QSO or where the quality of the observation was too poor to establish an estimate for the continuum flux. We also excluded apparent or known broad absorption line QSOs from our sample due to the difficulties in studying intervening absorbers in their spectra. Next we examined the Phase II proposals for each observation to determine if any knowledge of the sight line characteristics were known prior to the execution of the proposal that may represent a bias. For example, QSOs specifically targeted because *International Ultraviolet Explorer (IUE)* data indicated the QSO was UV-bright may bias our sample against LLSs. We identified all such potentially biased observations and removed them from our sample. There were also 2 gravitationally lensed QSOs for which we only included one of the pair in our sample, excluding the absorber associated with the lensing galaxy. QSOs targeted because of absorption features known from previous observations, such as Mg II absorption, DLAs, and 21 cm absorption represented the most common selection bias in the present sample. We did not include any LLSs in our statistical sample that were associated with previously identified systems toward these QSOs (these systems are listed in Table 4 with appropriate bias indicators). We did however, include the redshift path covered by these QSOs and any LLSs that occurred at redshifts higher than the targeted absorber redshift. There is a concern that including these observations, in particular the targeted strong Mg II absorbers, may bias our sample against detecting strong H I absorbers along the included redshift path. For the majority of the targeted Mg II observations, additional absorption systems along the line of sight were not accounted for when selecting the QSOs for observation (S. Rao, private communication, 2011). Because of this, we believe there is no significant bias in including the redshift path and non-targeted LLSs of

² The data are available through <http://lithops.as.arizona.edu/~jill/QuasarSpectra/>.

these observations. In § 5 we have examined a subset of these observations to show the statistical properties of the observations are consistent with the entire statistical sample. The remaining 249 objects listed in Table 3 comprise our sample.

3.2. Survey Redshift Path

To quantify the absorption features found in our sample, we must determine the portion of each spectral observation that is amenable to a robust search. This quantity is referred to as the redshift path of the survey and results from translating the observed spectral wavelengths into redshifts. For our survey we calculated two redshift paths, corresponding to robust searches for LLSs defined as absorbers where $\tau_{\text{LLS}} \geq 1$ and $\tau_{\text{LLS}} \geq 2$. For these two cases, we require the local continuum flux to exceed four times the estimated error array (i.e. $S/N \gtrsim 4$) and to exceed two and a half times the estimated error array (i.e. $S/N \gtrsim 2.5$), respectively. Requiring the S/N of the observation to be above this threshold allowed us to empirically define an acceptable wavelength range (i.e., redshift path) over which we can reliably detect LLSs. We also require the survey path to end at the redshift z_{prox} which corresponds to 3000 km s^{-1} blueward of z_{em} . The S/N limits for our redshift path definitions were deduced through the analysis of real and simulated spectra; these limits correspond to our ability to detect $\tau \geq 1$ or 2 at the 95% confidence level. The second redshift path requirement is an attempt to minimize the effect of the QSO and its environment on the analysis of intervening absorption systems. We note that for objects in our sample, we redefine the quantity z_{max} as the lesser value of the maximum redshift that satisfies the S/N requirement and z_{prox} .

In their recent high redshift survey ($z > 3.5$), Prochaska et al. (2010) note several biases that impacted their survey due to the presence of PLLSs. Unidentified PLLSs in their surveys had two main effects, neither of which particularly impacts our survey. In the first, unidentified PLLSs in their spectra could cause the local S/N to drop below their threshold criterion. These authors calculate the S/N for comparison against their selection criterion at the wavelength of the QSO Lyman limit and use all of the available path of the observation, unless they are able to identify a PLLS that depresses the S/N below the threshold at a lower redshift. Thus, not identifying a PLLS could cause them to overestimate the redshift path appropriate for a given QSO. However, we calculate a local S/N at each point in our spectra and are able to note which regions of a spectrum are unsuitable for use in our survey. Any effect that causes the S/N to fall below the threshold would shorten the redshift path, even if it were not identified as, e.g., a PLLS. In the second effect discussed by Prochaska et al. (2010), unidentified PLLSs at redshifts just above a higher optical depth absorber caused them to assign a redshift for the latter too high by up to $\Delta z = 0.1$. This had the effect of reducing the total redshift path of their survey by a sizable amount, since their typical redshift path per QSO was only $\Delta z \sim 0.2$. They estimate this caused overestimates in $l(z)$ by 30 to 50%. This has a negligible effect on our survey for several reasons. First, $\sim 90\%$ of the redshifts assigned in our survey come from measurements of Lyman-series lines associated with the LLSs rather

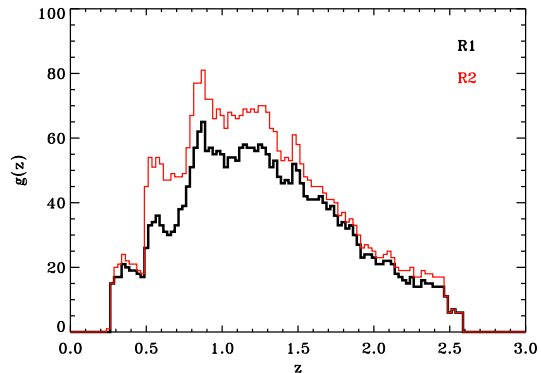


FIG. 1.— The redshift path surveyed with our samples of $\tau_{\text{LLS}} \geq 1$ (black) and $\tau_{\text{LLS}} \geq 2$ (red) spectra. The function $g(z)$ is the number of unique QSOs in our *HST* sample that probe the redshift interval $\Delta z = 0.025$, at redshift z , for LLSs.

than from the break itself. These measurements should be unaffected by the aforementioned bias. Furthermore, the probability of having two overlapping systems, and the resulting impact on the path length calculation, are much smaller at the lower redshifts of our survey. Typically our redshift path per QSO is a factor of ~ 4 larger than the mean of the Prochaska survey, while the number density of absorbers is smaller by a factor of ~ 4 . Even based on these considerations alone, the impact would be mitigated by more than a factor of 10. Furthermore, because the number density of absorbers per unit redshift is significantly lower, the probability of having two in close proximity is also lower by a factor of ~ 10 . Together these diminish the impact of this bias to below a $\sim 1\%$ effect that only impacts the sight lines without measurements based on Lyman series lines, i.e., $< 10\%$ of our sample of LLSs. Altogether, then, these biases play little role in our survey.

Table 3 summarizes the properties of the QSO sight lines that meet these selection criteria. For each object, we give the emission redshift, z_{em} , and the maximum and minimum redshifts meeting our redshift path criteria for each optical depth regime, z_{max} and z_{min} , where z_{min} corresponds to the greater value of the minimum redshift that satisfies the S/N requirement and 20 \AA above the minimum wavelength coverage of the observation. We refer to the QSO sightlines in which we can reliably detect a LLS with $\tau_{\text{LLS}} \geq 1$ as the R1 sample, which contains 229 QSOs and 61 LLSs, while the objects in which we can reliably detect a LLS with $\tau_{\text{LLS}} \geq 2$ is the R2 sample, which contains 249 QSOs and 50 LLSs.

Figure 1 shows the $g(z)$ distributions, which represents the number of QSOs with spectral coverage of λ_{LLS} , as a function of redshift for the R1 and R2 samples. Both samples are most sensitive to the detection of LLSs over the redshifts $0.8 \leq z \leq 1.5$. The total integrated redshift path,

$$\Delta z = \int g(z) dz \quad (3)$$

is $\Delta z(R1) = 79$ and $\Delta z(R2) = 96$. Our survey probes a factor of $\gtrsim 4$ larger redshift path than previous surveys at $z < 2.6$ ($\Delta z = 21$, Jannuzi et al. 1998). Our survey probes a redshift path very similar to the recent high redshift survey of Prochaska et al. (2010), where $\Delta z = 96$ for LLSs at $3.3 \leq z \leq 5.0$.

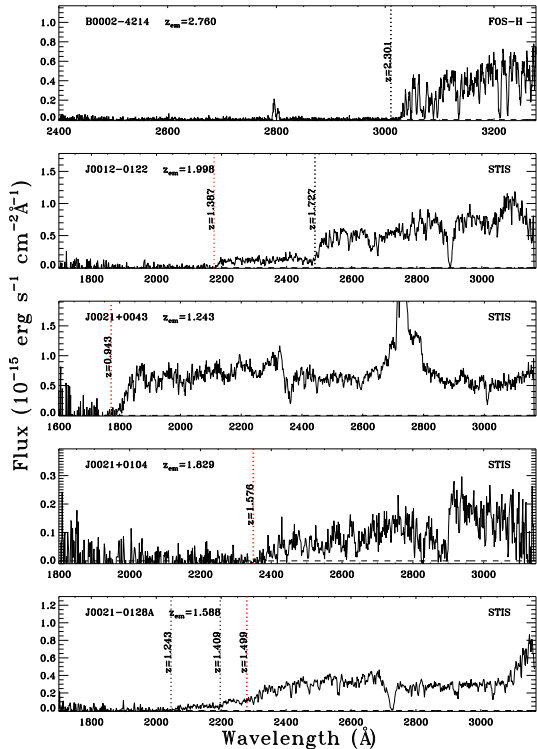


FIG. 2.— The first five observations of the LLSs listed in Table 4. The vertical, dashed lines represent LLSs included in sample R1/R2. The vertical, dashed red lines represent the absorbers that were identified but not included in the statistical analysis for various reasons (see Table 4 for more information). Spectra for each LLS listed in Table 4 can be found in the online version.

4. IDENTIFYING AND CHARACTERIZING LYMAN LIMIT SYSTEMS

We select LLSs on the basis of their Lyman limit absorption (i.e., we do not include absorbers in our statistical sample based only on strong line absorption) for redshifts where the data satisfied our redshift path criteria. The entire list of 206 LLSs found while examining our unabridged sample is given in Table 4. The absorbers used in the statistical analysis are designated with R1 or R2. There are 61 LLSs in the R1 sample and 50 LLSs in the R2 sample. A sample of the spectra for the observations can be found in Figure 2, where each QSO spectrum is plotted with a vertical dashed line at the location of an established H I absorber. The red dashed lines indicate systems which were identified but not included in our statistical analysis. The complete sample of LLSs identified in this work are available in the online version of Figure 2.

In general, as seen in Figure 2, the break produced by a $\tau_{\text{LLS}} \geq 1$ LLS is abrupt enough to be found in even low S/N (~ 4) and resolution spectra. However, as we discussed above the occasional presence of PLLSs can complicate the situation. In particular, assigning the continuum flux level redward of the Lyman break can become difficult. To minimize the potential error associated with this effect, we adopt a two-step process. First we use an automated search to identify potential Lyman limits. This automated search was checked by-eye and found to highlight absorbers with $\tau \geq 1$ quite well. These methods allowed us to identify absorbers where

$\tau < 1$, but we stress the sample of PLLSs detected is not complete. Subsequently we use an interactive routine to fit the continuum flux, the optical depth of the system, and the characteristic continuum recovery blueward of a Lyman limit (see below). While our statistical sample contains only LLSs that satisfy our $\tau_{\text{LLS}} \geq 1$ or $\tau_{\text{LLS}} \geq 2$ criteria, we have attempted to identify every optically thick and partially optically thick absorber present in our spectra. This is important for accurate continuum fitting and provides a sample of PLLSs that we use in the analysis of the $f(N_{\text{HI}})$ distribution presented in § 5.4.

We adopted the composite QSO spectrum developed by Zheng et al. (1997) as a general model of the QSO continuum. We scaled the continuum to each QSO spectrum over a relatively absorption free wavelength range of the spectrum. We found the majority of QSO observations were fitted well by this composite. We then used a running chi-square tool to identify portions of the spectrum where the QSO spectrum deviated from the composite. For each pixel in the spectrum, a running χ^2 goodness of fit parameter was calculated comparing the fitted continuum with the observed spectrum over $\sim 30 \text{ \AA}$.³ This largely excluded false identifications due to strong absorption lines present throughout the spectrum. Spectra not well fitted by this routine were individually examined for the possibility of a Lyman break, although the number of such spectra is very small.

Once a spectrum was flagged as containing a possible LLS, the spectrum was examined more thoroughly to identify the redshift of the break and any Lyman series lines present. When possible, the Lyman series lines were used to determine the redshift of the absorber. However, if the Lyman limit was located near the maximum wavelength of the spectrum or the resolution of a spectrum was too low to identify individual absorption lines (i.e. the majority of FOS-L observations) we used the Lyman break to set the redshift. We define the redshift of a LLS determined from the break as

$$z_{\text{LLS}} = \frac{\lambda_{\text{LLS}}}{912\text{\AA}} - 1, \quad (4)$$

where λ_{LLS} is the wavelength of the observed Lyman break. In Table 4, we list z_{LLS} from our analysis. The typical statistical error on the redshift determination from the Lyman series lines is $\sigma_z = 0.001$ for the FOS-H and STIS spectra. The statistical errors on z_{LLS} are larger when using the break, about 0.010 for the FOS-H and STIS spectra and 0.014 for the FOS-L spectra. As we used two different methods to determine z_{LLS} , possible systematics may be introduced. We tested this by using LLSs for which the redshift could be determined from both the Lyman lines and break. We found a systematic shift of 0.007 in the redshifts determined from the break in the FOS-H and STIS spectra, but not for the FOS-L (possibly because the resolution is far cruder). For the few redshifts of the LLS determined from the Lyman break in the FOS-H and STIS spectra, we systematically corrected z_{LLS} by the 0.007 shift.

³ At low redshift the attenuation of the QSO flux blueward of 912 Å (in the rest frame of the QSO) due to intervening Lyman- α lines is quite small compared to high redshift. This allowed us to model the QSO flux with the composite spectrum quite well over all wavelengths, including regions which probed the lower redshift Lyman- α forest.

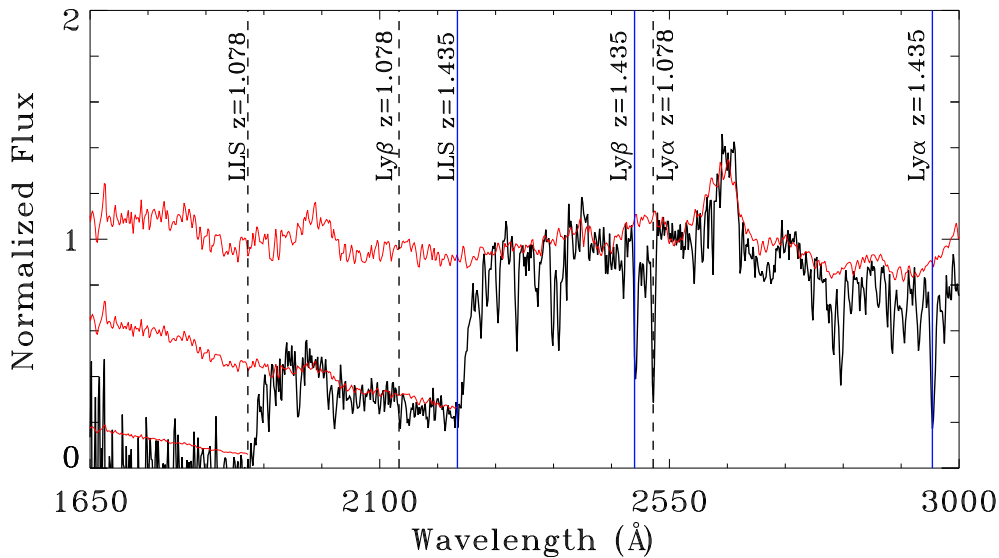


FIG. 3.— The spectrum of J1322+4739 with a composite spectrum overplotted (in red). The Lyman limit at $z = 1.435$ ($\tau = 1.27 \pm 0.04$) is identified with blue lines. Blueward of the limit, the composite is overplotted again with the characteristic recovery of the flux. The Lyman limit at $z = 1.078$ ($\tau > 2.44$) is identified with the dashed black lines. This is a snapshot of the plots produced using our method to identify LLSs and characterize their properties.

Once a redshift is assigned, we measure the optical depth at the Lyman limit for each absorber. We iteratively refined the fit of the composite QSO continuum model to each spectrum. We determine the optical depth at the limit by comparing the continuum flux, F_{QSO} , with the observed (absorbed) flux, F_{OBS} , as in Equation 1. For many PLLSs and a few LLSs, the residual flux below the limit is sufficient to satisfy our S/N selection criteria for further LLS searches at $z < z_{\text{LLS}}$ of the highest redshift system. We derive a continuum blueward of the highest redshift LLS in a spectrum by modeling the recovery of the flux due to the wavelength dependence of the optical depth. The continuum flux in the recovery region, F_{REC} , is

$$F_{\text{REC}} = F_{\text{QSO}} e^{-\tau_{\text{LLS}} \left(\frac{\lambda}{912\text{\AA}} \right)^3}, \text{ for } \lambda < 912\text{\AA}. \quad (5)$$

Once F_{REC} is defined, we repeat our LLS search for systems at redshifts below the initial system after renormalizing our best fit continuum fit according to Equation 5. Figure 3 shows the method of fitting the continuum onto a QSO spectrum, identifying a LLS, and modeling the recovery of the spectrum blueward of a Lyman limit.

For absorption systems where the residual absorbed flux blueward of the break was determined to the 3σ level, we report optical depth measurements with accompanying errors. For systems where we could not detect the residual absorbed flux to the 3σ level, we treat the optical depth measurement as a lower limit and report the 2σ lower limit. The optical depth measurements can be found in Table 4, where N_{HI} is also reported.

5. STATISTICAL ANALYSIS AND RESULTS

In this section we present the results of our survey. The first subsection examines the redshift density of LLSs and how the results from sample R1 and R2 compare to past studies of LLSs. The following subsections introduce a Λ CDM cosmology to connect the statistical treatment of our samples to physical structures throughout the uni-

verse such as the mean separation of LLSs, the incidence of LLSs as a function of absorption distance, and the column density distribution function. In each subsection, we first generalize the analysis, as to make it applicable to both of our samples. Following the general treatment, the individual samples are explored and discussed when appropriate.

5.1. The Redshift Density of Intervening LLSs

The redshift density of LLSs, $l(z)$,⁴ is a statistical quantity that is directly related to the QSO observations. The standard method for estimating $l(z)$ is to simply calculate the ratio of the number of LLSs, N , detected in a redshift interval to the total survey path, Δz (defined in Equation 3), contained in that redshift interval:

$$l(z) = \frac{N}{\Delta z}. \quad (6)$$

Figure 4 presents the values of $l(z)$ for both samples, R1 and R2. We first estimated $l(z)$ in redshift intervals where the binning was arbitrarily selected to provide approximately the same number of LLSs in each interval. Table 5 lists the properties of these redshift intervals for the R1 and R2 samples. Following previous work (e.g. Tytler 1982), we model the redshift evolution in $l(z)$ as a power law of the form:

$$l(z) = l_* \left(\frac{1+z}{1+z_*} \right)^\gamma. \quad (7)$$

This functional form was originally chosen when the Einstein-de Sitter models were the preferred cosmologies. At the time, evolution in the LLS distribution was found if $\gamma \neq 1$ for $q_0 = 0$ or $\gamma \neq 0.5$ for $q_0 = 0.5$. We use this functional form for the historical significance and the usefulness it provides in comparing our results with previous

⁴ This quantity has often been denoted in the past by a variety of symbols including $N(z)$, $n(z)$, and dN/dz .

surveys, but we note there is no physical or a priori reason to expect a particular functional form. However, the power law fit does do a reasonable job fitting the $l(z)$ distribution.

Using the maximum-likelihood method (e.g. Tytler 1982; Sargent et al. 1989), a best-fit estimate for γ , and from that l_* , can be determined for both samples. For the R1 sample ($\tau_{\text{LLS}} \geq 1$) we find $\gamma = 1.19 \pm 0.56$ and $l_* = 0.85$. For sample R2 ($\tau_{\text{LLS}} \geq 2$) we find $\gamma = 1.33 \pm 0.61$ and $l_* = 0.59$. For both samples we adopt $z_* = 1.5$, which corresponds to $\langle z_{\text{LLS}} \rangle = 1.5$ and can be chosen arbitrarily. These best-fit models are overplotted on the $l(z)$ data in Figure 4.

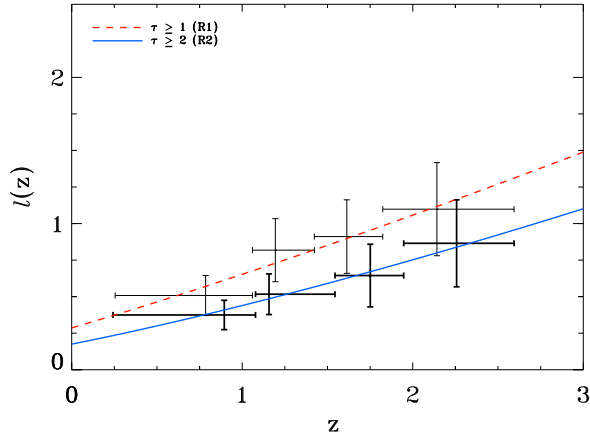


FIG. 4.— The evolution of the redshift density, $l(z)$. The values for $l(z)$ can be found in Table 5. From a maximum-likelihood analysis, the best fit power law: $l(z) = l_*[(1+z)/(1+z_*)]^\gamma$, with $z_* = 1.5$, is $l_* = 0.85$ and $\gamma = 1.19 \pm 0.56$ (for $\tau_{\text{LLS}} \geq 1$) and $l_* = 0.59$ and $\gamma = 1.33 \pm 0.61$ (for $\tau_{\text{LLS}} \geq 2$).

To check if the difference between the observed distribution and the adopted power law expression is statistically significant, we test the null hypothesis, that the observed and predicted cumulative distributions of LLSs with redshift are distinct, using a Kolmogorov-Smirnov test. The KS test yields a minimum probability of $P=0.95$ that we can reject the null hypothesis, using the entire redshift range encompassed by both the low and high redshift samples. Thus there is a strong probability that we can reject this null hypothesis.

As mentioned in § 3.1, we examined the potential biases associated with including redshift paths toward QSOs with targeted strong Mg II absorbers, which constitute a significant fraction of our statistical sample ($\sim 25\%$). To empirically test for any bias, we separately analyzed the statistical properties of these observations and compared their properties with the statistical properties of the total sample. From the STIS observations of Rao et al. (PID 9382 & 8569), we composed a sample of 79 QSO observations. This sample contained 17 (16) $\tau \geq 1$ (2) LLSs over a redshift path of $\Delta z = 22.65$ (28.01), giving $l(z) = 0.75 \pm 0.20$ (0.57 ± 0.14). These values are well within 1σ of the $l(z)$ for the full sample (0.77 ± 0.11 and 0.52 ± 0.08 for $\tau \geq 1$ and 2, respectively; Table 5). As a further check, we then separately analyzed the remaining 170 QSO observations to compare with the statistical properties of the total sample. This sample contained 44 (34) $\tau \geq 1$ (2) LLSs over a redshift path of $\Delta z = 56.57$ (68.13), giving $l(z) = 0.78 \pm 0.13$

(0.49 ± 0.09), which again is well within the 1σ values for the full sample (Table 5). This suggests any biases associated with these observations have a negligible impact on our analysis and results.

Over the past 30 years, there have been a variety of LLS surveys (Tytler 1982; Sargent et al. 1989; Lanzetta 1991; Storrie-Lombardi et al. 1994; Stengler-Larrea et al. 1995; Jannuzi et al. 1998; Prochaska et al. 2010; Songaila & Cowie 2010), and, as a result, a variety of estimates of $l(z)$. Many of these previous surveys examined large redshift intervals (typically spanning $0 \lesssim z \lesssim 4$) but have largely been statistically dominated by high redshift ($z \gtrsim 2.5$) LLSs. It is due to this inhomogeneity, combined with the lack of low redshift LLSs, that there is uncertainty as to the true statistical distribution of LLSs over the redshift range $0 \lesssim z \lesssim 4$. Lanzetta (1991) was the first to argue for a potential break in the evolution of the redshift density of LLSs at $z \sim 2.5$, where he found the low redshift ($z < 2.5$) LLSs showed relatively constant $l(z)$ and the high redshift ($z > 2.5$) LLSs showed a rapidly evolving $l(z)$. However, both Storrie-Lombardi et al. (1994) and Stengler-Larrea et al. (1995) argued, based on samples spanning the redshift range $0 \lesssim z \lesssim 4$, that the $l(z)$ for LLSs is best described as moderately evolving over the entire range and fit by a single power law in $(1+z)$. Figure 5 presents $l(z)$ values from the R1 sample, as well as the $l(z)$ fits from these previous surveys (with the parameters listed in Table 6). These previous surveys used a $\tau_{\text{LLS}} \geq 1$ criterion for inclusion in the sample, but it is not clear this was applied in a uniform manner (Stengler-Larrea et al. 1995). Our results for $l(z)$ over $0.25 \leq z \leq 2.6$ are consistent with the surveys of Storrie-Lombardi et al. (1994) and Stengler-Larrea et al. (1995), both of which fit $l(z)$ over the redshift range $0 \lesssim z \lesssim 4$.

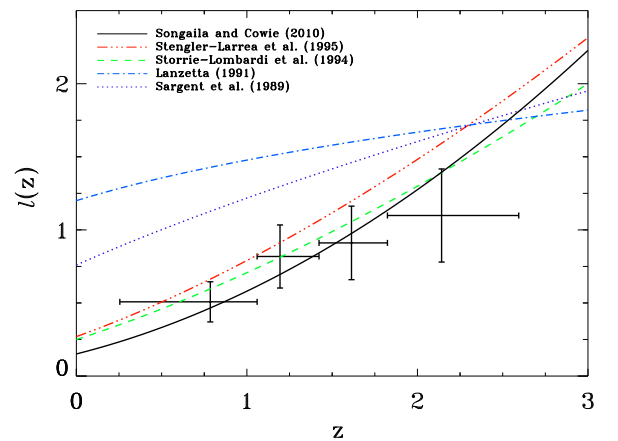


FIG. 5.— Estimates for the functional form of $l(z)$ from previous studies of $\tau_{\text{LLS}} \geq 1$ LLSs plotted on top of our R1 sample. The fits are parameterized as power laws with individual parameters listed in Table 6. Our results are consistent with the results of Stengler-Larrea et al. (1995) and Storrie-Lombardi et al. (1994), studies which probed the range $0 < z < 4$.

Recently, Prochaska et al. (2010) released a survey of high redshift LLSs (with $\tau_{\text{LLS}} \geq 2$) using the SDSS-DR7 that samples a redshift range ($3.5 \leq z \leq 4.4$) that does not overlap our survey redshifts. They find the $l(z)$ for high redshift LLSs can be described as rapidly evol-

ing over the range $3.5 \leq z \leq 4.4$. Our model of $l(z)$ is inconsistent with the Prochaska et al. (2010) survey when extrapolated to $z > 3$, as the Prochaska results are inconsistent with ours if extrapolated to $z < 2.6$. It was a similar disagreement seen in the high and low redshift samples of the Lanzetta (1991) work that led to the argument for a break in the power law description of $l(z)$ for LLSs. To investigate the possibility and significance of a broken power law fit to the redshift density of LLSs, we combine the recent high redshift sample from Prochaska et al. (2010) with our low redshift sample to examine the statistical nature of LLSs from $0 \lesssim z \lesssim 5$.

We refer to the combined R2 and Prochaska et al. (2010) samples as the RP10 sample. This combined sample of *HST* and SDSS observations contains 685 QSOs and 206 LLSs with $\tau_{\text{LLS}} \geq 2$. The total redshift path probed in RP10 is $\Delta z = 172$. This redshift path is a factor of ~ 2 greater than the recent LLS survey from Songaila & Cowie (2010), which spanned redshifts up to $z \sim 6$. In Figure 6, we present our estimate for $l(z)$ over this expanded redshift range. We find $l(z)$ from the combined sample can be described by a single power law (Equation 7) with $\gamma = 1.83 \pm 0.21$ and $l_* = 1.62$, for $z_* = 3.23$. Table 7 lists the properties of the $l(z)$ bins used for display purposes in Figure 6 and the values associated with each bin. To confirm the observations are well modeled by a single power law, a KS test was applied to the cumulative distribution function of observed and predicted LLSs (see Figure 6). The KS test yields a probability of at least $P = 0.95$ that the null hypothesis, the observed and predicted distributions represent different distributions, can be discarded. Thus the RP10 sample supports the conclusions of Storrie-Lombardi et al. (1994), Stengler-Larrea et al. (1995), and more recently Songaila & Cowie (2010), that a single power law is sufficient to describe $l(z)$ over $0 < z < 5$.

It should be noted that in the original analysis of the SDSS-DR7 sample, Prochaska et al. (2010) limited the redshift path to $z \leq 4.4$. This was done because the inclusion of $z > 4.4$ into their sample appeared to produce an artificially low $l(z)$ result for $4.4 < z < 5.0$, which they argued was unlikely to be physical. We include this extra redshift path from their sample, under the reasoning that arbitrary binning of the data for display purposes can produce artificial departures from a trend that in no way affects the statistical analysis of the maximum likelihood method. In our redefined bins, the artificial drop apparent at $z > 4.4$ is no longer present. To insure the extra redshift path is not solely responsible for our ability to fit the combined sample with a single power law, we conducted our analysis on the combined *HST*/SDSS for both situations ($z_{\text{max}} \leq 4.4$ and unrestricted z_{max}) and found both conditions produce single power law fits that are consistent and good describers of the data. It is also interesting to note that if z_{max} is unrestricted for the SDSS sample alone, the best fit curve for the high redshift sample is described by $\gamma = 2.79 \pm 1.46$ and $l_* = 1.94$. This description of $l(z)$ for the high redshift LLSs presents a less convincing argument for the need of a break in the power law, because the difference in power law indices between low and high redshift is less extreme.

Our analysis indicates that it is not necessary to introduce a broken power law to model the statistical evolution of the redshift density of LLSs over $0 \lesssim z \lesssim 5$.

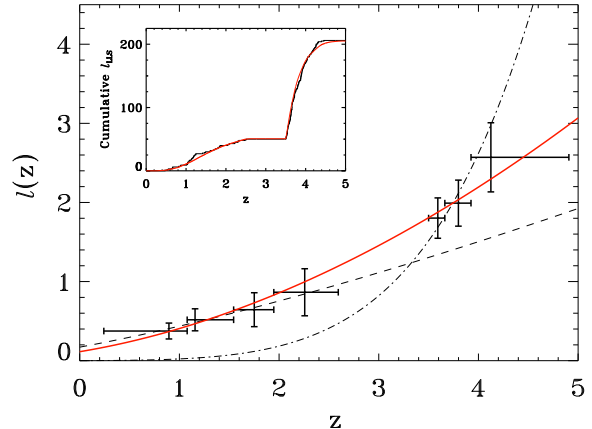


FIG. 6.— The incidence of LLSs per redshift, $l(z)$, for the combined SDSS-DR7 and R2 samples (RP10, $\tau \geq 2$). The single power law: $l(z) = l_* [(1+z)/(1+z_*)]^\gamma$, with $z_* = 3.23$, is $l_* = 1.62$ and $\gamma = 1.83 \pm 0.21$, is plotted with the $l(z)$ values taken from Table 7. To check the statistical significance of the single power law, a KS test was administered to the sample. The cumulative distribution function for the observations overplotted with the predicted distribution from our best fit power law can be found in the insert. The KS test gives a probability $P = 0.95$ that we can reject the null-hypothesis that the two distributions originate from different populations. The dashed and dot-dashed curves are the power law fits derived for the low and high redshift samples respectively.

However, we stress a sample with coverage of the $2.5 \lesssim z \lesssim 3.5$ region will be needed to truly rule out a break (J. O’Meara et al. in prep.). We note that the redshift density is really an observational statistic, and the difference between a single or broken power law may not carry much significance over to the physical quantities with which it is related. In § 5.2, § 5.3, and § 5.4 we put these results into the context of a cosmology and discuss the implications for the evolution and nature of LLSs to $z \sim 5$.

5.2. The Incidence of LLSs per Absorption Distance

The number of LLSs per absorption length, $l(X)$ (Bahcall & Peebles 1969), is defined as

$$l(X)dX = l(z)dz \quad (8)$$

where

$$dX = \frac{H_0}{H(z)}(1+z)^2 dz, \quad (9)$$

and

$$H(z) = H_0(\Omega_\Lambda + \Omega_m(1+z)^3)^{1/2}. \quad (10)$$

The quantity $l(X)$ is defined such that it is constant if the product of the comoving number density of structures giving rise to LLSs, n_{LLS} , and the average physical cross section of the structure, σ_{LLS} , is constant, i.e., $l(X) \propto n_{\text{LLS}}\sigma_{\text{LLS}}$.

Figure 7 shows the quantity $l(X)$ plotted as a function of fractional lookback time for the RP10 sample ($\tau_{\text{LLS}} \geq 2$). We see that $l(X)$ experiences a rapid decrease of ~ 0.6 Gyr corresponding to a decrease in redshift from $z = 4.9$ to 3.5 . After this rapid drop, $l(X)$ decreased slowly over ~ 8 Gyr, from $z = 2.6$ to 0.25 (See Table 7). The results in Table 7 show that $l(X)$ fell by a factor of ~ 1.5 over ~ 0.6 Gyr at high redshift and by another factor of 1.5 over ~ 8 Gyr at low redshift.

Figure 7 demonstrates why differing results are found regarding the broken (or not) power laws in the statistical treatment of the redshift density of LLSs. The dashed red line and dotted blue line in the plot are the best fit power laws for $l(z)$ (transformed into $l(X)$ using Equation 8 and 9) for our low redshift sample and the high redshift sample of Prochaska et al. (2010). The solid black line is the best fit power law to the RP10 sample (again transformed into $l(X)$ using Equation 8 and 9). The nature of power laws makes it difficult to extrapolate a fit based on observations in only the low or high redshift regime (in the regime where the power law is derived, the fit is nearly linear, making it extremely difficult to match observations in a regime outside of where it was derived). It is only when the observations are combined that we are able to produce a consistent single power law. We have mentioned the need for a study of the intermediate redshift regime ($2.5 \leq z \leq 3.5$, J. O’Meara et al. in prep.), which will allow for a more definitive assessment of the absorber distribution.

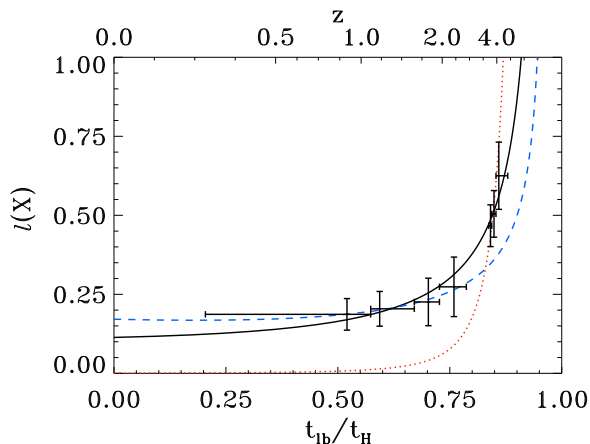


FIG. 7.— The incidence of LLSs per absorption distance, $l(X)$, plotted as a function of fractional look-back time. The values for $l(X)$ can be found in Table 7. The solid line is the power law result for the maximum-likelihood analysis on the RP10 sample ($\tau \geq 2$). The dashed blue line and the dotted red line are the power law fits from the R2 sample and high redshift sample from (Prochaska et al. 2010). This figure illustrates the problems that arise when attempting to fit the high and low redshift regimes with power law fits derived in either the high or low redshift only.

As previously stated, the behavior in $l(X)$ is related to the comoving number density of LLSs as well as the physical size of the absorbers. This rapid decrease in $l(X)$ over a short timescale at high redshift indicates either the physical size of LLSs has decreased substantially in this time or the comoving number density of LLSs has dropped significantly. A moderate decrease in both properties could also give rise to this behavior, but as we will show in § 6, when we associate LLSs with galaxies we find the physical size of LLSs must undergo significant evolution from $z \sim 5$ to 2.

5.3. The Mean Proper Separation of LLSs

The number density of optically thick absorbers throughout the Universe determines the mean free path of hydrogen ionizing photons, and in turn, sets the shape and intensity of the UVB. We can calculate an upper limit to this mfp using $l(X)$ of $\tau_{\text{LLS}} \geq 2$ absorbers, as

calculated in § 5.2. It is only an upper limit because we have not included the $\tau_{\text{LLS}} < 2$ absorbers that contribute to the overall absorption of hydrogen ionizing photons. Using $l(X)$, we can calculate the average proper distance, Δr_{LLS} , a photon travels before encountering a $\tau_{\text{LLS}} \geq 2$ LLS (e.g., Prochaska et al. 2010) as

$$\Delta r_{\text{LLS}} = \frac{c}{H_0} \frac{1}{(1+z)^3 l(X)}. \quad (11)$$

With the RP10 sample we find that Δr_{LLS} varies from $\sim 50 - 3700 h_{70}^{-1}$ Mpc proper distance from $z \sim 5$ to 0.3 (Table 7, also note Δr_{LLS} was calculated for R1 and R2 in Table 5). In Figure 8 Δr_{LLS} is shown as a function of redshift (data points and red curve), along with the mean free path of hydrogen ionizing photons (black curve) estimated by Faucher-Giguère et al. (2009) (It should be noted that while the calculation of the mean free path by Faucher-Giguère et al. (2009) is dependent on an assumed H I distribution, their estimated mean free path is in agreement with the mean free path calculation from Prochaska et al. (2009)). The shaded region emphasizes the difference between the two curves, which can be associated with the contribution from PLLSs and $\tau_{\text{LLS}} < 2$ LLSs that were not included in this calculation. We note the ratio between the distance a photon travels before encountering a $\tau_{\text{LLS}} \geq 2$ LLS and the mean free path of a hydrogen ionizing photon is increasing with decreasing redshift. Consider the extreme redshifts of the plot; at $z \sim 5$, Δr_{LLS} is a factor of ~ 1.5 larger than the predicted mean free path, while at $z \sim 0$, Δr_{LLS} is a factor of ~ 3.5 larger than the predicted mean free path. Assuming a mean free path consistent with Faucher-Giguère et al. (2009), this suggests that the $\tau_{\text{LLS}} < 2$ hydrogen absorption systems have become increasingly more important for absorption of Lyman continuum photons as the universe has evolved.

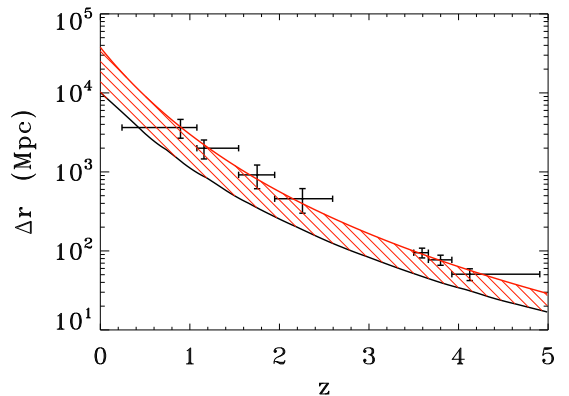


FIG. 8.— The average proper distance a photon travels before encountering a $\tau \geq 2$ LLS, plotted as a function of redshift. The data points correspond to values taken from Table 7, with the solid red line representing the interpolated functional form for Δr_{LLS} . We have included in this plot the mean free path of a hydrogen ionizing photon (solid black line), taken from the recent work on the ionizing background spectrum by Faucher-Giguère et al. (2009). The shaded region highlights the difference in the two curves, which corresponds to the effect PLLSs and $\tau_{\text{LLS}} < 2$ LLSs (which were not included in our RP10 statistical sample) have on the opacity of the universe.

5.4. The Differential Column Density Distribution Function

In this subsection, we combine our low redshift sample with previous works on the low- z ($z \lesssim 2.6$) IGM to place constraints on the differential column density distribution $f(N_{\text{HI}})$ over 10 orders of magnitude in N_{HI} . This distribution is defined such that $f(N_{\text{HI}}, X)dXdN_{\text{HI}}$ is the number of absorption systems with column density between N_{HI} and $N_{\text{HI}} + dN_{\text{HI}}$ and redshift path between X and $X + dX$ (e.g., Tytler 1987),

$$f(N_{\text{HI}})dN_{\text{HI}}dX = \frac{m}{\Delta N_{\text{HI}}\Sigma\Delta X}dN_{\text{HI}}dX, \quad (12)$$

where m is the observed number of absorption systems in a column density range ΔN_{HI} centered on N_{HI} and $\Sigma\Delta X$ is the total absorption distance covered by the spectra. The first moment of the distribution is also the incidence of absorbers per absorption distance, $l(X) = \int_{N_1}^{N_2} f(N)dN$. Empirically, it has been shown that at low and high redshift, $f(N_{\text{HI}})$ may be fitted by a power law for various N_{HI} regimes (e.g., Tytler 1987; Rao et al. 2006; Lehner et al. 2007; O’Meara et al. 2007):

$$f(N_{\text{HI}})dN_{\text{HI}}dX = C_{\text{HI}}N_{\text{HI}}^{-\beta}dN_{\text{HI}}dX. \quad (13)$$

The slope, β , may vary with the considered z or N_{HI} intervals, and, as discussed below and elsewhere (e.g., Wolfe et al. 2005; Prochaska & Wolfe 2009), the functional form can be more complicated than a single power law, especially when the entire observed N_{HI} range is considered. In Figure 9, we show the $f(N_{\text{HI}})$ column density distribution at $z \lesssim 2.6$. The data and analyses for different N_{HI} regimes come from various origins that we detail below. In the studies where another cosmology was chosen to calculate ΔX (Lehner et al. 2007; Williger et al. 2010), we have updated the cosmology to that used in the present study (see Equation 9). At $z < 1.65$, the DLA sample was selected based on known strong Mg II–Fe II systems (Rao et al. 2006). Their sample consist principally of data similar to those presented in this work (but rejected from our sample of LLSs because they were specifically targeted) with the addition of *IUE* spectra. Owing to their selection criteria, the sample has selection biases (Rao et al. 2006; Prochaska & Wolfe 2009), although Rao et al. (2006) argued that they are relatively well understood and dealt with (in the DLA regime). Rao et al. (2006) found that their DLA ($\log N_{\text{HI}} \geq 20.3$) sample could be fitted with $\beta = 1.4$ (represented by the solid red line in Figure 9). The dot-dashed cyan curve shows a fit assuming the power law index for the DLA at high redshift with $\beta = 1.8$ ($20.3 \lesssim \log N_{\text{HI}} \lesssim 21.8$) (Prochaska et al. 2010), which seems to provide a reasonable fit to the DLA measurements for $z < 1.65$ as well. The similar slope of $f(N_{\text{HI}})$ at both high and low z is consistent with a non-evolution of $f(N_{\text{HI}})$ for the DLA as argued by Prochaska & Wolfe (2009).

At the other end of the N_{HI} spectrum, $\log N_{\text{HI}} \lesssim 16$ —the Lyman- α forest regime, we consider two complementary samples that probe $z < 0.5$ (Lehner et al. 2007) and $0.5 < z < 2.0$ (Janknecht et al. 2006). We also complement the lower redshift interval with the 3C 273 sightline analyzed by Williger et al. (2010). At $z < 0.5$, the data come from the high resolution STIS E140M echelle

mode while at higher redshift the data come from STIS E230M as well as VLT/UVES and Keck/HIRES data. The H I column densities (and Doppler parameters) were derived by fitting the Lyman- α line (and higher Lyman series lines if present) thanks to the high resolution of these spectra. This method works well for systems with $\log N_{\text{HI}} \lesssim 15.5$ if several Lyman series lines are used (e.g., Lehner et al. 2006) or with $\log N_{\text{HI}} \lesssim 14$ (depending on the b -value) if only the Lyman- α transition is used. For the $z < 0.5$ sample, several Lyman series lines were used when possible. For the higher redshift sample, Janknecht et al. (2006) also used different atomic transitions to constrain the Doppler parameter. We note that their sample include a few PLLSs and LLSs, but the H I column densities of these systems often have errors in excess of 1 dex. We excluded those systems from our analysis. Using the maximum-likelihood method, we first fitted the two Lyman- α forest samples separately, finding no difference between these two redshift regimes. We therefore combined both samples and fitted them simultaneously. We find $\beta = 1.72 \pm 0.02$ and $\log C_{\text{HI}} = 11.14$ in the $\log N_{\text{HI}}$ interval [13.2, 14.5] (which is shown by the blue line in Figure 9). Changing the upper bound by +2 dex and the lower bound by +0.5 dex gives consistent results (within $\lesssim 1\sigma$). However, changing the lower bound by -0.1 dex decreases β by -0.05 (more than 2σ), and β drops even more if the lower bound decreases further. As indicated in Figure 9, there is a turnover in the distribution at $\log N_{\text{HI}} \simeq 13.2$, which is likely due to the incompleteness of the sample at these column densities.⁵ While the slope derived for Lyman- α forest is very similar to that predicted in recent cosmological simulations (Davé et al. 2010), the observations do not indicate an evolution of β in this redshift regime, as inferred in the simulations.

Finally, the column density distributions of the PLLSs, LLSs, and SLLSs ($19 \leq \log N_{\text{HI}} < 20.3$) have so far remained largely uncategorized at $z \leq 2.6$. For the SLLSs, τ_{LLS} is far too large to estimate N_{HI} from the Lyman break, but in this regime, the amount of H I is large enough that the Lyman- α transition produces damping wing from which N_{HI} can be estimated. In our sample, Lyman- α is covered in just 7 sightlines when $\tau_{\text{LLS}} > 3.5$. In two of these cases, there is no detection of Lyman- α , but the data were obtained from the low resolution FOS observations. In the other five cases, Lyman- α is observed, but in four of them, the equivalent width implies column densities around 10^{19} cm^{-2} or less. As the spectral resolution of the data is low and line contamination is likely, we relied on other recent works to constrain $f(N_{\text{HI}})$ in the SLLS regime. Specifically, we use the surveys of O’Meara et al. (2007) and Péroux et al. (2003), which include 16 SLLS at $1.7 < z < 2.6$, overlapping the high redshift portion of our LLS sample and the

⁵ Janknecht et al. (2006) typically found $\beta \simeq 1.60$ – 1.64 , but they set a completeness for their sample at $\log N_{\text{HI}} = 12.9$. Setting the lower bound to 12.9 dex, we found $\beta = 1.61$, a value very similar to theirs and substantially smaller than $\beta = 1.72 \pm 0.02$. Their completeness value was not justified, and based on our analysis a lower limit of 13.2 dex appears more appropriate. The signal-to-noise in 9 of the 11 sight lines (depending on the wavelength) indeed is not dissimilar from the lower redshift sample, where Lehner et al. (2007) showed that the completeness was 13.2 dex based on an analysis of the column density distribution.

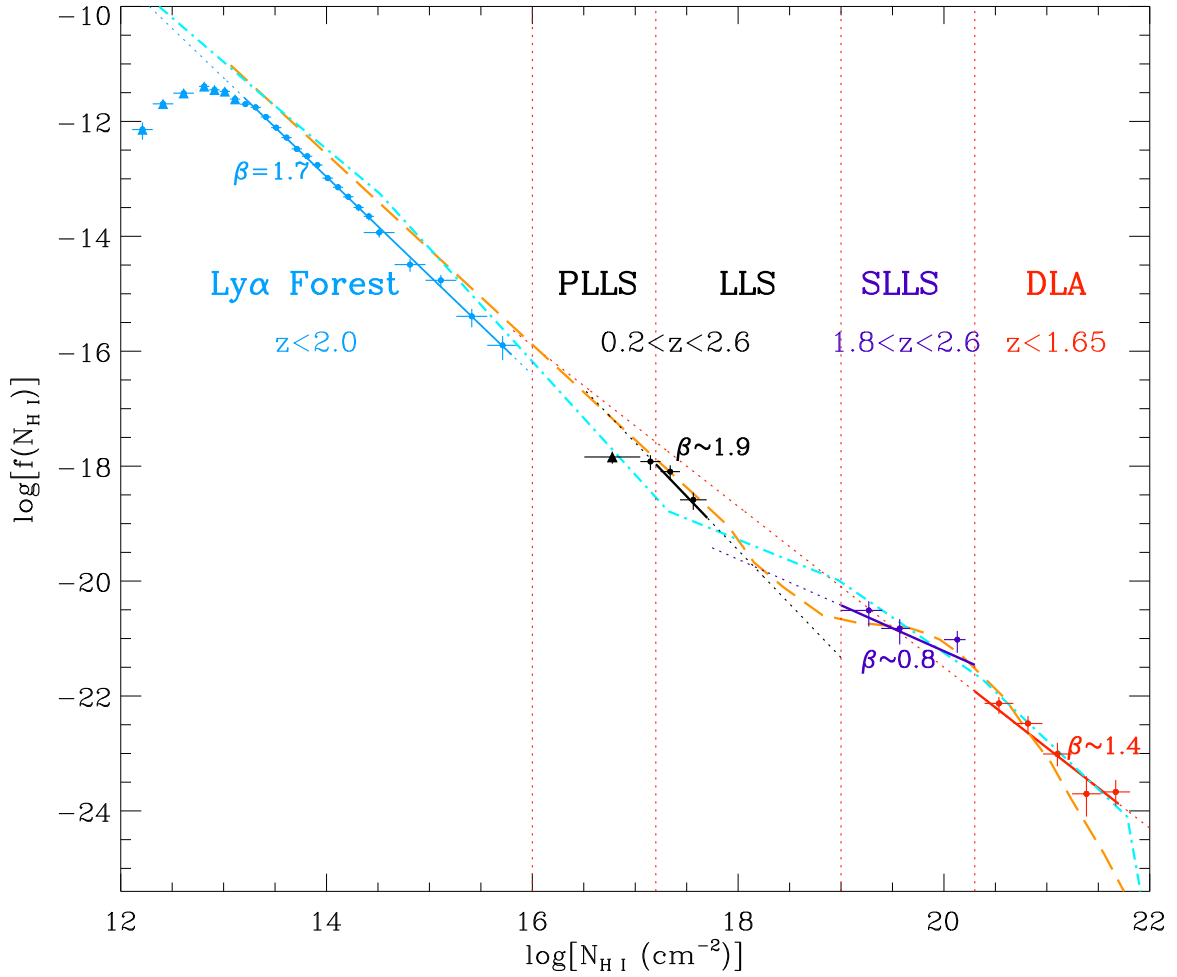


FIG. 9.— The differential density distribution ($f(N_{\text{HI}})$) is plotted against $\log N_{\text{HI}}$. The data are shown with filled circles or triangles and error bars. The triangles indicate that the sample is incomplete at these column densities. The blue, black, violet, and red solid curves are maximum-likelihood fits to the Lyman- α forest, LLS, SLLS, and DLA samples where the fit was undertaken, and the dotted part is the extension in other N_{HI} regimes. The dot-dashed cyan curve is the estimation of $f(N_{\text{HI}})$ at $z \sim 3.7$ by Prochaska et al. (2010, the solid black curve in their Figure 14; bear in mind that for $14.5 \leq \log N_{\text{HI}} < 19$, $f(N_{\text{HI}})$ is quite uncertain). The orange long-dashed curve is a model from Corbelli & Bandiera (2002) at low z where $f(N_{\text{HI}})$ is assumed to follow a single power law, but $f(N_{\text{HI}})$ deviates from a single power law as a result of photoionization by the UV background (see §5.4 for more details).

Lyman- α forest samples.⁶ We estimate the total absorption path probed for the SLLS searches to be $\Delta X \simeq 107$ ($\Delta X \simeq 29$ for the Péroux et al. sample, and $\Delta X \simeq 78$ for the O’Meara et al. sample). The bins of display of the data were chosen so there are ~ 5 systems per bin (see Figure 9). For the PLLSs and LLSs, we considered our sample of QSO sightlines, where we reject sight lines having LLSs with only limits on the optical depth (and hence on N_{HI}). The main effect of the removal of the limits is to increase slightly the normalization of the fit by ~ 0.1 dex. This is too small a difference to have any impact on our result and should not impact the power law slope. This reduces our sample to 50 systems and a total absorption path $\Delta X = 156$. In Figure 9 we show the adopted bins for $16.5 \leq \log N_{\text{HI}} \leq 17.8$. The first bin corresponds to optical depths in the intervals $[0.2, 0.7]$, i.e. where our sample is incomplete; we treat this bin as a lower limit.

⁶ Péroux et al. (2005) subsequently produced a second survey of SLLS, but their redshift coverage mostly targeted higher redshifts with a negligible redshift path at $z < 2.6$.

We used the maximum-likelihood method to fit the data with a power law distribution in $f(N_{\text{HI}})$ (Equation 13). Our first attempt was to fit the LLS and SLLS simultaneously, but no adequate fit was found with a single slope β . We, therefore, fitted the LLS and SLLS separately. For the SLLS, we find $\beta = 0.8^{+0.3}_{-0.1}$ for $19.1 \leq \log N_{\text{HI}} \leq 20.2$ (where the upper and lower bounds were allowed to vary by ± 0.1 dex to estimate the errors). For LLS, we derived $\beta \approx 1.9 \pm 0.3$ for $17.2 \leq \log N_{\text{HI}} \leq 17.7$ (as the N_{HI} interval spans only 0.5 dex, changing the upper and lower bounds by ± 0.1 dex led to an unstable fit; we consider this result as tentative). We note that if we integrate $f(N_{\text{HI}})$ in the intervals $\log N_{\text{HI}} = [17.3, 18.2]$ and $\log N_{\text{HI}} = [18.2, 20.2]$, with the respective β functional forms (where we assume that each is correct to the point where they intersect at ~ 18.2 dex, see Figure 9), we find $l(X) \sim 0.5$, which is not too dissimilar from the results presented in Table 5 that gives $l(X) \simeq 0.3$, providing some independent support to our results. It is evident that more data are needed in the PLLS and the LLS/SLLS regimes to better discern the

true shape of $f(N_{\text{HI}})$ in these N_{HI} intervals. However, our analysis suggests that there must be an inflection point in $f(N_{\text{HI}})$ in the LLS regime, and, likely, a second inflection point in order to connect the PLLS to the Lyman- α forest systems. We note that the $\beta = 1.7$ slope distribution fits well the H I systems with $N_{\text{HI}} \lesssim 10^{16} \text{ cm}^{-2}$ (see Figure 9), so the flattening should likely occur between 10^{16} and 10^{17} cm^{-2} . The $\log N_{\text{HI}} = [17.7, 18]$ interval will likely remain largely unconstrained owing to the difficulty in measuring N_{HI} in this regime requiring either to fit the Lyman series lines (e.g., Lehner et al. 2009a) or to have very high quality S/N data to discern the damping wings in the Lyman- α absorption.

In Figure 9 we also show one of the $f(N_{\text{HI}})$ models in the local universe by Corbelli & Bandiera (2002) (long-dashed orange curve; see their Figure 2 where we adjusted vertically their model to fit the DLA and SLLS distributions – the model with $f(N_{\text{H}}) \propto N_{\text{H}}^{-3.3}$ is shown). In their models, they investigated if the flattening of $f(N_{\text{HI}})$ between the LLSs and DLAs could be explained if $f(N_{\text{H}})$ (H = H I + H II) follows a single power law, while $f(N_{\text{HI}})$ can deviate from a single power owing to the change of the ionization fraction as function of N_{HI} . While the low N_{HI} systems are not well matched (in part because they attempted to fit data based on equivalent width measurements), the higher column density regimes are quite remarkably well reproduced. Other models explored the self-shielding effect on the $f(N_{\text{HI}})$ of DLAs and LLSs using spherical isothermal gaseous halos (Murakami & Ikeuchi 1990; Petitjean et al. 1992; Zheng & Miralda-Escudé 2002), which yields a somewhat similar functional form. Hence photoionization of a single power law population in $f(N_{\text{HI}})$ could be the main cause for the complicated shape of the $f(N_{\text{HI}})$ distribution.

In the higher redshift regime, Petitjean et al. (1993) also noted that a single $f(N_{\text{HI}})$ over the entire N_{HI} regime was not statistically adequate, and, in particular, their data hinted as well to two flattenings in the column density distribution function, one in the PLLS regime and the other one in LLS/SLLS regime that they explained as transitions between the H I systems to metal absorbers and between the neutral and ionized systems, respectively. The most recent study on $f(N_{\text{HI}})$ at $z \sim 3.7$, by Prochaska et al. (2010) suggests an even more complicated $f(N_{\text{HI}})$ distribution. We show in Figure 9 their $f(N_{\text{HI}})$ distribution over the same range of H I column density. We emphasize that while the Lyman- α forest (up to $\log N_{\text{HI}} \lesssim 14$), SLLS, DLA, and to a lesser extent LLS distributions are relatively well constrained, the PLLSs and H I interval $14 \lesssim \log N_{\text{HI}} \lesssim 16$ are not (see their Figure 14 for the amplitude of possible $f(N_{\text{HI}})$ in each N_{HI} region). As already mentioned above, there appears to be no evolution in the DLA portion of $f(N_{\text{HI}})$ with redshift, and a steeper slope than found by Rao et al. (2006) seems more appropriate for connecting the DLAs and SLLSs at low- z . While a similar flattening is observed in the SLLS regime, in the low- z universe $f(N_{\text{HI}})$ appears (tentatively) even flatter. A larger sample of SLLSs will be needed to confirm this as other explanations (e.g., an evolving normalization at different mean redshift or the presence of another inflection point) could account for the observed behavior.

In the lower N_{HI} regime, $f(N_{\text{HI}})$ appears to evolve from the high to low- z universe. At $\log N_{\text{HI}} \leq 14.5$, where $f(N_{\text{HI}})$ is well constrained at both low and high z , the slope becomes steeper as z decreases and there is a drop in the number of systems with redshift. Without a steep decline in the UV background flux (stemming from a drop of the number of QSOs at low z), the number of systems would be predicted to be much lower at low z , suggesting that the changes in the UV background may be the dominant reason for the evolution of the Lyman- α forest (e.g., Theuns et al. 2002b). Numerical simulations of a cold dark matter universe with a photoionized background dominated by the QSO light can, indeed, reproduce these properties to some extents (e.g., Theuns et al. 2002b; Davé et al. 2010), but the observed evolution rate of β is smaller than predicted. Part of the discrepancy between the models and observations could be due to the models ignoring the galactic contribution to the UV background, or more generally to an uncertainty in the strength and shape of the UV background. Large-scale galactic outflows could be thought as another uncertainty because (in the regime where $\log N_{\text{HI}} > 14$) they likely increase the H I absorbing cross section via deposit of cool gas in the outermost edges of galactic halos (Davé et al. 2010). Cosmological simulations however, suggest that galactic feedback has little impact on $f(N_{\text{HI}})$ of the Lyman- α forest as they only fill a small fraction of the volume, leaving the IGM filaments unscathed (Theuns et al. 2002a). Hence, the possible differences seen at $14.5 \lesssim \log N_{\text{HI}} \lesssim 19$ may occur owing to the evolution of both the UV background and galactic feedback. Current and future efforts to provide better statistics for the PLLSs and LLSs at both low and high- z should provide direct constraints on the UV background evolution and cosmological simulations.

6. LLSS AND THE GASEOUS HALOS OF GALAXIES

At very low redshift, the connection between LLSs, galaxies, and large-scale structures has been examined for a small number of individual systems discovered using *HST* and the *Far Ultraviolet Spectroscopic Explorer* (*FUSE*). These studies have found LLSs associated with individual galaxies ($0.2L_* \lesssim L \lesssim 3.4L_*$) at impact parameters $\rho \sim 30 - 100$ kpc (Chen & Prochaska 2000; Jenkins et al. 2003; Tripp et al. 2005; Cooksey et al. 2008; Lehner et al. 2009a). Some low redshift LLSs are metal enriched (i.e., $Z \gtrsim 0.3Z_{\odot}$, e.g., Chen & Prochaska 2000; Prochaska et al. 2006b; Lehner et al. 2009a) while some are relatively metal-poor (i.e., $Z \lesssim 0.1Z_{\odot}$, e.g., Prochaska & Burles 1999; Cooksey et al. 2008; Zonak et al. 2004). The presence of metal-enriched material far from the central star forming regions of galaxies suggests some LLSs are sensitive to the nature of feedback in galaxies. The existence of extremely metal-poor systems suggests the gas probed by some LLS absorption originates outside of galaxies, perhaps tracing IGM matter falling onto a galaxy. An example of a LLS tracing very low metallicity ($Z \sim 0.02Z_{\odot}$) gas falling onto a near solar, $0.3L_*$ galaxy at $z \sim 0.274$ will be described in J. Ribaldo et al. (in prep.). In addition to the observational evidence, numerical simulations also predict a physical association of LLSs with the gravitational potential of galaxies. These simulations show LLSs arising from infalling streams of intergalactic gas as well as out-

flowing gas ejected from galaxies due to stellar feedback (Gardner et al. 2001; Dekel & Birnboim 2006; Kohler & Gnedin 2007; Keres et al. 2009; Kacprzak et al. 2010, Fumagalli et al. 2011, Stewart et al. 2011; but also see, Mo & Miralda-Escudé 1996; Maller et al. 2003).

Based on these observational and theoretical studies, LLSs appear to be associated with circumgalactic environments. With this knowledge, we can calculate the characteristic sizes of such gaseous galactic envelopes using our survey of LLSs and knowledge of the galaxy population with which they are associated. We rewrite $l(X) \propto n_{\text{LLS}}\sigma_{\text{LLS}}$ as:

$$l(X)_{\text{LLS}} \propto n_{\text{GAL}}\sigma_{\text{GAL}}, \quad (14)$$

where n_{GAL} is the comoving number density of galaxies giving rise to LLS absorption and σ_{GAL} is the projected physical cross section of galaxies to columns $\log N_{\text{HI}} \geq 17.5$ (for comparison with R2,RP10 samples). The comoving number density of galaxies at a given redshift is calculated from the integration of an observationally constrained galaxy luminosity function. We investigate the size of absorbers assuming only galaxies with $L \geq L_{\text{min}}$ give rise to LLS absorption. Thus, following Tytler (1987), we rewrite Equation 14 as:

$$l(X) = \frac{c}{H_0} \int_{L_{\text{min}}}^{\infty} f_c \pi R^2(L) \Phi(L) dL, \quad (15)$$

where $f_c \pi R^2(L)$ is the cross section for absorption, σ_{GAL} , with a covering factor f_c and $\Phi(L)dL = \Phi_*(L/L_*)^\alpha \exp(-L/L_*)d(L/L_*)$ is the assumed form of the galaxy luminosity function (Schechter 1976). The comoving number density of galaxies that contribute to the LLS population is determined by our choice of L_{min} , and we use all galaxies with $L \geq L_{\text{min}}$ in this estimation of the mean σ_{GAL} . We note that several previous treatments of the gaseous halos around galaxies have allowed for a Holmberg-like scaling of the physical extent of the gas with $R(L) = R_*(L/L_*)^{\beta_L}$, where R_* is the projected radial extent of the absorbing gas associated with an L_* galaxy (Tytler 1987). Numerous galaxy-absorber studies have shown if the radial extent of galaxies is allowed to scale with luminosity, $R(L)$ serves as the effective cutoff for observed absorption out to that projected distance (i.e., Kacprzak et al. 2010; Chen et al. 2010; Kacprzak et al. 2008; Chen et al. 2001). However, we are considering the physical extent of absorbing gas averaged over all galaxy types and sizes, with our only selection criterion being $L \geq L_{\text{min}}$, and over a very wide range in redshift. Over time, the galaxies giving rise to LLSs may be best described with an evolving β_L , but as we are generalizing our analysis to the size of the gaseous envelope around a “mean” galaxy, averaged over all morphologies, star formation properties, sizes, etc., we adopt $\beta_L = 0.0$. Our results therefore describe the mean extent of circumgalactic gas about galaxies $L \geq L_{\text{min}}$.

Equation 15 can be solved using the incomplete Γ function, giving the statistical absorption radius of a galaxy

$$R_s = f_c^{0.5} R = \left[\frac{c\pi\Phi_*}{H_0 l(X)} \Gamma \left(2\beta_L + \alpha + 1, \frac{L_{\text{min}}}{L_*} \right) \right]^{-0.5}. \quad (16)$$

The radius R_s is therefore the mean radial extent of gas about an average host galaxy scaled by $f_c^{0.5}$, while

$\pi R_s^2 = \sigma_{\text{GAL}}$ is the projected area of such a galaxy for which $\log N_{\text{HI}} \geq 17.5$ for a given choice of L_{min} . We plot R_s in Figure 10 as a function of the assumed L_{min} in the left panel and redshift in the right panel. In the left panel, the shaded regions correspond to different luminosity function parameters, which are appropriate for the redshift ranges given in the legend. The luminosity function parameters are observationally determined and restricted to the redshift range probed by each survey. The right panel shows the statistical absorption radius as a function of redshift for three snapshots of L_{min} . The width of the shaded regions is determined from the redshift range of the survey used to calculate the luminosity function. The height of each region spans the R_s value predicted for the range in redshift. The recent study of Mg II absorbers and galaxies at $z < 0.5$ by Chen et al. (2010) found $f_c = 0.70$ for the strongest Mg II absorbers out to $R_* = 75$ kpc (with $\beta_L = 0.35$). The introduction of a non-unity covering factor will thus increase the values for R by ~ 10 – 30% compared with R_s .

From Figure 10, we can draw several inferences about the evolution and properties of the galactic environments giving rise to LLS absorption, albeit with some limitations. We are describing the mean extent of $\tau \geq 2$ H I gas with no assumptions about which galaxies give rise to the absorption. The evolution in R_s does not track the evolution of individual galaxies, only the mean galaxy with $L \geq L_{\text{min}}$ for each z . Any change in the physical cross section for the mean galaxy at each redshift does not imply individual galaxies are evolving on that timescale, as it is likely the case the galaxies giving rise to LLSs at $z \sim 5$ are not the same galaxies giving rise to LLSs at $z \sim 1$. With these limitations in mind, several inferences can be drawn from this approach.

The $L \geq L_*$ galaxies alone cannot account for the observed population of LLSs, because R_s would be inconsistent with previous galaxy-absorber observations, especially at $z \geq 2$ where the sizes implied for LLSs would be quite large compared with observations (Steidel et al. 2010). Extending the integration of Equation 15 to sub- L_* galaxies produces R_s values more consistent with the impact parameters found independently by other studies (e.g. Bouché et al. 2007; Kacprzak et al. 2010; Chen et al. 2010). It is not clear how small L_{min} should be before we can account for the entire population of LLSs, but Figure 10 highlights the importance and need for deep observations of QSO fields to confidently relate absorbers to specific galaxies. This conclusion is not surprising as Mg II studies and individual LLS observations show sub- L_* ($0.25 \lesssim L/L_* \lesssim 0.76$) galaxies contribute to the population of optically thick absorbers (e.g. Steidel et al. 2010; Kacprzak et al. 2010; Chen et al. 2010; Lehner et al. 2009a; Kacprzak et al. 2008). However, our analysis suggests the less luminous galaxy population may be the dominant source of LLSs. A similar scenario has been suggested for Mg II absorbers over the redshifts $0.37 \leq z \leq 0.82$, where Caler et al. (2010) find evidence that at least 70–75% of the Mg II absorber host galaxies are fainter than $0.56L_*$.

Figure 10 also highlights a significant evolution in the physical cross section of the mean absorbing galaxy as a function of redshift. For $L_{\text{min}} \sim 0.1L_*$, R_s decreases by a factor of ~ 3 from $z \sim 5$ to 2, but remains relatively constant from $z \sim 2$ to 0.3. This is remarkable as it suggests

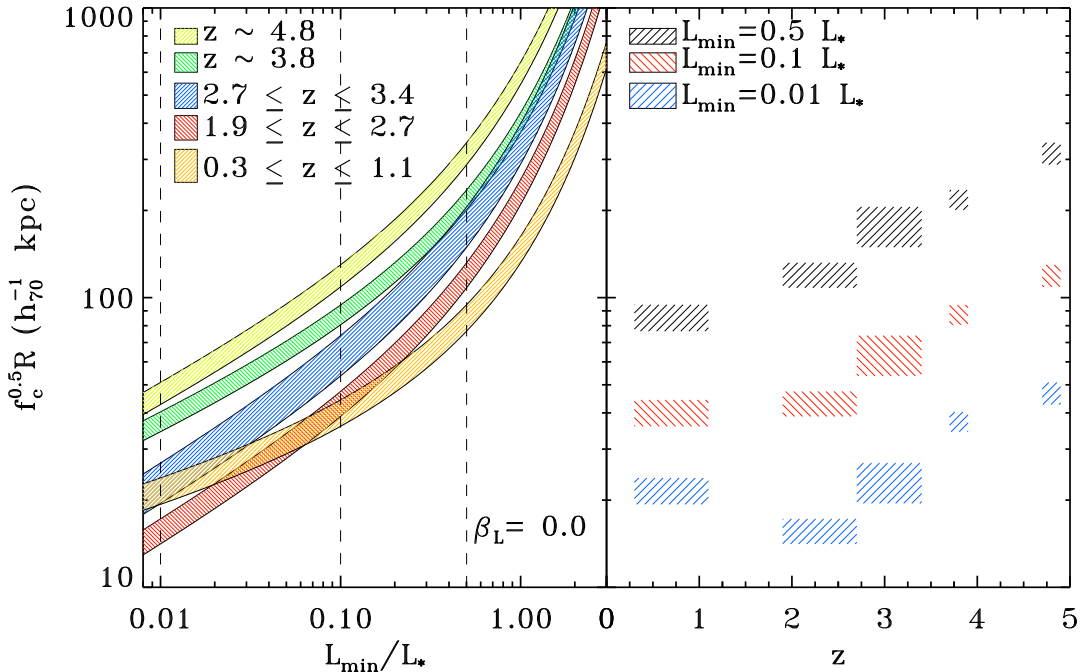


FIG. 10.— The left panel shows the statistical absorption distance ($f_c^{0.5}R$) plotted against L_{\min}/L_* , where L_{\min} is the assumed minimum luminosity for a galaxy to give rise to LLS absorption (see Equation 16). The shaded areas represent the absorption distance for specific redshift ranges, each with different luminosity function parameters. The orange region corresponds to the average α and Φ_* values determined by Faber et al. (2007) using DEEP2 over the redshift range $0.3 \lesssim z \lesssim 1.1$. The red and blue regions correspond to the analysis of Reddy & Steidel (2009) over the redshift range $1.9 \lesssim z \lesssim 2.7$ and $2.7 \lesssim z \lesssim 3.4$, respectively. Lastly, the green and yellow regions correspond to the analysis of van der Burg et al. (2010) using the CFHT Legacy Survey Deep fields at redshifts $z \sim 3.8$ and $z \sim 4.8$. The right panel shows the evolution of the statistical absorption distance as a function of redshift. The colored shaded regions correspond to a minimum luminosity cut designated in the left panel with the dashed lines. The width of the regions corresponds to the redshift range probed by the particular survey used to calculate the galaxy luminosity function and the height of the regions correspond to the range in R_s seen as we vary the redshift over the acceptable range. Note the evolution in the physical size of absorbers in the right panel does not imply single galaxies are evolving on the same timescale. Rather, the right panel implies the physical size of the gaseous envelope of a mean galaxy at a specific redshift undergoes significant evolution over cosmic time.

the physical cross section of the gaseous envelopes of a mean galaxy has decreased significantly over a very short epoch, but for the majority of cosmic time the physical extent of gas about a mean galaxy has been fairly constant. This relatively constant nature of absorption cross section at low- z was also noted by Nestor et al. (2005), who found evidence for little evolution in the physical size of Mg II absorbers as a function of redshift over $0.3 \leq z \leq 1.2$ (for $0.001 \leq L_{\min}/L_* \leq 0.25$).

Changes in physical cross section can be brought on by evolution in the typical covering factor as well as typical radial extent. However, changes in f_c alone likely cannot be responsible for the large drop in the physical cross section of the mean galaxy given the typical values observed at low redshift. While a change in the typical radial extent, R , is a likely cause, other factors could influence our perception of the cross section for the mean galaxy at a given redshift. Evolution in the power law index, β_L , associated with changes in the relative fraction of high versus low luminosity galaxies giving rise to LLSs could alter the mean cross section calculated here. For example, if at high redshifts ($z \sim 5$) the majority of LLSs arise in the circumgalactic gas of relatively high mass, bright galaxies, but at low redshifts ($z \sim 0.3 - 1$) the majority of LLSs arise in the environments of low mass, relatively low luminosity galaxies, we would expect an evolution in the mean physical cross section of LLS absorption simi-

lar to what is shown in Figure 10. An evolution in L_{\min} with redshift would have an affect similar to an evolving β_L .

As we alluded to above, there are two commonly invoked scenarios for producing circumgalactic gas at such large distances from the central regions of galaxies. In the first, galactic-scale outflows drive gas to large radial distances from the main body of a galaxy providing for Mg II and LLS absorption (Bouché et al. 2006). Evidence for this has been presented by Bouché et al. (2007), who found starburst galaxies within 50 kpc for $\sim 70\%$ of a sample of strong Mg II absorbers. Prochter et al. (2006) have also argued the importance of outflows to Mg II selected systems based on the similarity in the evolution in the redshift incidence of strong Mg II absorbers and the star formation rate density of the Universe for $z < 2$. Combined with constraints on the size of the galaxies giving rise to the Mg II absorption, this suggests such systems are produced through feedback processes in low mass galactic halos. In addition, other recent works have connected Mg II selected absorbers to galactic outflows at $z \sim 0.7$ (Nestor et al. 2010), $0.5 < z < 1.4$ (Ménard & Chelouche 2009), and $2 \lesssim z \lesssim 3$ (Steidel et al. 2010).

The second scenario assumes much of the circumgalactic material traced by LLSs is intergalactic gas being accreted onto the galaxies. To maintain the low

apparent ionization conditions of LLSs (Lehner et al. 2009a; Cooksey et al. 2008), the gas should not be shock heated as it is accreted. Such low-ionization gas falls under the phenomenon of cold mode accretion (CMA) (Kereš et al. 2005) predicted to be directed along the filamentary structure of the Universe, allowing galaxies to draw gas from large distances. CMA can account for the observational properties of galaxies inconsistent with the traditional shock-heated accretion models, such as the color bimodality of galaxies and the decline of the cosmic star formation rate at low redshifts (Kereš et al. 2005; Dekel & Birnboim 2006; Dekel et al. 2009a,b; Kereš et al. 2009). Support for CMA has been suggested in recent studies of Mg II absorbers where no correlation between the Mg II absorption strength and galaxy color was found, indicating the origin of the absorbers is not tied to the star formation history of the associated galaxy (Chen et al. 2010). Chen et al. (2010) conclude Mg II absorbers (and LLSs as an extension) are a generic feature of galaxy environments and that the gas probed by Mg II absorption is likely intergalactic in origin. There is more direct observational evidence to support this origin for some LLSs. The nearly primordial LLS detected by J. Ribaud et al. (in prep.) within 40 kpc of a near solar galaxy is similar in ionization state and metallicity to the low-metallicity absorbers reported in Cooksey et al. (2008) and Zonak et al. (2004).

While outflows and infall must play an important role in the composition and maintenance of circumgalactic environments, observations of a few systems suggest gas ejected to large distances during galaxy mergers and tidal interactions could also be responsible for some of the observed LLSs (e.g., Jenkins et al. 2003; Lehner et al. 2009a). Other studies have suggested the high velocity clouds (HVCs) seen about the Milky Way may be analogs for the higher redshift LLSs or Mg II systems (Charlton et al. 2000; Richter et al. 2009; Stocke et al. 2010). In the Milky Way and the nearby Magellanic Clouds, the HVCs probe outflows related to galactic fountains and winds (Keeney et al. 2006; Zech et al. 2008; Lehner & Howk 2007; Lehner et al. 2009b), the infall of low-metallicity gas (e.g., Wakker 2001; Wakker et al. 2008; Thom et al. 2008), and the tidal debris stripped from the Magellanic Clouds (and others) as they interact with each other and the Milky Way (e.g., Putman et al. 2003). Thus, these potential LLS analogs have a wide range of origins, although many of the Milky Way HVCs tend to reside at much smaller impact parameters than suggested for the LLSs ($\rho \leq 10 - 20$ kpc Lehner & Howk 2010; Wakker et al. 2008; Thom et al. 2008). On the other hand tidal remnants from galactic interactions or gas outflows from its satellites are about 50–100 kpc from the Milky Way. These local analogs underline the complex task in defining what kind of phenomena the LLSs trace and if one dominates over the others.

Discriminating between these scenarios using only the correlations of redshifts and equivalent widths of the Mg II lines with other parameters has been difficult. The availability of H I column density information for a large number of LLSs offers a path to studying the metallicities of the LLSs/Mg II systems at low redshifts. Further studies specifically targeting the galactic environments of LLSs, where the metallicities of the LLSs and the galaxies

can be compared, will be critical to further characterize the nature of the absorbers and the role these systems play in the movement of gas into and out of the halos of galaxies. With metallicity playing a fundamental role in discriminating between these two scenarios (e.g., Fumagalli et al. 2011), absorbers will need to be selected based on H I absorption to provide a comprehensive picture of the nature and origin of circumgalactic gas.

7. SUMMARY AND CONCLUDING REMARKS

Using FOS and STIS *HST* archival observations, we have compiled the largest sample of QSOs to date with coverage of the Lyman limit over the redshift range $0.24 \leq z \leq 2.59$. We have used these observations to study the population of LLSs over these redshifts. In considering candidates for our R1 (R2) sample, we included only the data from objects where the spectral quality was judged to be sufficient to reliably detect a LLS with $\tau_{\text{LLS}} \geq 1$ ($\tau_{\text{LLS}} \geq 2$). The sample R1 (R2) contains 229 (249) QSOs, covering a total redshift path of $\Delta z = 79$ (96) and a total of 61 (50) LLSs. This marks a factor of $\sim 3 - 4$ increase in the number of LLSs and redshift path sampled over the most up-to-date work by Stengler-Larrea et al. (1995) and Jannuzi et al. (1998) in this redshift regime. In addition to our statistical sample, we have catalogued 206 low redshift LLSs from the FOS and STIS archives, which increases the sample of LLSs by a factor of ~ 10 for the $z \leq 2.6$ sample. The robustness of our samples allowed us to examine the evolution of LLSs over $0.24 \leq z \leq 2.59$ for the R1 and R2 samples and from $0.2 \lesssim z \lesssim 5.0$ for the RP10 sample that combines our R2 sample with the high redshift sample of Prochaska et al. (2010). Our main results are as follows:

1. We find the redshift density to be well fitted by the power law $l(z) \propto (1+z)^\gamma$ (Equation 7). We find for sample R1 (R2) $\gamma = 1.19 \pm 0.56$ (1.33 ± 0.61). For the RP10 sample at $z \leq 5$, $l(z)$ is well modeled by a single power law with $\gamma = 1.83 \pm 0.21$ (for $\tau_{\text{LLS}} \geq 2$).
2. Assuming a standard Λ CDM cosmology with our RP10 sample, we find $l(X)$, which is proportional to the product of the comoving number density of absorbers, n_{LLS} , and the average physical size of an absorber, σ_{LLS} , decreases by a factor 1.5 from $z \sim 5$ to 3. The evolution of $l(X)$ at $z \leq 2.6$ has slowed considerably, decreasing by a similar factor for $z \sim 2.6$ to 0.25. This indicates the environments which give rise to LLSs experienced dramatic changes in the first ~ 2 Gyr after $z \sim 5$, then more slowly evolved over the following ~ 8 Gyr.
3. We calculate the average proper distance, Δr_{LLS} , a photon travels before encountering a $\tau_{\text{LLS}} \geq 2$ LLS and compare this result with the predicted mean free path of hydrogen ionizing photons. The ratio of Δr_{LLS} and the mean free path from $z \sim 5$ to 0 suggests the $\tau_{\text{LLS}} < 2$ absorption systems have become increasingly more important for absorption of Lyman continuum photons as the Universe has evolved.
4. We model the column density distribution function, $f(N_{\text{HI}})$, for the various N_{HI} regimes at $z \leq 2.6$

using a functional form $f(N_{\text{HI}}) \propto N_{\text{HI}}^{-\beta}$. We show that a single power law cannot fit the entire observed N_{HI} regime. Instead several slopes are needed. For the LLSs, we derive $\beta \sim 1.9$. The functional form in the Lyman- α forest regime ($\beta = 1.72 \pm 0.02$) and in the SLLS regime ($\beta \sim 0.8$) suggests the distribution has two inflection points. For the DLA regime, $\beta \sim 1.8$ seems appropriate for connecting $f(N_{\text{HI}})$ between the DLAs and SLLSs. Simple models assuming a single power law in $f(N_{\text{HI}})$ with absorbers photoionized by the UV background reproduce the $f(N_{\text{HI}})$ distribution remarkably well.

5. We observe little redshift evolution in $f(N_{\text{HI}})$ for the SLLSs and DLAs from high ($z \sim 3.7$) to low ($z \leq 2.6$) redshifts. However, there is evidence that $f(N_{\text{HI}})$ evolves from high to low redshift at $\log N_{\text{HI}} \lesssim 17.7$, which coincides with the strong evolution seen in the UV background and star-formation rates of galaxies over similar redshifts.

6. Assuming LLSs arise in circumgalactic gas, we find the physical cross section of the mean galaxy at each redshift to LLS absorption decreased by a factor of ~ 9 from $z \sim 5$ to 2 and subsequently stayed relatively constant. We argue sub- L_* galaxies must contribute significantly to the absorber population.

The authors wish to thank J.X. Prochaska who kindly made their data available for comparison with this sample prior to publication. We would also like to thank the referee for useful and insightful comments, as well as J.X. Prochaska and J. O'Meara for their valuable comments. Support for this research was provided by NASA through grant HST-AR-11762.01-A from the Space Telescope Science Institute, which is operated by the Association of Universities for Research in Astronomy, Incorporated, under NASA contract NAS5-26555. Further support comes from NASA grant NNX08AJ31G. This research has made use of the NASA Astrophysics Data System Abstract Service and the Centre de Données de Strasbourg (CDS).

REFERENCES

- Bahcall, J. N., & Peebles, P. J. E. 1969, *ApJ*, 156, L7
- Bechtold, J., Dobrzycki, A., Wilden, B., Morita, M., Scott, J., Dobrzycka, D., Tran, K.-V., & Aldcroft, T. L. 2002, *ApJS*, 140, 143
- Bouché, N., Murphy, M. T., Péroux, C., Davies, R., Eisenhauer, F., Förster Schreiber, N. M., & Tacconi, L. 2007, *ApJ*, 669, L5
- Bouché, N., Murphy, M. T., Péroux, C., Csabai, I., & Wild, V. 2006, *MNRAS*, 371, 495
- Calder, M. A., Sheth, R. K., & Jain, B. 2010, *MNRAS*, 406, 1269
- Charlton, J. C., & Churchill, C. W. 1998, *ApJ*, 499, 181
- Charlton, J. C., Churchill, C. W., & Rigby, J. R. 2000, *ApJ*, 544, 702
- Chen, H.-W., Helsby, J. E., Gauthier, J.-R., Sheckman, S. A., Thompson, I. B., & Tinker, J. L. 2010, *ApJ*, 714, 1521
- Chen, H.-W., Lanzetta, K. M., & Webb, J. K. 2001, *ApJ*, 556, 158
- Chen, H.-W., & Prochaska, J. X. 2000, *ApJ*, 543, L9
- Churchill, C. W., Mellon, R. R., Charlton, J. C., Jannuzi, B. T., Kirhakos, S., Steidel, C. C., & Schneider, D. P. 2000, *ApJS*, 130, 91
- Churchill, C., Steidel, C., & Kacprzak, G. 2005, *Extra-Planar Gas*, 331, 387
- Cooksey, K. L., Prochaska, J. X., Chen, H.-W., Mulchaey, J. S., & Weiner, B. J. 2008, *ApJ*, 676, 262
- Corbelli, E., & Bandiera, R. 2002, *ApJ*, 567, 712
- Danforth, C. W., & Shull, J. M. 2008, *ApJ*, 679, 194
- Davé, R., Oppenheimer, B. D., Katz, N., Kollmeier, J. A., & Weinberg, D. H. 2010, *MNRAS*, 408, 2051
- Dekel, A., Sari, R., & Ceverino, D. 2009a, *ApJ*, 703, 785
- Dekel, A., et al. 2009b, *Nature*, 457, 451
- Dekel, A., & Birnboim, Y. 2006, *MNRAS*, 368, 2
- Faber, S. M., et al. 2007, *ApJ*, 665, 265
- Faucher-Giguère, C.-A., Lidz, A., Zaldarriaga, M., & Hernquist, L. 2009, *ApJ*, 703, 1416
- Fumagalli, M., Prochaska, J. X., Kasen, D., Dekel, A., Ceverino, D., & Primack, J. R. 2011, *arXiv:1103.2130*
- Gardner, J. P., Katz, N., Hernquist, L., & Weinberg, D. H. 2001, *ApJ*, 559, 131
- Haardt, F., & Madau, P. 1996, *ApJ*, 461, 20
- Janknecht, E., Reimers, D., Lopez, S., & Tytler, D. 2006, *A&A*, 458, 427
- Jannuzi, B. T., et al. 1998, *ApJS*, 118, 1
- Jena, T., et al. 2005, *MNRAS*, 361, 70
- Jenkins, E. B., Bowen, D. V., Tripp, T. M., Sembach, K. R., Leighly, K. M., Halpern, J. P., & Lauroesch, J. T. 2003, *AJ*, 125, 2824
- Kacprzak, G. G., Churchill, C. W., Ceverino, D., Steidel, C. C., Klypin, A., & Murphy, M. T. 2010, *ApJ*, 711, 533
- Kacprzak, G. G., Churchill, C. W., Steidel, C. C., & Murphy, M. T. 2008, *AJ*, 135, 922
- Keeney, B. A., Danforth, C. W., Stocke, J. T., Penton, S. V., Shull, J. M., & Sembach, K. R. 2006, *ApJ*, 646, 951
- Kereš, D., & Hernquist, L. 2009, *ApJ*, 700, L1
- Kereš, D., Katz, N., Weinberg, D. H., & Davé, R. 2005, *MNRAS*, 363, 2
- Kereš, D., Katz, N., Fardal, M., Davé, R., & Weinberg, D. H. 2009, *MNRAS*, 395, 160
- Keyes, C.D., Koratkar, A.P., Dahlem, M., Hayes, J., Christensen, J., & Martin, S. 1995, v6.0
- Kohler, K., & Gnedin, N. Y. 2007, *ApJ*, 655, 685
- Komatsu, E., et al. 2009, *ApJS*, 180, 330
- Kulkarni, V. P., Khare, P., Péroux, C., York, D. G., Lauroesch, J. T., & Meiring, J. D. 2007, *ApJ*, 661, 88
- Lanzetta, K. M. 1991, *ApJ*, 375, 1
- Lehner, N., & Howk, J. C. 2010, *ApJ*, 709, L138
- Lehner, N., Prochaska, J. X., Kobulnicky, H. A., Cooksey, K. L., Howk, J. C., Williger, G. M., & Cales, S. L. 2009a, *ApJ*, 694, 734
- Lehner, N., Staveley-Smith, L., & Howk, J. C. 2009b, *ApJ*, 702, 940
- Lehner, N., Savage, B. D., Richter, P., Sembach, K. R., Tripp, T. M., & Wakker, B. P. 2007, *ApJ*, 658, 680
- Lehner, N., & Howk, J. C. 2007, *MNRAS*, 377, 687
- Lehner, N., Savage, B. D., Wakker, B. P., Sembach, K. R., & Tripp, T. M. 2006, *ApJS*, 164, 1
- Maller, A. H., Prochaska, J. X., Somerville, R. S., & Primack, J. R. 2003, *MNRAS*, 343, 268
- Ménard, B., & Chelouche, D. 2009, *MNRAS*, 393, 808
- Miralda-Escudé, J., Cen, R., Ostriker, J. P., & Rauch, M. 1996, *ApJ*, 471, 582
- Mo, H. J., & Miralda-Escudé, J. 1996, *ApJ*, 469, 589
- Murakami, I., & Ikeuchi, S. 1990, *PASJ*, 42, L11
- Nagamine, K., Choi, J.-H., & Yajima, H. 2010, *arXiv:1006.5345*
- Nestor, D. B., Johnson, B. D., Wild, V., Ménard, B., Turnshek, D. A., Rao, S., & Pettini, M. 2010, *arXiv:1003.0693*
- Nestor, D. B., Turnshek, D. A., & Rao, S. M. 2005, *ApJ*, 628, 637
- O'Meara, J. M., in prep.
- O'Meara, J. M., Prochaska, J. X., Burles, S., Prochter, G., Bernstein, R. A., & Burgess, K. M. 2007, *ApJ*, 656, 666
- Penton, S. V., Stocke, J. T., & Shull, J. M. 2004, *ApJS*, 152, 29
- Péroux, C., Dessauges-Zavadsky, M., D'Odorico, S., Sun Kim, T., & McMahon, R. G. 2005, *MNRAS*, 363, 479
- Péroux, C., Dessauges-Zavadsky, M., D'Odorico, S., Kim, T.-S., & McMahon, R. G. 2003, *MNRAS*, 345, 480

- Péroux, C., Dessauges-Zavadsky, M., Kim, T., McMahon, R. G., & D'Odorico, S. 2002, *Ap&SS*, 281, 543
- Petitjean, P., Webb, J. K., Rauch, M., Carswell, R. F., & Lanzetta, K. 1993, *MNRAS*, 262, 499
- Petitjean, P., Bergeron, J., & Puget, J. L. 1992, *A&A*, 265, 375
- Petitjean, P., & Bergeron, J. 1990, *A&A*, 231, 309
- Prochaska, J. X., O'Meara, J. M., & Worseck, G. 2010, *ApJ*, 718, 392
- Prochaska, J. X., Worseck, G., & O'Meara, J. M. 2009, *ApJ*, 705, L113
- Prochaska, J. X., Weiner, B. J., Chen, H.-W., & Mulchaey, J. S. 2006a, *ApJ*, 643, 680
- Prochaska, J. X., O'Meara, J. M., Herbert-Fort, S., Burles, S., Prochter, G. E., & Bernstein, R. A. 2006b, *ApJ*, 648, L97
- Prochaska, J. X., & Wolfe, A. M. 2009, *ApJ*, 696, 1543
- Prochaska, J. X., Chen, H.-W., Howk, J. C., Weiner, B. J., & Mulchaey, J. 2004, *ApJ*, 617, 718
- Prochaska, J. X., & Burles, S. M. 1999, *AJ*, 117, 1957
- Prochter, G. E., Prochaska, J. X., & Burles, S. M. 2006, *ApJ*, 639, 766
- Putman, M. E., Staveley-Smith, L., Freeman, K. C., Gibson, B. K., & Barnes, D. G. 2003, *ApJ*, 586, 170
- Rao, S. M., Turnshek, D. A., & Nestor, D. B. 2006, *ApJ*, 636, 610
- Rauch, M. 1998, *ARA&A*, 36, 267
- Reddy, N. A., & Steidel, C. C. 2009, *ApJ*, 692, 778
- Ribaudo, J., in prep.
- Richter, P., Charlton, J. C., Fangano, A. P. M., Bekhti, N. B., & Masiero, J. R. 2009, *ApJ*, 695, 1631
- Sargent, W. L. W., Steidel, C. C., & Boksenberg, A. 1989, *ApJS*, 69, 703
- Schechter, P. 1976, *ApJ*, 203, 297
- Shull, J. M., Roberts, D., Giroux, M. L., Penton, S. V., & Fardal, M. A. 1999, *AJ*, 118, 1450
- Simcoe, R. A., Sargent, W. L. W., Rauch, M., & Becker, G. 2006, *ApJ*, 637, 648
- Songaila, A., & Cowie, L. L. 2010, arXiv:1007.3262
- Spitzer, L. 1978, New York Wiley-Interscience
- Steidel, C. C., Erb, D. K., Shapley, A. E., Pettini, M., Reddy, N., Bogosavljević, M., Rudie, G. C., & Rakic, O. 2010, *ApJ*, 717, 289
- Steidel, C. C., & Sargent, W. L. W. 1992, *ApJS*, 80, 1
- Stengler-Larrea, E. A., et al. 1995, *ApJ*, 444, 64
- Stocke, J. T., Keeney, B. A., & Danforth, C. W. 2010, *Publications of the Astronomical Society of Australia*, 27, 256
- Storrie-Lombardi, L. J., McMahon, R. G., Irwin, M. J., & Hazard, C. 1994, *ApJ*, 427, L13
- Theuns, T., Viel, M., Kay, S., Schaye, J., Carswell, R. F., & Tzanavaris, P. 2002a, *ApJ*, 578, L5
- Theuns, T., Zaroubi, S., Kim, T.-S., Tzanavaris, P., & Carswell, R. F. 2002b, *MNRAS*, 332, 367
- Thom, C., Peek, J. E. G., Putman, M. E., Heiles, C., Peek, K. M. G., & Wilhelm, R. 2008, *ApJ*, 684, 364
- Tripp, T. M., Jenkins, E. B., Bowen, D. V., Prochaska, J. X., Aracil, B., & Ganguly, R. 2005, *ApJ*, 619, 714
- Tytler, D. 1982, *Nature*, 298, 427
- Tytler, D. 1987, *ApJ*, 321, 49
- van der Burg, R. F. J., Hildebrandt, H., & Erben, T. 2010, arXiv:1009.0758
- Veron-Cetty, M. P., & Veron, P. 2010, *VizieR Online Data Catalog*, 7258, 0
- Wakker, B. P., York, D. G., Wilhelm, R., Barentine, J. C., Richter, P., Beers, T. C., Ivezić, Ž., & Howk, J. C. 2008, *ApJ*, 672, 298
- Wakker, B. P. 2001, *ApJS*, 136, 463
- Williger, G. M., et al. 2010, *MNRAS*, 405, 1736
- Wolfe, A. M., Gawiser, E., & Prochaska, J. X. 2005, *ARA&A*, 43, 861
- Zech, W. F., Lehner, N., Howk, J. C., Dixon, W. V. D., & Brown, T. M. 2008, *ApJ*, 679, 460
- Zheng, W., Kriss, G. A., Telfer, R. C., Grimes, J. P., & Davidsen, A. F. 1997, *ApJ*, 475, 469
- Zheng, Z., & Miralda-Escudé, J. 2002, *ApJ*, 578, 33
- Zonak, S. G., Charlton, J. C., Ding, J., & Churchill, C. W. 2004, *ApJ*, 606, 196
- Zuo, L., & Phinney, E. S. 1993, *ApJ*, 418, 28

TABLE 1
OBSERVATIONS FROM STIS ARCHIVE

| Object | R.A. (J2000) | DEC. (J2000) | Grating | Exp. (s) | Id |
|-------------|--------------|--------------|---------|----------|------|
| J0001+0709 | 00 01 40.580 | +07 09 54.62 | G230L | 2304 | 8569 |
| J0012-0122 | 00 12 10.880 | -01 22 07.74 | G230L | 2304 | 8569 |
| J0018-3529 | 00 18 41.430 | -35 29 04.70 | G140L | 2392 | 8287 |
| J0021+0104 | 00 21 27.886 | +01 04 20.10 | G230L | 2355 | 9382 |
| J0021+0043 | 00 21 33.264 | +00 43 00.73 | G230L | 2379 | 9382 |
| J0021-0128A | 00 21 51.800 | -01 28 34.11 | G230L | 7900 | 8126 |
| J0022-0128B | 00 22 04.890 | -01 28 48.07 | G230L | 7900 | 8126 |
| J0032-2144 | 00 32 44.690 | -21 44 22.14 | G230L | 5037 | 8225 |
| J0038-3501 | 00 38 05.540 | -35 01 40.35 | G230L | 8156 | 8126 |
| J0038-3504 | 00 38 17.450 | -35 04 05.37 | G230L | 11087 | 8126 |
| J0039-3529 | 00 39 37.280 | -35 29 17.10 | G230L | 11075 | 8126 |
| J0039-3528 | 00 39 42.570 | -35 28 00.48 | G230L | 8156 | 8126 |
| J0043-2622 | 00 43 42.730 | -26 22 09.17 | G230L | 2374 | 8569 |
| J0051+0041 | 00 51 30.470 | +00 41 49.76 | G230L | 2190 | 9051 |
| J0100-5113 | 01 00 27.110 | -51 13 54.21 | G140L | 850 | 9858 |
| J0102-0853 | 01 02 49.610 | -08 53 44.01 | G230L | 2150 | 9051 |
| J0103-3009 | 01 03 55.090 | -30 09 46.40 | G140L | 2348 | 8287 |
| J0105-2736 | 01 05 34.770 | -27 36 58.40 | G230L | 13266 | 7359 |
| J0106+0105 | 01 06 03.883 | +01 05 06.22 | G230L | 5236 | 9382 |
| J0107-0019 | 01 07 37.049 | -00 19 11.89 | G230L | 5252 | 9382 |
| J0109-2307 | 01 09 02.960 | -23 07 30.03 | G230L | 4738 | 8225 |
| J0109-2102 | 01 09 25.130 | -21 02 54.00 | G140L | 2289 | 8287 |
| J0110+0019 | 01 10 56.938 | +00 19 11.21 | G230L | 2367 | 9382 |
| J0116-0043 | 01 16 15.528 | -00 43 35.33 | G230L | 2363 | 9382 |
| J0122+1339 | 01 22 31.920 | +13 39 40.90 | G140L | 600 | 9067 |
| J0123-0058 | 01 23 03.219 | -00 58 19.38 | G230L | 5160 | 9382 |
| J0126-2222 | 01 26 14.940 | -22 22 33.49 | G230L | 4738 | 8225 |
| J0126-0105 | 01 26 30.353 | -01 05 01.03 | G230L | 2371 | 9382 |
| J0128-3029 | 01 28 24.840 | -30 29 41.64 | G140L | 1594 | 9506 |
| J0132+0116 | 01 32 33.876 | +01 16 07.10 | G230L | 5236 | 9382 |
| J0134+0051 | 01 34 05.743 | +00 51 09.65 | G230L | 5252 | 9382 |
| J0137-2430 | 01 37 38.310 | -24 30 53.70 | G230L | 5037 | 8225 |
| J0138-0005 | 01 38 25.497 | -00 05 33.97 | G230L | 5244 | 9382 |
| J0139-0023 | 01 39 38.664 | -00 23 47.80 | G230L | 5236 | 9382 |
| J0139+0619 | 01 39 55.780 | +06 19 22.89 | G230L | 8073 | 9894 |
| J0139+0619 | 01 39 55.780 | +06 19 22.89 | G140L | 13819 | 9894 |
| J0141-0024 | 01 41 23.010 | -00 24 21.68 | G230L | 2150 | 9051 |
| J0145-3520 | 01 45 50.610 | -35 20 50.05 | G230L | 900 | 9507 |
| J0152+0023 | 01 52 49.687 | +00 23 14.78 | G230L | 5260 | 9382 |
| J0153+0052 | 01 53 09.041 | +00 52 50.38 | G230L | 5236 | 9382 |
| J0153+0009 | 01 53 18.101 | +00 09 11.63 | G230L | 2379 | 9382 |
| J0157-0048 | 01 57 33.826 | -00 48 24.26 | G230L | 5260 | 9382 |
| J0157-0106 | 01 57 41.563 | -01 06 29.59 | G140L | 600 | 9067 |
| J0208-0503 | 02 08 02.990 | -05 03 00.01 | G230L | 2150 | 9051 |
| J0210-0152 | 02 10 39.840 | -01 52 13.53 | G230L | 2190 | 9051 |
| J0232+3423 | 02 32 28.980 | +34 23 46.57 | G230L | 2372 | 8569 |
| J0240-1851 | 02 40 32.560 | -18 51 51.26 | G140L | 720 | 9506 |
| J0241-1514 | 02 41 56.500 | -15 14 42.04 | G230L | 2304 | 8569 |
| J0244-2904 | 02 44 49.110 | -29 04 48.10 | G140L | 2338 | 8287 |
| J0253+0107 | 02 53 16.464 | +01 07 59.77 | G230L | 8141 | 9382 |
| J0253-5441 | 02 53 29.190 | -54 41 51.13 | G230L | 900 | 9507 |
| J0256+0110 | 02 56 07.250 | +01 10 37.92 | G230L | 5240 | 9382 |
| J0256-3315 | 02 56 47.840 | -33 15 26.15 | G140L | 2412 | 8569 |
| J0304-0008 | 03 04 49.820 | -00 08 13.60 | G230L | 4774 | 7272 |
| J0304-0008 | 03 04 49.820 | -00 08 13.60 | G140L | 23282 | 7575 |
| J0308-3250 | 03 08 23.480 | -32 50 10.19 | G140L | 720 | 9506 |
| J0311-6039 | 03 11 06.880 | -60 39 03.40 | G140L | 2520 | 8287 |
| J0318-2012 | 03 18 25.200 | -20 12 19.49 | G230L | 5016 | 8569 |
| J0329-2357 | 03 29 54.070 | -23 57 09.17 | G230L | 4798 | 8225 |
| J0349-5344 | 03 49 28.500 | -53 44 47.68 | G140L | 1498 | 9858 |
| J0354-2724 | 03 54 05.570 | -27 24 20.15 | G230L | 2376 | 8569 |
| J0355-5451 | 03 55 13.340 | -54 51 57.19 | G230L | 720 | 9507 |
| J0411-4956 | 04 11 00.840 | -49 56 56.38 | G230L | 900 | 9507 |
| J0416-2056 | 04 16 04.340 | -20 56 27.37 | G230L | 5053 | 8225 |
| J0423-0120 | 04 23 15.760 | -01 20 34.06 | G230L | 2304 | 8569 |
| J0436-5258 | 04 36 50.790 | -52 58 48.58 | G140L | 856 | 9506 |
| J0438-2608 | 04 38 10.210 | -26 08 38.22 | G230L | 720 | 9507 |
| J0439-2422 | 04 39 09.320 | -24 22 08.41 | G230L | 2206 | 8225 |
| J0439-5311 | 04 39 38.661 | -53 11 32.00 | G140L | 720 | 9506 |
| J0439-4540 | 04 39 44.810 | -45 40 42.12 | G230L | 7126 | 9894 |
| J0439-4540 | 04 39 44.810 | -45 40 42.12 | G140L | 11390 | 9894 |
| J0440-5248 | 04 40 11.940 | -52 48 18.29 | G140L | 720 | 9506 |
| J0441-4313 | 04 41 17.280 | -43 13 43.82 | G140L | 2510 | 9382 |
| J0443-2820 | 04 43 20.760 | -28 20 52.33 | G230L | 900 | 9507 |
| J0448+0950 | 04 48 21.680 | +09 50 52.31 | G230L | 4958 | 8569 |
| J0452-1640 | 04 52 14.229 | -16 40 16.76 | G230L | 2304 | 8569 |

TABLE 1 — *Continued*

| Object | R.A. (J2000) | DEC. (J2000) | Grating | Exp. (s) | Id |
|------------|--------------|--------------|---------|----------|------|
| J0452-2201 | 04 52 44.769 | -22 01 20.09 | G230L | 2202 | 8225 |
| J0453-1305 | 04 53 13.480 | -13 05 55.84 | G230L | 2304 | 8569 |
| J0504-2944 | 05 04 19.010 | -29 44 39.15 | G140L | 720 | 9506 |
| J0504-2944 | 05 04 19.019 | -29 44 39.11 | G230L | 900 | 9507 |
| J0509-3232 | 05 09 17.701 | -32 32 44.97 | G140L | 2144 | 9506 |
| J0514-3326 | 05 14 10.783 | -33 26 22.50 | G230L | 16588 | 9165 |
| J0732+6159 | 07 32 18.571 | +61 59 05.43 | G140L | 720 | 9506 |
| J0739+8146 | 07 39 03.389 | +81 46 01.66 | G230L | 2726 | 8569 |
| J0744+3208 | 07 44 17.360 | +32 08 05.01 | G230L | 2156 | 9051 |
| J0749+4152 | 07 49 27.907 | +41 52 42.39 | G140L | 600 | 9067 |
| J0753+4231 | 07 53 03.342 | +42 31 30.76 | G140L | 600 | 9067 |
| J0800+4435 | 08 00 06.324 | +44 35 55.64 | G140L | 600 | 9067 |
| J0800+3051 | 08 00 23.020 | +30 51 01.26 | G230L | 87 | 9759 |
| J0801+5210 | 08 01 17.750 | +52 10 35.12 | G140L | 1543 | 9506 |
| J0804+6459 | 08 04 30.300 | +64 59 52.89 | G140L | 2570 | 7617 |
| J0806+5041 | 08 06 20.460 | +50 41 24.65 | G230L | 2420 | 9051 |
| J0814+5029 | 08 14 35.186 | +50 29 46.54 | G140L | 600 | 9067 |
| J0825+5127 | 08 25 35.193 | +51 27 06.40 | G140L | 600 | 9067 |
| J0827+1052 | 08 27 06.509 | +10 52 23.81 | G230L | 2304 | 8569 |
| J0839+5256 | 08 39 52.354 | +52 56 24.28 | G140L | 600 | 9067 |
| J0857+1855 | 08 57 26.810 | +18 55 24.20 | G140L | 2352 | 8569 |
| J0904+1309 | 09 04 23.361 | +13 09 21.20 | G140L | 2318 | 8287 |
| J0912+2450 | 09 12 17.769 | +24 50 37.70 | G140L | 720 | 9506 |
| J0915+4426 | 09 15 10.748 | +44 26 55.94 | G140L | 600 | 9759 |
| J0926+3055 | 09 26 36.299 | +30 55 06.00 | G140L | 576 | 8582 |
| J0944+2554 | 09 44 42.341 | +25 54 42.53 | G230L | 2140 | 8569 |
| J0948+4323 | 09 48 35.922 | +43 23 02.01 | G230L | 2333 | 9051 |
| J0949+2955 | 09 49 41.100 | +29 55 18.80 | G140L | 64800 | 8284 |
| J0949+2955 | 09 49 41.100 | +29 55 18.80 | G230L | 25920 | 8284 |
| J0950+5846 | 09 50 11.257 | +58 46 57.72 | G140L | 600 | 9067 |
| J0950+5801 | 09 50 13.989 | +58 01 38.00 | G140L | 576 | 8582 |
| J0953-0038 | 09 53 23.588 | -00 38 03.62 | G230L | 5248 | 9382 |
| J0955+5940 | 09 55 11.331 | +59 40 30.70 | G140L | 600 | 9067 |
| J0958+3224 | 09 58 20.991 | +32 24 02.37 | G140L | 1200 | 9506 |
| J1000+0005 | 10 00 17.659 | +00 05 22.56 | G230L | 2354 | 8569 |
| J1001+5553 | 10 01 20.739 | +55 53 55.10 | G230L | 1903 | 8336 |
| J1001+5553 | 10 01 20.889 | +55 53 49.20 | G230L | 1904 | 8336 |
| J1001+5610 | 10 01 42.601 | +56 10 44.00 | G140L | 576 | 8582 |
| J1007+0042 | 10 07 15.472 | +00 42 58.03 | G230L | 4731 | 9382 |
| J1007+1248 | 10 07 26.100 | +12 48 56.00 | G230L | 2292 | 9432 |
| J1008-0223 | 10 08 34.739 | -02 23 02.50 | G140L | 600 | 9067 |
| J1008-0018 | 10 08 37.317 | -00 18 35.21 | G230L | 5248 | 9382 |
| J1009-1226 | 10 09 02.618 | -12 26 18.14 | G230L | 900 | 9507 |
| J1009-0026 | 10 09 30.421 | -00 26 19.10 | G230L | 2383 | 9382 |
| J1009+0036 | 10 09 45.143 | +00 36 33.23 | G230L | 5236 | 9382 |
| J1010+0003 | 10 10 18.160 | +00 03 51.37 | G230L | 2375 | 9382 |
| J1010-0047 | 10 10 33.398 | -00 47 24.40 | G230L | 2375 | 9382 |
| J1013+5615 | 10 13 36.299 | +56 15 36.97 | G140L | 576 | 8582 |
| J1014+4300 | 10 14 47.131 | +43 00 30.90 | G140L | 2441 | 8287 |
| J1017+5356 | 10 17 42.729 | +53 56 35.39 | G230L | 5580 | 9051 |
| J1022+3041 | 10 22 30.278 | +30 41 04.86 | G140L | 2376 | 8569 |
| J1022+0101 | 10 22 59.777 | +01 01 23.20 | G230L | 5236 | 9382 |
| J1026+6136 | 10 26 19.102 | +61 36 28.90 | G140L | 600 | 9067 |
| J1026+6746 | 10 26 32.571 | +67 46 12.65 | G140L | 720 | 9506 |
| J1028-0100 | 10 28 36.980 | -01 00 27.86 | G230L | 5256 | 9382 |
| J1031+5053 | 10 31 18.472 | +50 53 36.51 | G140L | 2094 | 9506 |
| J1031-0036 | 10 31 48.779 | -00 36 03.28 | G230L | 2351 | 9382 |
| J1032+5051 | 10 32 16.190 | +50 51 20.65 | G140L | 1543 | 9506 |
| J1032+0003 | 10 32 39.163 | +00 03 53.39 | G230L | 2400 | 9382 |
| J1037+0028 | 10 37 44.392 | +00 28 08.51 | G230L | 2367 | 9382 |
| J1040+5145 | 10 40 57.700 | +51 45 05.86 | G140L | 600 | 9759 |
| J1047-0047 | 10 47 33.395 | -00 47 01.07 | G230L | 5248 | 9382 |
| J1048+0032 | 10 48 52.533 | +00 32 29.40 | G230L | 2367 | 9382 |
| J1051-0051 | 10 51 51.460 | -00 51 18.16 | G140L | 150 | 7295 |
| J1054-0020 | 10 54 40.950 | -00 20 49.13 | G230L | 2375 | 9382 |
| J1057-0139 | 10 57 13.250 | -01 39 13.90 | G140L | 600 | 9067 |
| J1103+3715 | 11 03 49.709 | +37 15 25.50 | G230L | 2188 | 9051 |
| J1104-1016 | 11 04 16.699 | -10 16 08.16 | G230L | 900 | 9507 |
| J1106-0052 | 11 06 31.740 | -00 52 53.52 | G140L | 190 | 7295 |
| J1107+0048 | 11 07 29.022 | +00 48 10.30 | G230L | 2383 | 9382 |
| J1107+0003 | 11 07 36.654 | +00 03 28.62 | G230L | 2367 | 9382 |
| J1108+3133 | 11 08 01.300 | +31 33 32.38 | G230L | 2200 | 9051 |
| J1108-0802 | 11 08 12.631 | -08 02 29.03 | G230L | 900 | 9507 |
| J1109+0051 | 11 09 36.361 | +00 51 10.40 | G230L | 8145 | 9382 |
| J1110+4831 | 11 10 38.591 | +48 31 16.51 | G140L | 720 | 9506 |
| J1110+3019 | 11 10 40.250 | +30 19 09.95 | G230L | 2236 | 9051 |
| J1110+0048 | 11 10 54.906 | +00 48 53.53 | G230L | 5244 | 9382 |

TABLE 1 — *Continued*

| Object | R.A. (J2000) | DEC. (J2000) | Grating | Exp. (s) | Id |
|------------|--------------|--------------|---------|----------|------|
| J1112+0013 | 11 12 56.118 | +00 13 43.28 | G230L | 2363 | 9382 |
| J1119+6004 | 11 19 14.352 | +60 04 56.84 | G140L | 1000 | 9506 |
| J1125+5910 | 11 25 53.899 | +59 10 21.00 | G140L | 1320 | 9874 |
| J1126+0034 | 11 26 02.783 | +00 34 18.01 | G230L | 2371 | 9382 |
| J1129-1941 | 11 29 30.461 | -19 41 00.37 | G140L | 720 | 9506 |
| J1137+3907 | 11 37 09.521 | +39 07 23.59 | G230L | 2260 | 9051 |
| J1143+3452 | 11 43 08.811 | +34 52 22.69 | G140L | 10538 | 8287 |
| J1200+3126 | 12 00 06.189 | +31 26 30.20 | G140L | 29185 | 8287 |
| J1201+0111 | 12 01 30.370 | +01 11 38.67 | G140L | 1320 | 9874 |
| J1203+1522 | 12 03 31.249 | +15 22 55.50 | G140L | 2316 | 8287 |
| J1205-2634 | 12 05 33.179 | -26 34 03.75 | G230L | 4772 | 8225 |
| J1209+0232 | 12 09 44.821 | +02 32 12.70 | G140L | 1320 | 9874 |
| J1210-2758 | 12 10 43.810 | -27 58 59.10 | G230L | 5071 | 8225 |
| J1214+1429 | 12 14 40.269 | +14 29 00.10 | G230L | 10811 | 7359 |
| J1220-2113 | 12 20 21.940 | -21 13 15.58 | G230L | 4738 | 8225 |
| J1220+3343 | 12 20 33.871 | +33 43 12.53 | G230L | 2380 | 8569 |
| J1220-0040 | 12 20 37.031 | -00 40 33.92 | G230L | 5248 | 9382 |
| J1224+0037 | 12 24 14.293 | +00 37 07.90 | G230L | 2363 | 9382 |
| J1225-2938 | 12 25 01.359 | -29 38 19.86 | G230L | 5079 | 8225 |
| J1225+0035 | 12 25 56.613 | +00 35 34.01 | G230L | 5240 | 9382 |
| J1225-0052 | 12 25 58.444 | -00 52 27.05 | G230L | 5236 | 9382 |
| J1226-0006 | 12 26 08.060 | -00 06 03.10 | G230L | 8145 | 9382 |
| J1226-2630 | 12 26 40.100 | -26 30 01.14 | G230L | 4772 | 8225 |
| J1228+1018 | 12 28 36.910 | +10 18 42.16 | G230L | 2334 | 8569 |
| J1232+5252 | 12 32 39.291 | +52 52 50.98 | G140L | 600 | 9759 |
| J1235+4736 | 12 35 31.099 | +47 36 05.98 | G140L | 576 | 8582 |
| J1238+1750 | 12 38 20.200 | +17 50 38.90 | G230L | 7928 | 7359 |
| J1242+0012 | 12 42 02.659 | +00 12 28.50 | G230L | 7910 | 7359 |
| J1246-0730 | 12 46 04.241 | -07 30 46.74 | G230L | 4898 | 9076 |
| J1247+3126 | 12 47 14.359 | +31 26 41.90 | G140L | 4728 | 8287 |
| J1249-0559 | 12 49 13.839 | -05 59 19.26 | G140L | 2072 | 7295 |
| J1301+5902 | 13 01 12.938 | +59 02 06.75 | G140L | 120 | 7295 |
| J1304-0037 | 13 04 24.001 | -00 37 57.10 | G140L | 600 | 9067 |
| J1313-2716 | 13 13 47.322 | -27 16 49.09 | G230L | 2376 | 8569 |
| J1314-3105 | 13 14 56.829 | -31 05 55.10 | G140L | 2360 | 8287 |
| J1317+3531 | 13 17 43.198 | +35 31 32.00 | G140L | 576 | 8582 |
| J1321+1106 | 13 21 18.878 | +11 06 48.96 | G230L | 2304 | 8569 |
| J1322+4739 | 13 22 39.331 | +47 39 27.97 | G230L | 8375 | 8126 |
| J1322+4739 | 13 22 50.720 | +47 39 36.55 | G230L | 8327 | 8126 |
| J1323-0021 | 13 23 23.745 | -00 21 56.56 | G230L | 2375 | 9382 |
| J1330-2056 | 13 30 07.657 | -20 56 16.65 | G140L | 2394 | 9382 |
| J1333+2539 | 13 33 09.412 | +25 39 18.10 | G140L | 2342 | 8287 |
| J1341+0059 | 13 41 54.236 | +00 59 48.30 | G230L | 2359 | 9382 |
| J1342+6021 | 13 42 13.250 | +60 21 42.90 | G230L | 8564 | 7356 |
| J1342+6021 | 13 42 13.250 | +60 21 42.90 | G140L | 14778 | 7356 |
| J1342-0035 | 13 42 46.238 | -00 35 44.27 | G230L | 2355 | 9382 |
| J1345-0023 | 13 45 47.820 | -00 23 23.86 | G230L | 2350 | 9382 |
| J1348+2818 | 13 48 11.671 | +28 18 02.50 | G140L | 2342 | 8287 |
| J1352-2649 | 13 52 10.302 | -26 49 28.43 | G230L | 5079 | 8225 |
| J1358-2352 | 13 58 32.728 | -23 52 21.43 | G230L | 2198 | 8225 |
| J1402-2822 | 14 02 02.289 | -28 22 25.47 | G230L | 5071 | 8225 |
| J1404-0130 | 14 04 45.839 | -01 30 22.07 | G230L | 2304 | 8569 |
| J1419-0036 | 14 19 21.017 | -00 36 53.86 | G230L | 2375 | 9382 |
| J1420-0054 | 14 20 50.442 | -00 54 27.00 | G230L | 5236 | 9382 |
| J1423+3252 | 14 23 26.122 | +32 52 21.07 | G230L | 2376 | 8569 |
| J1426+0051 | 14 26 50.867 | +00 51 50.18 | G230L | 5240 | 9382 |
| J1431+3952 | 14 31 20.541 | +39 52 41.51 | G230L | 2292 | 9051 |
| J1431-0050 | 14 31 43.744 | -00 50 12.48 | G230L | 2375 | 9382 |
| J1433+3131 | 14 33 16.051 | +31 31 26.00 | G140L | 2364 | 8287 |
| J1436-0051 | 14 36 45.004 | -00 51 51.26 | G230L | 5248 | 9382 |
| J1436+4952 | 14 36 47.629 | +49 52 55.80 | G230L | 8375 | 7359 |
| J1438-0658 | 14 38 16.150 | -06 58 20.70 | G230L | 720 | 9507 |
| J1438+6211 | 14 38 44.780 | +62 11 54.39 | G230L | 4260 | 8569 |
| J1439+2954 | 14 39 12.261 | +29 54 49.00 | G140L | 2342 | 8287 |
| J1455-0045 | 14 55 08.163 | -00 45 08.39 | G230L | 2375 | 9382 |
| J1501+0019 | 15 01 23.452 | +00 19 39.04 | G230L | 2375 | 9382 |
| J1502-4154 | 15 02 55.210 | -41 54 29.81 | G230L | 5457 | 8244 |
| J1503+6105 | 15 03 08.851 | +61 05 51.69 | G140L | 600 | 9759 |
| J1503-4152 | 15 03 33.929 | -41 52 23.70 | G140L | 6000 | 8244 |
| J1503-4152 | 15 03 33.929 | -41 52 23.70 | G230L | 2457 | 8244 |
| J1504+0122 | 15 04 50.171 | +01 22 15.49 | G140L | 1320 | 9874 |
| J1505+0342 | 15 05 56.561 | +03 42 26.31 | G140L | 1320 | 9874 |
| J1508+6717 | 15 08 40.411 | +67 17 47.51 | G140L | 2448 | 7762 |
| J1510+0058 | 15 10 24.932 | +00 58 44.00 | G140L | 1320 | 9874 |
| J1516+1900 | 15 16 53.240 | +19 00 48.10 | G140L | 2857 | 9161 |
| J1516+1900 | 15 16 53.240 | +19 00 48.10 | G230L | 2311 | 9161 |
| J1521-0009 | 15 21 01.974 | -00 09 04.32 | G230L | 5236 | 9382 |

TABLE 1 — *Continued*

| Object | R.A. (J2000) | DEC. (J2000) | Grating | Exp. (s) | Id |
|------------|--------------|--------------|---------|----------|------|
| J1525+0026 | 15 25 10.598 | +00 26 32.75 | G230L | 2387 | 9382 |
| J1527+2452 | 15 27 01.761 | +24 52 49.62 | G230L | 2200 | 9051 |
| J1537+0021 | 15 37 13.740 | +00 21 15.48 | G230L | 5232 | 9382 |
| J1537+3358 | 15 37 31.022 | +33 58 37.95 | G230L | 2236 | 9051 |
| J1544+5912 | 15 44 20.101 | +59 12 26.00 | G140L | 2139 | 8485 |
| J1544+5912 | 15 44 20.101 | +59 12 26.00 | G230L | 600 | 8485 |
| J1554+0822 | 15 54 44.601 | +08 22 22.00 | G230L | 900 | 9507 |
| J1557-2029 | 15 57 21.200 | -20 29 13.24 | G230L | 2321 | 8569 |
| J1559-2442 | 15 59 41.418 | -24 42 39.00 | G230L | 5057 | 8569 |
| J1614+4859 | 16 14 26.810 | +48 59 58.71 | G140L | 600 | 9759 |
| J1614+4704 | 16 14 34.658 | +47 04 20.31 | G230L | 2369 | 9051 |
| J1619+3813 | 16 19 46.860 | +38 13 28.81 | G140L | 1320 | 9874 |
| J1631+4048 | 16 31 11.331 | +40 48 05.11 | G140L | 1543 | 9506 |
| J1631+1156 | 16 31 45.179 | +11 56 03.17 | G230L | 2304 | 8569 |
| J1636+7205 | 16 36 15.139 | +72 05 12.73 | G140L | 1543 | 9506 |
| J1637+2509 | 16 37 55.239 | +25 09 30.58 | G230L | 2200 | 9051 |
| J1649+3047 | 16 49 19.010 | +30 47 18.00 | G230L | 49158 | 8266 |
| J1649+3046 | 16 49 28.868 | +30 46 52.40 | G230L | 27540 | 8266 |
| J1701+6412 | 17 01 00.612 | +64 12 09.90 | G230L | 2166 | 9982 |
| J1701+6412 | 17 01 00.612 | +64 12 09.90 | G140L | 2245 | 9982 |
| J1702+6058 | 17 02 11.199 | +60 58 50.00 | G140L | 3500 | 8024 |
| J1702+6058 | 17 02 11.199 | +60 58 50.00 | G230L | 700 | 8024 |
| J1704+7057 | 17 04 26.104 | +70 57 34.93 | G230L | 2691 | 8569 |
| J1706+3615 | 17 06 34.109 | +36 15 08.40 | G230L | 2268 | 9051 |
| J1710+5923 | 17 10 14.517 | +59 23 26.48 | G230L | 600 | 9759 |
| J1711+6052 | 17 11 34.417 | +60 52 40.48 | G140L | 600 | 9759 |
| J1712+5559 | 17 12 44.092 | +55 59 50.57 | G230L | 4380 | 9382 |
| J1714+5757 | 17 14 13.411 | +57 57 11.15 | G230L | 4380 | 9382 |
| J1715+6453 | 17 15 30.498 | +64 53 19.25 | G140L | 600 | 9759 |
| J1715+4606 | 17 15 32.483 | +46 06 40.19 | G230L | 2337 | 9051 |
| J1715+5747 | 17 15 39.814 | +57 47 22.03 | G230L | 4380 | 9382 |
| J1716+5654 | 17 16 23.730 | +56 54 45.26 | G230L | 9840 | 9382 |
| J1717+5500 | 17 17 53.079 | +55 00 47.98 | G140L | 600 | 9067 |
| J1722+5442 | 17 22 37.031 | +54 42 04.18 | G230L | 4380 | 9382 |
| J1727+5302 | 17 27 38.943 | +53 02 29.40 | G230L | 4380 | 9382 |
| J1728-1415 | 17 28 19.797 | -14 15 56.15 | G140L | 1140 | 8264 |
| J1728-1415 | 17 28 19.797 | -14 15 56.15 | G230L | 781 | 8264 |
| J1729+7032 | 17 29 11.440 | +70 32 58.78 | G140L | 720 | 9506 |
| J1729+5758 | 17 29 58.799 | +57 58 38.32 | G230L | 4380 | 9382 |
| J1733+5533 | 17 33 23.064 | +55 33 00.26 | G230L | 4380 | 9382 |
| J1736+5938 | 17 36 44.253 | +59 38 39.74 | G230L | 4380 | 9382 |
| J1742+1827 | 17 42 06.958 | +18 27 21.15 | G140L | 8138 | 8684 |
| J1742+1827 | 17 42 06.958 | +18 27 21.15 | G230L | 5267 | 8684 |
| J1858+5645 | 18 58 26.917 | +56 45 56.17 | G230L | 4260 | 8569 |
| J1939+7007 | 19 39 29.407 | +70 07 49.47 | G140L | 1344 | 9506 |
| J1940-6907 | 19 40 25.569 | -69 07 56.01 | G140L | 49924 | 7272 |
| J1944+7705 | 19 44 54.902 | +77 05 52.00 | G140L | 576 | 8582 |
| J2006-0223 | 20 06 08.518 | -02 23 35.09 | G230L | 2304 | 8569 |
| J2051+1950 | 20 51 12.642 | +19 50 06.99 | G230L | 2332 | 8569 |
| J2114+0607 | 21 14 52.581 | +06 07 42.92 | G140L | 1100 | 9277 |
| J2114+0607 | 21 14 52.581 | +06 07 42.92 | G230L | 900 | 9277 |
| J2115-4323 | 21 15 06.877 | -43 23 11.10 | G230L | 5315 | 7359 |
| J2120-4426 | 21 20 11.609 | -44 26 52.90 | G230L | 8279 | 7359 |
| J2139-2454 | 21 39 13.271 | -24 54 14.89 | G230L | 5057 | 8225 |
| J2144-0754 | 21 44 32.717 | -07 54 42.85 | G230L | 2110 | 9051 |
| J2151+2130 | 21 51 45.828 | +21 30 13.50 | G230L | 2333 | 8569 |
| J2153-1514 | 21 53 19.138 | -15 14 12.11 | G140L | 503 | 9858 |
| J2154-4414 | 21 54 51.160 | -44 14 05.85 | G140L | 720 | 9506 |
| J2155-0922 | 21 55 01.531 | -09 22 24.40 | G230L | 1667 | 9181 |
| J2155-0922 | 21 55 01.531 | -09 22 24.40 | G140L | 2640 | 9181 |
| J2159-2417 | 21 59 24.961 | -24 17 52.10 | G230L | 4738 | 8225 |
| J2211-1705 | 22 11 15.417 | -17 05 25.84 | G230L | 7904 | 7359 |
| J2215-2944 | 22 15 16.040 | -29 44 23.61 | G230L | 2376 | 8569 |
| J2218-6150 | 22 18 51.042 | -61 50 42.80 | G140L | 2520 | 8287 |
| J2221-1857 | 22 21 39.492 | -18 57 07.20 | G140L | 2312 | 8287 |
| J2233-6033 | 22 33 37.668 | -60 33 28.95 | G230L | 22124 | 7633 |
| J2233-6033 | 22 33 37.668 | -60 33 28.95 | G140L | 18480 | 8076 |
| J2236+1343 | 22 36 07.690 | +13 43 55.40 | G230L | 900 | 9507 |
| J2252-5021 | 22 52 43.938 | -50 21 37.71 | G140L | 2530 | 8287 |
| J2253-3658 | 22 53 10.693 | -36 58 15.70 | G140L | 2392 | 8287 |
| J2255-5435 | 22 55 57.429 | -54 35 26.20 | G140L | 2530 | 8287 |
| J2258-2758 | 22 58 06.028 | -27 58 21.15 | G230L | 2223 | 8225 |
| J2304+0311 | 23 04 45.000 | +03 11 46.00 | G140L | 2200 | 7358 |
| J2316-2849 | 23 16 16.223 | -28 49 00.20 | G140L | 2342 | 8287 |
| J2316-3349 | 23 16 43.228 | -33 49 12.30 | G140L | 2364 | 8287 |
| J2328+0022 | 23 28 20.354 | +00 22 37.09 | G230L | 5260 | 9382 |
| J2330-5506 | 23 30 01.838 | -55 06 23.57 | G230L | 900 | 9507 |

TABLE 1 — *Continued*

| Object | R.A. (J2000) | DEC. (J2000) | Grating | Exp. (s) | Id |
|------------|--------------|--------------|---------|----------|------|
| J2331+0038 | 23 31 21.804 | +00 38 06.29 | G230L | 2379 | 9382 |
| J2334+0052 | 23 34 39.983 | +00 52 00.16 | G230L | 8157 | 9382 |
| J2339-0029 | 23 39 17.827 | -00 29 44.34 | G230L | 2347 | 9382 |
| J2346-0016 | 23 46 25.671 | -00 16 00.48 | G140L | 600 | 9067 |
| J2350-4326 | 23 50 34.241 | -43 26 00.00 | G140L | 2120 | 8875 |
| J2350-4326 | 23 50 34.241 | -43 26 00.00 | G230L | 1280 | 8875 |
| J2351-1427 | 23 51 29.839 | -14 27 56.80 | G140L | 2318 | 8287 |
| J2352-0028 | 23 52 53.511 | -00 28 51.31 | G230L | 2375 | 9382 |
| J2353-0028 | 23 53 21.614 | -00 28 41.66 | G230L | 2379 | 9382 |
| J2358-5440 | 23 58 33.442 | -54 40 42.21 | G140L | 2530 | 8287 |

TABLE 2
OBSERVATIONS FROM FOS ARCHIVE (G160L)

| Object | R.A. (J2000) | DEC. (J2000) | Exp. (s) | Id |
|------------|--------------|--------------|----------|------|
| preCOSTAR | | | | |
| J0017+8135 | 00 17 08.563 | +81 35 08.91 | 600 | 1027 |
| J0017+8135 | 00 17 08.563 | +81 35 08.91 | 25 | 1027 |
| J0017+8135 | 00 17 08.563 | +81 35 08.91 | 25 | 1027 |
| J0027+2241 | 00 27 15.400 | +22 41 58.50 | 1331 | 2424 |
| J0047+0319 | 00 47 05.900 | +03 19 54.90 | 530 | 2424 |
| J0057-2643 | 00 57 58.012 | -26 43 14.14 | 1200 | 3199 |
| J0117-0841 | 01 17 23.338 | -08 41 32.38 | 1127 | 3268 |
| J0117-0841 | 01 17 23.338 | -08 41 32.38 | 1143 | 4856 |
| J0117-0841 | 01 17 23.338 | -08 41 32.38 | 1143 | 4856 |
| J0117-0841 | 01 17 23.338 | -08 41 32.38 | 1143 | 4856 |
| J0117-0841 | 01 17 23.338 | -08 41 32.38 | 1143 | 4856 |
| J0117-0841 | 01 17 23.338 | -08 41 32.38 | 345 | 4856 |
| J0120+2133 | 01 20 17.250 | +21 33 46.30 | 420 | 4396 |
| J0145-0120 | 01 45 51.189 | -01 20 30.73 | 50 | 1027 |
| J0145-0120 | 01 45 51.189 | -01 20 30.73 | 1200 | 1027 |
| J0145-0120 | 01 45 51.189 | -01 20 30.73 | 50 | 1027 |
| J0148+3854 | 01 48 24.400 | +38 54 04.00 | 420 | 4396 |
| J0152-2001 | 01 52 27.291 | -20 01 07.29 | 2000 | 3051 |
| J0152-2001 | 01 52 27.291 | -20 01 07.29 | 100 | 3051 |
| J0152-2001 | 01 52 27.291 | -20 01 07.29 | 2000 | 3051 |
| J0152-2001 | 01 52 27.291 | -20 01 07.29 | 2000 | 3051 |
| J0152-2001 | 01 52 27.291 | -20 01 07.29 | 2000 | 3051 |
| J0156+0445 | 01 56 36.001 | +04 45 28.47 | 1200 | 3199 |
| J0235-0402 | 02 35 07.260 | -04 02 05.80 | 1803 | 4799 |
| J0256-0126 | 02 56 16.520 | -01 26 37.40 | 360 | 4396 |
| J0336-3607 | 03 36 09.280 | -36 07 33.30 | 420 | 4396 |
| J0351-1429 | 03 51 28.600 | -14 29 09.10 | 530 | 2424 |
| J0357-4812 | 03 57 21.900 | -48 12 15.00 | 420 | 4396 |
| J0448-2044 | 04 48 58.810 | -20 44 45.70 | 480 | 4396 |
| J0449-3911 | 04 49 42.299 | -39 11 09.00 | 420 | 4396 |
| J0745+3142 | 07 45 41.700 | +31 42 55.70 | 563 | 3791 |
| J0813+4813 | 08 13 36.059 | +48 13 02.49 | 2172 | 3939 |
| J0813+4813 | 08 13 36.059 | +48 13 02.49 | 2172 | 3939 |
| J0813+4813 | 08 13 36.059 | +48 13 02.49 | 1200 | 1193 |
| J0813+4813 | 08 13 36.059 | +48 13 02.49 | 2173 | 3939 |
| J0813+4813 | 08 13 36.059 | +48 13 02.49 | 2172 | 3939 |
| J0813+4813 | 08 13 36.061 | +48 13 02.69 | 1620 | 5351 |
| J0813+4813 | 08 13 36.061 | +48 13 02.69 | 1580 | 5351 |
| J0837+4450 | 08 37 52.745 | +44 50 25.96 | 1400 | 3545 |
| J0837+4450 | 08 37 52.745 | +44 50 25.96 | 1400 | 3545 |
| J0837+4450 | 08 37 52.745 | +44 50 25.96 | 1400 | 3545 |
| J0837+4450 | 08 37 52.745 | +44 50 25.96 | 1400 | 3545 |
| J0837+4450 | 08 37 52.745 | +44 50 25.96 | 1400 | 3545 |
| J0853+4349 | 08 53 34.200 | +43 49 01.00 | 530 | 2424 |
| J0859+4637 | 08 59 24.320 | +46 37 17.39 | 480 | 4952 |
| J0919+5106 | 09 19 57.700 | +51 06 10.01 | 563 | 2424 |
| J0949+2955 | 09 49 41.107 | +29 55 19.12 | 100 | 3200 |
| J0949+2955 | 09 49 41.107 | +29 55 19.12 | 1768 | 3200 |
| J1003+6813 | 10 03 06.801 | +68 13 17.50 | 563 | 3791 |
| J1010+4132 | 10 10 27.499 | +41 32 39.10 | 563 | 3791 |
| J1011+1304 | 10 11 10.800 | +13 04 12.00 | 420 | 4952 |
| J1024+1912 | 10 24 44.901 | +19 12 19.60 | 1464 | 2424 |
| J1041+0610 | 10 41 17.201 | +06 10 16.60 | 1331 | 2424 |
| J1042+1203 | 10 42 44.601 | +12 03 31.30 | 1545 | 2424 |
| J1058+1951 | 10 58 17.900 | +19 51 51.00 | 1061 | 2424 |
| J1107+1628 | 11 07 15.000 | +16 28 02.40 | 563 | 3791 |
| J1125+5910 | 11 25 53.851 | +59 10 21.19 | 360 | 4952 |
| J1126+3918 | 11 26 27.990 | +39 18 44.79 | 360 | 4952 |
| J1133+1052 | 11 33 30.300 | +10 52 23.00 | 563 | 2424 |
| J1139-1350 | 11 39 10.701 | -13 50 43.10 | 530 | 2424 |
| J1139+6547 | 11 39 57.100 | +65 47 49.41 | 530 | 2424 |
| J1208+4540 | 12 08 58.000 | +45 40 36.00 | 530 | 2424 |
| J1218+1105 | 12 18 26.100 | +11 05 05.30 | 1677 | 2424 |
| J1232-0224 | 12 32 00.000 | -02 24 05.34 | 1000 | 1193 |
| J1232-0224 | 12 32 00.088 | -02 24 07.57 | 2029 | 3939 |
| J1232-0224 | 12 32 00.088 | -02 24 07.57 | 2029 | 3939 |
| J1247+3209 | 12 47 20.801 | +32 09 00.99 | 1331 | 2424 |
| J1249-0559 | 12 49 13.843 | -05 59 19.34 | 901 | 4081 |
| J1254+1141 | 12 54 38.199 | +11 41 06.10 | 853 | 2424 |
| J1256+0427 | 12 56 59.901 | +04 27 34.10 | 853 | 3791 |
| J1308+3005 | 13 08 29.689 | +30 05 39.00 | 480 | 4952 |
| J1319+5148 | 13 19 46.230 | +51 48 06.09 | 480 | 4953 |
| J1319+2728 | 13 19 56.301 | +27 28 08.40 | 798 | 2424 |
| J1321+2847 | 13 21 14.736 | +28 47 48.68 | 1000 | 1144 |
| J1323+2910 | 13 23 20.581 | +29 10 06.90 | 480 | 4953 |

TABLE 2 — *Continued*

| Object | R.A. (J2000) | DEC. (J2000) | Exp. (s) | Id |
|------------|--------------|--------------|----------|------|
| J1331+3030 | 13 31 08.295 | +30 30 32.86 | 900 | 1193 |
| J1334+5501 | 13 34 11.660 | +55 01 25.50 | 480 | 4953 |
| J1336+1725 | 13 36 02.000 | +17 25 13.00 | 530 | 2424 |
| J1336-0048 | 13 36 47.131 | -00 48 57.74 | 1127 | 3268 |
| J1341+4123 | 13 41 00.798 | +41 23 14.10 | 798 | 2424 |
| J1343+2844 | 13 43 00.201 | +28 44 08.00 | 1061 | 2424 |
| J1349+5341 | 13 49 34.698 | +53 41 17.40 | 1539 | 2424 |
| J1351-0007 | 13 51 50.420 | -00 07 39.70 | 480 | 4953 |
| J1354+0052 | 13 54 58.700 | +00 52 10.00 | 530 | 2424 |
| J1357+1919 | 13 57 04.501 | +19 19 06.60 | 530 | 2424 |
| J1407+2827 | 14 07 00.399 | +28 27 14.63 | 1530 | 6799 |
| J1409+2618 | 14 09 23.877 | +26 18 21.21 | 676 | 2424 |
| J1418+1703 | 14 18 03.699 | +17 03 24.90 | 1519 | 2424 |
| J1427-1203 | 14 27 38.101 | -12 03 49.90 | 563 | 2424 |
| J1437-0147 | 14 37 48.259 | -01 47 11.30 | 1450 | 6103 |
| J1437-0147 | 14 37 48.259 | -01 47 11.30 | 1510 | 6103 |
| J1437-0147 | 14 37 48.270 | -01 47 11.40 | 360 | 4953 |
| J1445+0958 | 14 45 16.469 | +09 58 36.12 | 1200 | 1027 |
| J1445+0958 | 14 45 16.469 | +09 58 36.12 | 50 | 1027 |
| J1445+0958 | 14 45 16.469 | +09 58 36.12 | 50 | 1027 |
| J1524+0958 | 15 24 24.529 | +09 58 29.46 | 1878 | 3200 |
| J1524+0958 | 15 24 24.529 | +09 58 29.46 | 1878 | 3200 |
| J1524+0958 | 15 24 24.529 | +09 58 29.46 | 100 | 3200 |
| J1524+0958 | 15 24 24.529 | +09 58 29.46 | 1878 | 3200 |
| J1539+4735 | 15 39 34.794 | +47 35 31.62 | 563 | 3791 |
| J1620+1736 | 16 20 21.801 | +17 36 24.00 | 563 | 2424 |
| J1630+3758 | 16 30 13.586 | +37 58 21.04 | 1000 | 1144 |
| J1630+3756 | 16 30 20.815 | +37 56 55.53 | 1000 | 1144 |
| J1658+0515 | 16 58 33.501 | +05 15 16.50 | 1061 | 2424 |
| J1902+3159 | 19 02 56.082 | +31 59 41.65 | 1460 | 6577 |
| J2246-1206 | 22 46 18.201 | -12 06 51.20 | 563 | 3791 |
| J2253+1608 | 22 53 57.803 | +16 08 53.40 | 530 | 2424 |
| J2303-6807 | 23 03 43.499 | -68 07 37.11 | 563 | 2424 |
| J2342-0322 | 23 42 56.602 | -03 22 26.50 | 563 | 4000 |
| J2342-0322 | 23 42 56.602 | -03 22 26.50 | 563 | 4000 |
| J2342-0322 | 23 42 56.602 | -03 22 26.50 | 516 | 4000 |
| J2346+0930 | 23 46 36.899 | +09 30 46.00 | 563 | 3791 |
| J2355-3357 | 23 55 25.598 | -33 57 55.80 | 563 | 2424 |
| COSTAR | | | | |
| J0102-2719 | 01 02 17.008 | -27 19 50.06 | 1080 | 5455 |
| J0102-2719 | 01 02 17.008 | -27 19 50.06 | 300 | 5455 |
| J0111+1753 | 01 11 49.793 | +17 53 50.73 | 1350 | 5095 |
| J0111+1753 | 01 11 49.793 | +17 53 50.73 | 1350 | 5095 |
| J0144+3411 | 01 44 11.780 | +34 11 56.23 | 1580 | 6577 |
| J0209-3939 | 02 09 28.570 | -39 39 40.00 | 2220 | 6093 |
| J0209-3939 | 02 09 28.570 | -39 39 40.00 | 2500 | 6093 |
| J0228-1011 | 02 28 39.150 | -10 11 10.30 | 1360 | 5455 |
| J0231+1322 | 02 31 45.910 | +13 22 54.47 | 1400 | 6577 |
| J0251+4315 | 02 51 34.590 | +43 15 15.70 | 1660 | 6577 |
| J0310-1909 | 03 10 28.079 | -19 09 43.82 | 1270 | 5097 |
| J0347+0105 | 03 47 40.200 | +01 05 14.25 | 1490 | 6799 |
| J0347+0105 | 03 47 40.200 | +01 05 14.25 | 2430 | 6799 |
| J0357-4812 | 03 57 21.870 | -48 12 15.30 | 2570 | 6103 |
| J0357-4812 | 03 57 21.870 | -48 12 15.30 | 1650 | 6103 |
| J0357-4812 | 03 57 21.870 | -48 12 15.30 | 1220 | 6103 |
| J0741+3111 | 07 41 10.681 | +31 11 59.75 | 1520 | 6577 |
| J0813+4813 | 08 13 36.061 | +48 13 02.69 | 1620 | 5351 |
| J0813+4813 | 08 13 36.061 | +48 13 02.69 | 1580 | 5351 |
| J0830+2410 | 08 30 52.101 | +24 10 59.45 | 1560 | 6577 |
| J0845+3420 | 08 45 38.661 | +34 20 43.30 | 1680 | 6091 |
| J0845+1328 | 08 45 47.271 | +13 28 58.41 | 1540 | 6577 |
| J0906+1722 | 09 06 38.214 | +17 22 23.16 | 450 | 5455 |
| J0906+1722 | 09 06 38.214 | +17 22 23.16 | 870 | 5455 |
| J0935+4953 | 09 35 53.009 | +49 53 13.79 | 1440 | 6314 |
| J0935+4953 | 09 35 53.130 | +49 53 13.60 | 1200 | 5455 |
| J0954+1743 | 09 54 56.851 | +17 43 31.09 | 1430 | 6577 |
| J1001+5553 | 10 01 20.739 | +55 53 55.10 | 240 | 5683 |
| J1001+5553 | 10 01 20.889 | +55 53 49.20 | 240 | 5683 |
| J1001+5454 | 10 01 29.722 | +54 54 38.13 | 1670 | 6577 |
| J1038-2752 | 10 38 08.434 | -27 52 37.99 | 1510 | 6577 |
| J1052+6125 | 10 52 32.849 | +61 25 20.56 | 1660 | 6577 |
| J1130-1449 | 11 30 07.020 | -14 49 27.60 | 1450 | 6577 |
| J1150-0023 | 11 50 43.861 | -00 23 55.10 | 1260 | 5095 |
| J1150-0023 | 11 50 43.861 | -00 23 55.10 | 1040 | 5095 |
| J1151+3825 | 11 51 29.290 | +38 25 53.04 | 1520 | 6577 |

TABLE 2 — *Continued*

| Object | R.A. (J2000) | DEC. (J2000) | Exp. (s) | Id |
|------------|--------------|--------------|----------|------|
| J1211+1030 | 12 11 40.620 | +10 30 02.50 | 1940 | 5351 |
| J1211+1030 | 12 11 40.620 | +10 30 02.50 | 1260 | 5351 |
| J1256+5652 | 12 56 14.216 | +56 52 25.08 | 770 | 6799 |
| J1311-0552 | 13 11 36.486 | -05 52 38.95 | 450 | 5455 |
| J1311-0552 | 13 11 36.486 | -05 52 38.95 | 930 | 5455 |
| J1407+2827 | 14 07 00.399 | +28 27 14.63 | 1530 | 6799 |
| J1415+1129 | 14 15 46.300 | +11 29 44.10 | 960 | 5455 |
| J1437-0147 | 14 37 48.259 | -01 47 11.30 | 1450 | 6103 |
| J1437-0147 | 14 37 48.259 | -01 47 11.30 | 1510 | 6103 |
| J1513+1011 | 15 13 29.330 | +10 11 05.87 | 1550 | 6577 |
| J1601+1714 | 16 01 20.350 | +17 14 15.75 | 2340 | 5095 |
| J1601+1714 | 16 01 20.350 | +17 14 15.75 | 1280 | 5095 |
| J1625+2646 | 16 25 48.907 | +26 46 58.76 | 1920 | 6577 |
| J1716+5328 | 17 16 35.310 | +53 28 15.27 | 1660 | 6577 |
| J1902+3159 | 19 02 56.082 | +31 59 41.65 | 1460 | 6577 |
| J2124-1744 | 21 24 41.660 | -17 44 45.90 | 1470 | 6799 |
| J2124-1744 | 21 24 41.660 | -17 44 45.90 | 2420 | 6799 |

TABLE 3
LIST OF OBJECTS USED IN SAMPLE R1/R2.

| Object ^a | z_{em} | R1 ^b | | R2 ^c | |
|---------------------|----------|-----------------|-----------|-----------------|-----------|
| | | z_{min} | z_{max} | z_{min} | z_{max} |
| J0001+0709 | 3.234 | 2.226 | 2.481 | 2.214 | 2.481 |
| B0002+0507 | 1.900 | 1.470 | 1.871 | 1.470 | 1.871 |
| B0002-4214 | 2.760 | 2.301 | 2.594 | 2.301 | 2.594 |
| B0003+1553 | 0.450 | 0.330 | 0.435 | 0.289 | 0.435 |
| J0012-0122 | 1.998 | 1.387 | 1.968 | 1.387 | 1.968 |
| J0021+0043 | 1.243 | 0.943 | 1.221 | 0.943 | 1.221 |
| J0021+0104 | 1.829 | 1.575 | 1.801 | 1.575 | 1.801 |
| J0021-0128A | 1.588 | 1.403 | 1.562 | 1.243 | 1.562 |
| J0022-0128B | 1.040 | 0.830 | 1.020 | 0.830 | 1.020 |
| J0027+2241 | 1.108 | 0.542 | 1.087 | 0.497 | 1.087 |
| J0038-3501 | 1.199 | 0.852 | 1.177 | 0.813 | 1.177 |
| J0038-3504 | 1.519 | 0.964 | 1.494 | 0.759 | 1.494 |
| J0039-3529 | 1.095 | 0.813 | 1.074 | 0.797 | 1.074 |
| J0043-2622 | 3.053 | 1.880 | 2.478 | 1.880 | 2.478 |
| J0047+0319 | 0.624 | ... | ... | 0.495 | 0.608 |
| J0051+0041 | 1.188 | 0.995 | 1.166 | 0.870 | 1.166 |
| B0058+0155 | 1.954 | 1.035 | 1.535 | 0.824 | 1.535 |
| J0102-0853 | 1.682 | 1.178 | 1.655 | 1.178 | 1.655 |
| J0106+0105 | 1.611 | 1.293 | 1.585 | 1.293 | 1.585 |
| B0107-0235 | 0.948 | 0.793 | 0.929 | 0.780 | 0.929 |
| J0116-0043 | 1.263 | 0.915 | 1.240 | 0.915 | 1.240 |
| B0119-0437 | 1.925 | 1.470 | 1.896 | 1.470 | 1.896 |
| J0120+2133 | 1.500 | 1.318 | 1.475 | 1.050 | 1.475 |
| B0122-0021 | 1.070 | 0.820 | 1.049 | 0.791 | 1.049 |
| J0123-0058 | 1.550 | 1.397 | 1.524 | 1.397 | 1.524 |
| J0126-0105 | 1.609 | 1.193 | 1.583 | 1.193 | 1.583 |
| J0128-3029 | 0.475 | 0.255 | 0.460 | 0.255 | 0.460 |
| J0134+0051 | 1.522 | 1.348 | 1.497 | 1.268 | 1.497 |
| J0137-2430 | 0.831 | 0.790 | 0.813 | 0.738 | 0.813 |
| J0138-0005 | 1.340 | 1.219 | 1.317 | 1.112 | 1.317 |
| J0139-0023 | 1.384 | 1.082 | 1.360 | 1.082 | 1.360 |
| J0141-0024 | 2.611 | 2.215 | 2.464 | 2.215 | 2.464 |
| B0143-0135 | 3.124 | 1.612 | 2.593 | 1.612 | 2.593 |
| J0144+3411 | 1.450 | 0.765 | 1.385 | 0.765 | 1.390 |
| J0148+3854 | 1.442 | ... | ... | 1.215 | 1.418 |
| B0150-2015 | 2.139 | 1.474 | 2.108 | 1.474 | 2.108 |
| J0152-2001 | 2.147 | 1.447 | 1.658 | 1.447 | 1.658 |
| J0153+0009 | 0.837 | 0.793 | 0.819 | 0.793 | 0.819 |
| J0153+0052 | 1.163 | 1.053 | 1.141 | 1.053 | 1.141 |
| J0157-0048 | 1.545 | 1.411 | 1.520 | 1.411 | 1.520 |
| B0207-3953 | 2.813 | 2.480 | 2.593 | 2.480 | 2.593 |
| J0208-0503 | 1.850 | 1.072 | 1.822 | 1.072 | 1.822 |
| B0219+4248 | 0.444 | ... | ... | 0.331 | 0.430 |
| J0235-0402 | 1.438 | 0.497 | 1.414 | 0.497 | 1.414 |
| J0240-1851 | 0.631 | 0.257 | 0.615 | 0.242 | 0.615 |
| J0241-1514 | 2.786 | ... | ... | 2.198 | 2.474 |
| J0251+4315 | 1.310 | 0.871 | 1.287 | 0.771 | 1.287 |
| B0254-3327b | 1.915 | 1.583 | 1.886 | 1.474 | 1.886 |
| J0256-0126 | 0.879 | 0.814 | 0.860 | 0.814 | 0.860 |
| J0304-0008 | 3.290 | 2.112 | 2.476 | 0.919 | 2.476 |
| J0318-2012 | 2.869 | ... | ... | 2.084 | 2.473 |
| J0336-3607 | 1.093 | ... | ... | 0.871 | 1.072 |
| J0351-1429 | 0.614 | 0.487 | 0.598 | 0.487 | 0.598 |
| J0354-2724 | 2.823 | ... | ... | 1.858 | 2.474 |
| J0357-4812 | 1.016 | 0.511 | 0.996 | 0.504 | 0.996 |
| J0411-4956 | 0.817 | 0.785 | 0.799 | 0.785 | 0.799 |
| B0421+0157 | 2.044 | 1.473 | 2.014 | 1.473 | 2.014 |
| J0423-0120 | 0.915 | 0.839 | 0.896 | 0.805 | 0.896 |
| B0424-1309 | 2.159 | 2.036 | 2.127 | 2.036 | 2.127 |
| J0436-5258 | 1.231 | 0.263 | 0.881 | 0.259 | 0.881 |
| J0439-2422 | 0.840 | 0.819 | 0.822 | 0.754 | 0.822 |
| J0440-5248 | 1.053 | 0.264 | 0.881 | 0.261 | 0.881 |
| J0441-4313 | 0.593 | 0.262 | 0.577 | 0.259 | 0.577 |
| J0448-2044 | 1.896 | 1.457 | 1.740 | 0.580 | 1.746 |
| J0452-1640 | 2.600 | 1.008 | 2.474 | 1.008 | 2.474 |
| J0453-1305 | 2.300 | 2.068 | 2.267 | 2.068 | 2.267 |
| B0453-4220 | 2.660 | 2.303 | 2.593 | 2.303 | 2.593 |
| B0454+0356 | 1.345 | 0.858 | 1.322 | 0.858 | 1.322 |
| B0454-2203 | 0.534 | 0.473 | 0.519 | 0.473 | 0.519 |
| J0504-2944 | 0.552 | 0.256 | 0.536 | 0.255 | 0.536 |
| J0514-3326 | 1.569 | 1.131 | 1.543 | 1.131 | 1.543 |
| B0624+6907 | 0.374 | 0.329 | 0.360 | 0.311 | 0.360 |
| J0741+3111 | 0.630 | 0.482 | 0.614 | 0.482 | 0.614 |
| J0806+5041 | 2.432 | 1.101 | 2.398 | 1.079 | 2.398 |

TABLE 3 — *Continued*

| Object ^a | z_{em} | R1 ^b | | R2 ^c | |
|---------------------|----------|-----------------|-----------|-----------------|-----------|
| | | z_{min} | z_{max} | z_{min} | z_{max} |
| J0830+2410 | 0.939 | 0.772 | 0.920 | 0.772 | 0.920 |
| J0839+5256 | 1.545 | 0.328 | 0.882 | 0.328 | 0.882 |
| J0845+1328 | 1.877 | 0.768 | 1.254 | 0.768 | 1.357 |
| J0853+4349 | 0.513 | ... | ... | 0.495 | 0.498 |
| J0859+4637 | 0.923 | 0.615 | 0.904 | 0.499 | 0.904 |
| J0912+2450 | 0.654 | 0.262 | 0.637 | 0.259 | 0.637 |
| J0919+5106 | 0.553 | 0.512 | 0.537 | 0.495 | 0.537 |
| B0933+7315 | 2.528 | 2.332 | 2.493 | 2.332 | 2.493 |
| B0935+4141 | 1.937 | 1.465 | 1.908 | 1.465 | 1.908 |
| J0944+2554 | 2.910 | 2.235 | 2.456 | 2.235 | 2.456 |
| J0948+4323 | 1.892 | 1.227 | 1.863 | 1.227 | 1.863 |
| B0953+5454 | 2.584 | 2.510 | 2.548 | 2.510 | 2.548 |
| J0953-0038 | 1.382 | 1.016 | 1.358 | 1.016 | 1.358 |
| J0954+1743 | 1.478 | 0.502 | 1.453 | 0.502 | 1.453 |
| B0954+5537 | 0.909 | 0.844 | 0.890 | 0.803 | 0.890 |
| B0955+3238 | 0.533 | ... | ... | 0.331 | 0.518 |
| J0958+3224 | 0.530 | 0.258 | 0.515 | 0.256 | 0.515 |
| B1001+2910 | 0.329 | 0.286 | 0.316 | 0.286 | 0.316 |
| J1003+6813 | 0.773 | 0.705 | 0.755 | 0.505 | 0.755 |
| J1008-0018 | 1.350 | 0.931 | 1.327 | 0.876 | 1.327 |
| J1009+0036 | 1.702 | 1.031 | 1.675 | 0.959 | 1.675 |
| J1009-0026 | 1.244 | 0.889 | 1.222 | 0.889 | 1.222 |
| J1010+0003 | 1.399 | 1.266 | 1.375 | 1.266 | 1.375 |
| J1010+4132 | 0.613 | 0.495 | 0.597 | 0.495 | 0.597 |
| J1010-0047 | 1.671 | 1.328 | 1.644 | 1.328 | 1.644 |
| J1011+1304 | 1.287 | 0.879 | 1.264 | 0.497 | 1.264 |
| B1017+2759 | 1.928 | 1.502 | 1.899 | 1.473 | 1.899 |
| J1017+5356 | 1.400 | 1.296 | 1.376 | 1.296 | 1.376 |
| J1022+0101 | 1.563 | ... | ... | 1.416 | 1.537 |
| J1022+3041 | 1.318 | 0.345 | 0.882 | 0.310 | 0.882 |
| J1024+1912 | 0.828 | 0.745 | 0.810 | 0.530 | 0.810 |
| J1028-0100 | 1.530 | 0.843 | 1.505 | 0.801 | 1.505 |
| J1032+0003 | 1.190 | 1.106 | 1.168 | 1.106 | 1.168 |
| J1037+0028 | 1.733 | 1.425 | 1.706 | 1.425 | 1.706 |
| J1038-2752 | 2.168 | 0.833 | 1.028 | 0.825 | 1.259 |
| J1041+0610 | 1.265 | 0.514 | 1.242 | 0.502 | 1.242 |
| J1042+1203 | 1.028 | 0.714 | 1.008 | 0.619 | 1.008 |
| B1047+5503 | 2.165 | 1.637 | 2.133 | 1.464 | 2.133 |
| J1048+0032 | 1.649 | 1.194 | 1.623 | 1.194 | 1.623 |
| J1054-0020 | 1.021 | ... | ... | 0.952 | 1.001 |
| J1058+1951 | 1.110 | 1.037 | 1.089 | 1.037 | 1.089 |
| B1100+7715 | 0.311 | ... | ... | 0.283 | 0.298 |
| B1100-2629 | 2.145 | 1.838 | 2.114 | 1.838 | 2.114 |
| J1103+3715 | 1.295 | 1.239 | 1.272 | 1.239 | 1.272 |
| B1104-1805a | 2.303 | 1.662 | 2.270 | 1.662 | 2.270 |
| J1107+0048 | 1.391 | 0.919 | 1.367 | 0.831 | 1.367 |
| J1107+1628 | 0.632 | 0.483 | 0.616 | 0.483 | 0.616 |
| J1108+3133 | 2.244 | 1.194 | 2.212 | 1.194 | 2.212 |
| J1109+0051 | 0.957 | 0.834 | 0.937 | 0.803 | 0.937 |
| J1110+3019 | 1.521 | 1.245 | 1.496 | 1.085 | 1.496 |
| B1115+0802a2 | 1.722 | 1.471 | 1.695 | 1.471 | 1.695 |
| J1125+5910 | 0.852 | 0.259 | 0.833 | 0.259 | 0.833 |
| J1130-1449 | 1.187 | 0.502 | 1.165 | 0.502 | 1.165 |
| J1139-1350 | 0.554 | ... | ... | 0.497 | 0.538 |
| J1143+3452 | 3.130 | 0.556 | 0.880 | 0.556 | 0.880 |
| B1146+1103e | 1.100 | 0.813 | 1.079 | 0.795 | 1.079 |
| B1146+1104b | 1.010 | 0.852 | 0.990 | 0.820 | 0.990 |
| B1148+5454 | 0.978 | 0.360 | 0.958 | 0.330 | 0.958 |
| J1150-0023 | 1.980 | 0.502 | 1.751 | 0.502 | 1.751 |
| J1151+3825 | 1.304 | 0.544 | 1.281 | 0.489 | 1.281 |
| J1208+4540 | 1.155 | 0.767 | 1.133 | 0.502 | 1.133 |
| J1211+1030 | 2.193 | 0.698 | 1.751 | 0.636 | 1.751 |
| B1216+0655 | 0.334 | 0.309 | 0.321 | 0.284 | 0.321 |
| J1218+1105 | 1.403 | 1.080 | 1.379 | 0.572 | 1.379 |
| J1220+3343 | 1.532 | 1.502 | 1.507 | 1.415 | 1.507 |
| J1220-0040 | 1.411 | 0.963 | 1.387 | 0.963 | 1.387 |
| B1222+2251 | 2.046 | 1.174 | 1.535 | 1.174 | 1.535 |
| J1224+0037 | 1.482 | 1.268 | 1.457 | 1.268 | 1.457 |
| J1225+0035 | 1.226 | 1.099 | 1.204 | 1.038 | 1.204 |
| B1225+3145 | 2.219 | 1.796 | 2.187 | 1.796 | 2.187 |
| J1225-0052 | 0.964 | 0.910 | 0.944 | 0.844 | 0.944 |
| J1226-0006 | 1.118 | ... | ... | 1.077 | 1.097 |
| J1228+1018 | 2.305 | 1.392 | 2.272 | 1.126 | 2.272 |
| J1232-0224 | 1.038 | 0.761 | 1.018 | 0.485 | 1.018 |
| B1247+2647 | 2.043 | 1.470 | 2.013 | 1.470 | 2.013 |

TABLE 3 — *Continued*

| Object ^a | z_{em} | R1 ^b | | R2 ^c | |
|---------------------|----------|-----------------|-----------|-----------------|-----------|
| | | z_{min} | z_{max} | z_{min} | z_{max} |
| J1247+3209 | 0.949 | 0.756 | 0.930 | 0.500 | 0.930 |
| B1248+3142 | 1.020 | 0.782 | 1.000 | 0.771 | 1.000 |
| B1248+4007 | 1.030 | 0.773 | 1.010 | 0.773 | 1.010 |
| B1249+2929 | 0.820 | 0.775 | 0.802 | 0.775 | 0.802 |
| J1254+1141 | 0.870 | 0.570 | 0.851 | 0.500 | 0.851 |
| B1259+5918 | 0.472 | 0.297 | 0.457 | 0.280 | 0.457 |
| J1313-2716 | 2.186 | 1.684 | 2.154 | 1.684 | 2.154 |
| J1319+2728 | 1.014 | 0.661 | 0.994 | 0.661 | 0.994 |
| J1319+5148 | 1.055 | 0.687 | 1.034 | 0.500 | 1.034 |
| B1320+2925 | 0.960 | 0.841 | 0.940 | 0.794 | 0.940 |
| J1321+1106 | 2.181 | 1.971 | 2.149 | 1.849 | 2.149 |
| J1321+2847 | 1.703 | 1.135 | 1.676 | 1.135 | 1.676 |
| J1322+4739 | 1.554 | 1.072 | 1.528 | 1.072 | 1.528 |
| J1322+4739 | 1.101 | 0.921 | 1.080 | 0.753 | 1.080 |
| J1323-0021 | 1.388 | 1.331 | 1.364 | 1.085 | 1.364 |
| B1328+3045 | 0.849 | 0.790 | 0.831 | 0.780 | 0.831 |
| B1329+4117 | 1.930 | 1.283 | 1.901 | 1.283 | 1.901 |
| J1331+3030 | 0.846 | 0.701 | 0.828 | 0.701 | 0.828 |
| B1334-0033 | 2.783 | 0.803 | 2.594 | 0.552 | 2.594 |
| J1336+1725 | 0.554 | 0.502 | 0.538 | 0.502 | 0.538 |
| J1341+0059 | 1.714 | 1.597 | 1.687 | 1.597 | 1.687 |
| J1341+4123 | 1.204 | 0.683 | 1.182 | 0.502 | 1.182 |
| J1342+6021 | 0.961 | 0.258 | 0.941 | 0.258 | 0.941 |
| J1343+2844 | 0.905 | 0.704 | 0.886 | 0.499 | 0.886 |
| J1345-0023 | 1.095 | 0.811 | 1.074 | 0.784 | 1.074 |
| J1351-0007 | 1.444 | 1.159 | 1.420 | 1.159 | 1.420 |
| J1354+0052 | 1.121 | 0.667 | 1.100 | 0.667 | 1.100 |
| J1357+1919 | 0.719 | 0.608 | 0.702 | 0.497 | 0.702 |
| J1404-0130 | 2.522 | 1.719 | 2.482 | 1.719 | 2.482 |
| J1409+2618 | 0.945 | 0.502 | 0.926 | 0.502 | 0.926 |
| J1418+1703 | 0.821 | 0.725 | 0.803 | 0.495 | 0.803 |
| J1419-0036 | 0.969 | 0.822 | 0.949 | 0.822 | 0.949 |
| J1420-0054 | 1.458 | 1.332 | 1.433 | 1.332 | 1.433 |
| J1423+3252 | 1.905 | 1.490 | 1.876 | 1.176 | 1.876 |
| J1426+0051 | 1.333 | 0.940 | 1.310 | 0.838 | 1.310 |
| J1427-1203 | 0.805 | ... | ... | 0.652 | 0.787 |
| J1431+3952 | 1.215 | 0.823 | 1.193 | 0.803 | 1.193 |
| J1431-0050 | 1.188 | 0.942 | 1.166 | 0.858 | 1.166 |
| B1435+6349 | 2.068 | 1.938 | 2.037 | 1.938 | 2.037 |
| J1436-0051 | 1.273 | 1.109 | 1.250 | 0.919 | 1.250 |
| J1437-0147 | 1.310 | 0.499 | 1.287 | 0.499 | 1.287 |
| J1455-0045 | 1.375 | 1.095 | 1.351 | 1.095 | 1.351 |
| J1501+0019 | 1.930 | 1.486 | 1.901 | 1.486 | 1.901 |
| J1502-4154 | 1.026 | ... | ... | 1.001 | 1.006 |
| J1504+0122 | 0.967 | 0.271 | 0.882 | 0.259 | 0.882 |
| J1513+1011 | 1.546 | 1.042 | 1.521 | 1.042 | 1.521 |
| B1517+2356 | 1.903 | 1.725 | 1.874 | 0.820 | 1.874 |
| B1517+2357 | 1.834 | 0.821 | 1.806 | 0.800 | 1.806 |
| J1521-0009 | 1.318 | 1.094 | 1.295 | 0.955 | 1.295 |
| J1524+0958 | 1.324 | 0.501 | 1.301 | 0.501 | 1.301 |
| J1527+2452 | 0.993 | ... | ... | 0.946 | 0.973 |
| J1537+0021 | 1.754 | 1.632 | 1.726 | 1.632 | 1.726 |
| J1537+3358 | 1.025 | 0.902 | 1.005 | 0.902 | 1.005 |
| J1539+4735 | 0.772 | 0.715 | 0.754 | 0.520 | 0.754 |
| B1542+5408 | 2.371 | 0.996 | 2.337 | 0.996 | 2.337 |
| B1544+4855 | 0.400 | 0.331 | 0.386 | 0.322 | 0.386 |
| J1544+5912 | 0.807 | 0.260 | 0.789 | 0.259 | 0.789 |
| J1601+1714 | 1.952 | 1.581 | 1.736 | 1.538 | 1.751 |
| J1614+4704 | 1.860 | 1.405 | 1.831 | 1.405 | 1.831 |
| J1619+3813 | 1.124 | 0.258 | 0.883 | 0.258 | 0.883 |
| J1620+1736 | 0.555 | 0.535 | 0.539 | 0.488 | 0.539 |
| B1622+2352 | 0.927 | 0.891 | 0.908 | 0.891 | 0.908 |
| B1623+2653 | 2.526 | 1.042 | 2.491 | 1.042 | 2.491 |
| J1629+3808 | 1.461 | 1.110 | 1.436 | 0.981 | 1.436 |
| J1631+1156 | 1.792 | 1.112 | 1.764 | 0.974 | 1.764 |
| J1637+2509 | 1.110 | 0.999 | 1.089 | 0.888 | 1.089 |
| J1649+3046 | 1.123 | 1.072 | 1.102 | 1.072 | 1.102 |
| J1658+0515 | 0.879 | 0.539 | 0.860 | 0.499 | 0.860 |
| B1704+6048 | 0.371 | 0.312 | 0.357 | 0.283 | 0.357 |
| J1704+7057 | 2.015 | 1.810 | 1.985 | 1.029 | 1.985 |
| J1706+3615 | 0.918 | 0.826 | 0.899 | 0.794 | 0.899 |
| J1712+5559 | 1.358 | 1.209 | 1.334 | 1.209 | 1.334 |
| B1715+5331 | 1.940 | 1.470 | 1.911 | 1.470 | 1.911 |
| J1716+5654 | 0.937 | ... | ... | 0.905 | 0.918 |
| B1718+4807 | 1.084 | 0.776 | 1.063 | 0.776 | 1.063 |

TABLE 3 — *Continued*

| Object ^a | z_{em} | R1 ^b | | R2 ^c | |
|---------------------|----------|-----------------|-----------|-----------------|-----------|
| | | z_{min} | z_{max} | z_{min} | z_{max} |
| J1722+5442 | 1.215 | 0.948 | 1.193 | 0.864 | 1.193 |
| J1727+5302 | 1.444 | 1.032 | 1.420 | 1.032 | 1.420 |
| J1729+5758 | 1.342 | 0.856 | 1.319 | 0.824 | 1.319 |
| J1733+5533 | 1.072 | 0.999 | 1.051 | 0.999 | 1.051 |
| B1821+1042 | 1.360 | 1.252 | 1.336 | 1.252 | 1.336 |
| J1858+5645 | 1.595 | 1.234 | 1.569 | 1.234 | 1.569 |
| J1902+3159 | 0.635 | 0.482 | 0.619 | 0.482 | 0.619 |
| J2051+1950 | 2.367 | 1.833 | 2.333 | 1.747 | 2.333 |
| B2145+0643 | 0.999 | 0.820 | 0.979 | 0.802 | 0.979 |
| J2151+2130 | 1.534 | 1.170 | 1.509 | 1.004 | 1.509 |
| J2154-4414 | 0.344 | 0.256 | 0.331 | 0.256 | 0.331 |
| J2215-2944 | 2.706 | 0.936 | 2.594 | 0.862 | 2.594 |
| B2216-0350 | 0.901 | ... | ... | 0.862 | 0.882 |
| J2233-6033 | 2.238 | 0.265 | 2.206 | 0.263 | 2.206 |
| J2246-1206 | 0.630 | 0.499 | 0.614 | 0.499 | 0.614 |
| J2253+1608 | 0.859 | 0.793 | 0.840 | 0.537 | 0.840 |
| J2258-2758 | 0.927 | 0.819 | 0.908 | 0.790 | 0.908 |
| J2328+0022 | 1.308 | 0.836 | 1.285 | 0.809 | 1.285 |
| J2331+0038 | 1.486 | 1.143 | 1.461 | 1.143 | 1.461 |
| J2334+0052 | 1.040 | 0.854 | 1.020 | 0.823 | 1.020 |
| J2339-0029 | 1.340 | ... | ... | 1.155 | 1.317 |
| J2342-0322 | 0.896 | 0.539 | 0.877 | 0.499 | 0.877 |
| J2346+0930 | 0.673 | 0.614 | 0.656 | 0.499 | 0.656 |
| J2352-0028 | 1.624 | 1.345 | 1.598 | 1.318 | 1.598 |
| J2355-3357 | 0.702 | 0.497 | 0.685 | 0.486 | 0.685 |

^a Objects with a B preface designate objects listed with coordinates from the Besselian epoch (1950). These objects were observed with the FOS high resolution gratings and can be found in Bechtold et al. (2002). Objects with a J preface designate objects listed with coordinates from the Julian epoch (2000). These objects were observed with either the FOS low resolution gratings or the

STIS low resolution gratings described in § 3 and listed in Table 1 and Table 2.

^b $\tau \geq 1$

^c $\tau \geq 2$

TABLE 4
LIST OF LLSs.

| Object ^a | z_{em} | z_{LLS}^b | τ_{LLS} | $\log N_{HI}$ | Sample ^c | Instrument ^d |
|---------------------|----------|--------------------|--------------|---|---------------------|-------------------------|
| B0002-4214 | 2.760 | 2.301 | > 4.06 | > 17.81 | R1,R2 | FOS-H |
| J0012-0122 | 1.998 | 1.727 | 1.70 ± 0.08 | 17.44 ^{+0.01} _{-0.02} | R1 | STIS |
| J0012-0122 | 1.998 | 1.387 | > 2.33 | > 17.57 | MgII | STIS |
| J0021+0043 | 1.243 | 0.943 | > 2.97 | > 17.67 | MgII | STIS |
| J0021+0104 | 1.829 | 1.576 | > 2.47 | > 17.59 | MgII | STIS |
| J0021-0128A | 1.588 | 1.499 | 0.96 ± 0.07 | 17.19 ^{+0.03} _{-0.04} | PLLS | STIS |
| J0021-0128A | 1.588 | 1.409 | 1.16 ± 0.13 | 17.27 ^{+0.04} _{-0.06} | R1 | STIS |
| J0021-0128A | 1.588 | 1.243 | > 2.01 | > 17.50 | R2 | STIS |
| J0038-3504 | 1.519 | 1.517 | 0.87 ± 0.04 | 17.14 ^{+0.02} _{-0.02} | PLLS,Prox | STIS |
| J0038-3504 | 1.519 | 1.114 | 0.22 ± 0.08 | 16.55 ^{+0.14} _{-0.20} | PLLS | STIS |
| J0039-3528 | 0.836 | 0.838 | > 1.84 | > 17.47 | Prox | STIS |
| J0043-2622 | 3.053 | 1.880 | 1.38 ± 0.15 | 17.34 ^{+0.05} _{-0.05} | R1 | STIS |
| J0043-2622 | 3.053 | 1.384 | > 1.71 | > 17.43 | LQ | STIS |
| B0058+0155 | 1.954 | 1.463 | 0.77 ± 0.05 | 17.09 ^{+0.03} _{-0.03} | PLLS | FOS-H |
| J0102-0853 | 1.682 | 1.185 | > 2.49 | > 17.60 | R1,R2 | STIS |
| J0106+0105 | 1.611 | 1.356 | > 2.68 | > 17.63 | MgII | STIS |
| J0109-2307 | 0.818 | 0.821 | > 1.72 | > 17.44 | Prox | STIS |
| J0116-0043 | 1.263 | 0.915 | > 1.89 | > 17.48 | MgII | STIS |
| B0119-0437 | 1.925 | 1.964 | 1.81 ± 0.04 | 17.46 ^{+0.01} _{-0.01} | Prox | FOS-H |
| J0120+2133 | 1.500 | 1.327 | 1.58 ± 0.06 | 17.40 ^{+0.02} _{-0.01} | R1 | FOS-L |
| J0120+2133 | 1.500 | 1.050 | 2.61 ± 0.31 | 17.62 ^{+0.05} _{-0.05} | R2 | FOS-L |
| J0123-0058 | 1.550 | 1.412 | > 2.79 | > 17.65 | MgII | STIS |
| J0126-0105 | 1.609 | 1.193 | > 2.73 | > 17.64 | MgII | STIS |
| J0134+0051 | 1.522 | 1.449 | 1.07 ± 0.09 | 17.23 ^{+0.04} _{-0.04} | R1 | STIS |
| J0134+0051 | 1.522 | 1.274 | > 1.81 | > 17.46 | LQ | STIS |
| J0138-0005 | 1.340 | 1.342 | 0.64 ± 0.10 | 17.01 ^{+0.06} _{-0.07} | PLLS,Prox | STIS |
| J0139-0023 | 1.384 | 1.089 | 1.65 ± 0.22 | 17.42 ^{+0.06} _{-0.06} | R1 | STIS |
| J0141-0024 | 2.611 | 2.215 ^b | > 2.95 | > 17.67 | R1,R2 | STIS |
| B0143-0135 | 3.124 | 1.612 | > 2.59 | > 17.61 | R1,R2 | FOS-H |
| J0144+3411 | 1.450 | 1.243 | 1.82 ± 0.07 | 17.46 ^{+0.02} _{-0.01} | MgII | FOS-L |
| J0148+3854 | 1.442 | 1.215 ^b | > 2.66 | > 17.62 | R2 | FOS-L |
| J0153+0009 | 0.837 | 0.773 | | | MgII,Blue | STIS |
| J0153+0052 | 1.163 | 1.062 | > 2.80 | > 17.65 | MgII | STIS |
| J0157-0048 | 1.545 | 1.417 | > 3.76 | > 17.78 | MgII | STIS |
| B0207-3953 | 2.813 | 2.480 | > 3.33 | > 17.72 | R1,R2 | FOS-H |
| J0208-0503 | 1.850 | 1.072 | > 1.80 | > 17.46 | DLA | STIS |
| J0210-0152 | 2.370 | 2.381 | 1.29 ± 0.38 | 17.31 ^{+0.12} _{-0.15} | LQ,Prox | STIS |
| J0210-0152 | 2.370 | 2.147 | > 1.66 | > 17.42 | LQ | STIS |
| J0241-1514 | 2.786 | 2.198 | 1.45 ± 0.32 | 17.36 ^{+0.09} _{-0.10} | LQ | STIS |
| J0241-1514 | 2.786 | 1.839 ^b | > 2.11 | > 17.52 | LQ | STIS |
| J0256-0126 | 0.879 | 0.814 ^b | > 3.43 | > 17.74 | R1,R2 | FOS-L |
| J0304-0008 | 3.290 | 2.112 | 0.79 ± 0.09 | 17.10 ^{+0.05} _{-0.05} | PLLS | STIS |
| J0304-0008 | 3.290 | 1.985 | 0.72 ± 0.11 | 17.06 ^{+0.06} _{-0.07} | PLLS | STIS |
| J0318-2012 | 2.869 | 2.090 | > 2.83 | > 17.65 | R2 | STIS |
| J0336-3607 | 1.093 | 0.871 ^b | > 2.14 | > 17.53 | R2 | FOS-L |
| J0354-2724 | 2.823 | 1.858 ^b | > 2.51 | > 17.60 | R2 | STIS |
| J0411-4956 | 0.817 | 0.785 | > 1.25 | > 17.30 | R1 | STIS |
| B0424-1309 | 2.159 | 2.036 | > 3.91 | > 17.79 | R1,R2 | FOS-H |
| J0452-1640 | 2.600 | 1.008 | > 2.11 | > 17.52 | MgII | STIS |
| J0453-1305 | 2.300 | 2.068 | > 4.28 | > 17.83 | R1,R2 | STIS |
| B0453-4220 | 2.660 | 2.304 | > 4.08 | > 17.81 | R1,R2 | FOS-H |
| B0454+0356 | 1.345 | 1.153 | 1.13 ± 0.04 | 17.26 ^{+0.01} _{-0.02} | R1 | FOS-H |
| B0454+0356 | 1.345 | 0.993 | 0.68 ± 0.04 | 17.04 ^{+0.02} _{-0.03} | PLLS | FOS-H |
| B0454+0356 | 1.345 | 0.858 | > 2.41 | > 17.58 | R1,R2 | FOS-H |
| B0454-2203 | 0.534 | 0.473 | > 3.43 | > 17.74 | R1,R2 | FOS-H |
| J0514-3326 | 1.569 | 1.138 | > 3.73 | > 17.77 | R1,R2 | STIS |
| J0514-3326 | 1.569 | 0.935 | | | Blue | STIS |
| J0806+5041 | 2.432 | 1.814 | 0.80 ± 0.05 | 17.10 ^{+0.03} _{-0.02} | PLLS | STIS |
| J0806+5041 | 2.432 | 1.677 | 0.68 ± 0.06 | 17.04 ^{+0.03} _{-0.04} | PLLS | STIS |
| J0806+5041 | 2.432 | 1.322 | 0.71 ± 0.09 | 17.06 ^{+0.05} _{-0.07} | PLLS | STIS |
| J0806+5041 | 2.432 | 1.065 | 0.50 ± 0.19 | 16.90 ^{+0.15} _{-0.21} | PLLS | STIS |
| J0813+4813 | 0.871 | 0.866 | > 2.11 | > 17.52 | Prox,21cm | FOS-L |
| J0839+5256 | 1.545 | 0.328 | 1.21 ± 0.27 | 17.29 ^{+0.09} _{-0.11} | R1 | STIS |
| B0848+1623 | 1.936 | 1.926 | > 4.71 | > 17.87 | Prox | FOS-H |
| J0912+2450 | 0.654 | 0.376 | 0.50 ± 0.05 | 16.90 ^{+0.04} _{-0.04} | PLLS | STIS |
| B0933+7315 | 2.528 | 2.332 | > 4.00 | > 17.80 | R1,R2 | FOS-H |
| B0933+7315 | 2.528 | 1.508 ^b | > 1.67 | > 17.42 | LQ | FOS-H |

TABLE 4 — *Continued*

| Object ^a | z_{em} | z_{LLS}^b | τ_{LLS} | $\log N_{HI}$ | Sample ^c | Instrument ^d |
|---------------------|----------|--------------------|-----------------|-------------------------|---------------------|-------------------------|
| B0935+4141 | 1.937 | 1.465 | > 4.81 | > 17.88 | R1,R2 | FOS-H |
| J0944+2554 | 2.910 | 2.235 | > 2.98 | > 17.67 | R1,R2 | STIS |
| J0944+2554 | 2.910 | 1.466 | 1.33 ± 0.32 | $17.33^{+0.09}_{-0.12}$ | LQ | STIS |
| J0948+4323 | 1.892 | 1.235 | > 3.00 | > 17.68 | DLA | STIS |
| B0953+5454 | 2.584 | 2.510 ^b | > 4.00 | > 17.80 | R1,R2 | FOS-H |
| J0953-0038 | 1.382 | 1.016 | > 2.30 | > 17.56 | R1,R2 | STIS |
| B0958+5509 | 1.750 | 1.733 | > 5.31 | > 17.93 | Prox | FOS-H |
| J1001+5553A | 1.413 | 1.392 | > 4.57 | > 17.86 | Prox | STIS |
| J1001+5553B | 1.413 | 1.392 | > 4.68 | > 17.87 | Prox,GL | STIS |
| J1008-0018 | 1.350 | 1.196 | 1.13 ± 0.06 | $17.26^{+0.02}_{-0.03}$ | R1 | STIS |
| J1009+0036 | 1.702 | 0.973 | > 2.17 | > 17.54 | MgII | STIS |
| J1009-0026 | 1.244 | 1.145 | 0.48 ± 0.08 | $16.88^{+0.07}_{-0.08}$ | PLLS | STIS |
| J1009-0026 | 1.244 | 1.118 | 0.33 ± 0.07 | $16.72^{+0.08}_{-0.11}$ | PLLS | STIS |
| J1009-0026 | 1.244 | 0.889 | > 1.87 | > 17.47 | MgII | STIS |
| J1009-0026 | 1.244 | 0.843 | | | MgII,Blue | STIS |
| J1010+0003 | 1.399 | 1.266 | > 3.12 | > 17.69 | MgII | STIS |
| J1010-0047 | 1.671 | 1.328 | > 3.58 | > 17.75 | MgII | STIS |
| J1011+1304 | 1.287 | 0.900 | 1.36 ± 0.11 | $17.34^{+0.03}_{-0.04}$ | R1 | FOS-L |
| B1017+2759 | 1.928 | 1.608 | 1.52 ± 0.05 | $17.39^{+0.01}_{-0.02}$ | R1 | FOS-H |
| J1017+5356 | 1.400 | 1.307 | > 3.13 | > 17.69 | DLA | STIS |
| J1022+0101 | 1.563 | 1.560 | 2.09 ± 0.11 | $17.52^{+0.03}_{-0.02}$ | Prox | STIS |
| J1022+0101 | 1.563 | 1.427 | > 1.89 | > 17.48 | MgII | STIS |
| J1022+3041 | 1.318 | 0.435 | 0.41 ± 0.08 | $16.82^{+0.07}_{-0.10}$ | PLLS | STIS |
| J1022+3041 | 1.318 | 0.346 | 2.40 ± 0.31 | $17.58^{+0.06}_{-0.06}$ | DLA | STIS |
| J1024+1912 | 0.828 | 0.530 ^b | > 2.23 | > 17.55 | R2 | FOS-L |
| J1032+0003 | 1.190 | 1.105 | > 2.72 | > 17.63 | MgII | STIS |
| J1037+0028 | 1.733 | 1.425 | > 2.97 | > 17.67 | MgII | STIS |
| J1042+1203 | 1.028 | 0.661 | 0.57 ± 0.13 | $16.96^{+0.09}_{-0.11}$ | PLLS | FOS-L |
| B1047+5503 | 2.165 | 1.637 | 0.84 ± 0.05 | $17.13^{+0.03}_{-0.03}$ | PLLS | FOS-H |
| J1048+0032 | 1.649 | 1.194 | > 2.61 | > 17.62 | R1,R2 | STIS |
| J1054-0020 | 1.021 | 0.952 | > 1.61 | > 17.41 | MgII | STIS |
| J1058+1951 | 1.110 | 1.037 | 2.22 ± 0.13 | $17.55^{+0.03}_{-0.02}$ | R1,R2 | FOS-L |
| B1100-2629 | 2.145 | 1.838 | > 5.42 | > 17.93 | R1,R2 | FOS-H |
| J1103+3715 | 1.295 | 1.246 | > 2.15 | > 17.53 | R1,R2 | STIS |
| B1103+6416 | 2.190 | 1.892 | 1.81 ± 0.03 | $17.46^{+0.01}_{-0.00}$ | IUE | FOS-H |
| B1103+6416 | 2.190 | 0.976 | 0.34 ± 0.07 | $16.73^{+0.09}_{-0.10}$ | IUE | FOS-H |
| B1104-1805a | 2.303 | 2.201 | 0.20 ± 0.03 | $16.51^{+0.06}_{-0.09}$ | PLLS | FOS-H |
| B1104-1805a | 2.303 | 1.662 | > 4.55 | > 17.86 | DLA | FOS-H |
| B1104-1805b | 2.303 | 2.201 | 0.60 ± 0.04 | $16.98^{+0.03}_{-0.03}$ | PLLS | FOS-H |
| B1104-1805b | 2.303 | 1.662 | 1.99 ± 0.21 | $17.50^{+0.05}_{-0.05}$ | DLA | FOS-H |
| J1107+0048 | 1.391 | 1.082 | 1.03 ± 0.06 | $17.22^{+0.02}_{-0.03}$ | MgII | STIS |
| J1108+3133 | 2.244 | 2.106 | 1.50 ± 0.07 | $17.38^{+0.02}_{-0.02}$ | R1 | STIS |
| J1108+3133 | 2.244 | 1.200 | > 2.11 | > 17.52 | R1,R2 | STIS |
| J1110+3019 | 1.521 | 1.030 | > 1.64 | > 17.41 | DLA | STIS |
| J1112+0013 | 1.433 | 1.423 | > 2.53 | > 17.60 | Prox | STIS |
| J1125+5910 | 0.852 | 0.558 | 0.33 ± 0.05 | $16.72^{+0.06}_{-0.06}$ | PLLS | STIS |
| J1126+0034 | 1.783 | 1.793 | > 3.49 | > 17.74 | Prox | STIS |
| J1143+3452 | 3.130 | 0.556 ^b | > 4.48 | > 17.85 | R1,R2 | STIS |
| J1150-0023 | 1.980 | 1.446 | 0.95 ± 0.05 | $17.18^{+0.02}_{-0.03}$ | PLLS | FOS-L |
| J1151+3825 | 1.304 | 0.548 | 1.69 ± 0.12 | $17.43^{+0.03}_{-0.03}$ | MgII | FOS-L |
| J1208+4540 | 1.158 | 0.928 | 0.79 ± 0.06 | $17.10^{+0.03}_{-0.04}$ | PLLS | FOS-L |
| J1218+1105 | 1.403 | 1.266 | 0.66 ± 0.06 | $17.02^{+0.04}_{-0.04}$ | PLLS | FOS-L |
| J1218+1105 | 1.403 | 1.110 | 0.74 ± 0.08 | $17.07^{+0.05}_{-0.04}$ | PLLS | FOS-L |
| J1220+3343 | 1.532 | 1.502 | 1.85 ± 0.13 | $17.47^{+0.03}_{-0.03}$ | R1 | STIS |
| J1220-0040 | 1.411 | 0.976 | > 1.97 | > 17.49 | MgII | STIS |
| B1222+2251 | 2.046 | 1.174 | 0.71 ± 0.13 | $17.05^{+0.08}_{-0.08}$ | PLLS | FOS-H |
| J1224+0037 | 1.482 | 1.364 | 0.68 ± 0.07 | $17.03^{+0.05}_{-0.04}$ | PLLS | STIS |
| J1224+0037 | 1.482 | 1.268 | > 2.69 | > 17.63 | MgII | STIS |
| B1225+3145 | 2.219 | 1.796 | > 5.75 | > 17.96 | R1,R2 | FOS-H |
| J1228+1018 | 2.305 | 0.939 | > 0.69 | > 17.04 | MgII | STIS |
| J1232-0224 | 1.045 | 0.832 | 1.26 ± 0.08 | $17.30^{+0.03}_{-0.03}$ | 21cm | FOS-L |
| J1232-0224 | 1.045 | 0.772 | 0.51 ± 0.09 | $16.92^{+0.07}_{-0.09}$ | 21cm | FOS-L |
| J1308+3005 | 0.803 | 0.821 | 2.93 ± 0.22 | $17.67^{+0.03}_{-0.03}$ | Prox | FOS-L |
| J1313-2716 | 2.186 | 1.684 | > 4.34 | > 17.84 | R1,R2 | STIS |
| J1319+2728 | 1.014 | 0.661 | 3.08 ± 0.26 | $17.69^{+0.04}_{-0.04}$ | R1,R2 | FOS-L |
| B1320+2925 | 0.960 | 0.872 | 1.37 ± 0.12 | $17.34^{+0.04}_{-0.04}$ | R1 | FOS-L |

TABLE 4 — *Continued*

| Object ^a | z_{em} | z_{LLS}^b | τ_{LLS} | $\log N_{HI}$ | Sample ^c | Instrument ^d |
|---------------------|----------|--------------------|-----------------|-------------------------|---------------------|-------------------------|
| J1321+1106 | 2.181 | 1.849 ^b | > 2.63 | > 17.62 | R2 | STIS |
| J1321+2847 | 1.703 | 1.135 | 2.56 ± 0.26 | $17.61^{+0.04}_{-0.04}$ | R1,R2 | FOS-L |
| J1322+4739 | 1.554 | 1.435 | 1.27 ± 0.04 | $17.31^{+0.01}_{-0.02}$ | R1 | STIS |
| J1322+4739 | 1.554 | 1.078 | > 2.44 | > 17.59 | R1,R2 | STIS |
| B1323+6530 | 1.618 | 1.609 | > 4.18 | > 17.82 | Prox | FOS-H |
| B1329+4117 | 1.930 | 1.841 | 0.38 ± 0.03 | $16.78^{+0.04}_{-0.03}$ | PLLS | FOS-H |
| B1329+4117 | 1.930 | 1.602 | 1.02 ± 0.04 | $17.21^{+0.02}_{-0.02}$ | MgII | FOS-H |
| B1329+4117 | 1.930 | 1.283 | > 2.76 | > 17.64 | MgII | FOS-H |
| B1334-0033 | 2.783 | 2.201 | 0.81 ± 0.03 | $17.12^{+0.01}_{-0.02}$ | PLLS | FOS-H |
| J1341+0059 | 1.714 | 1.597 | > 3.25 | > 17.71 | R1,R2 | STIS |
| J1341+4123 | 1.204 | 1.063 | 0.58 ± 0.04 | $16.97^{+0.03}_{-0.04}$ | PLLS | FOS-L |
| J1351-0007 | 1.444 | 1.159 ^b | > 3.67 | > 17.76 | R1,R2 | FOS-L |
| J1354+0052 | 1.121 | 0.666 ^b | > 3.74 | > 17.77 | R1,R2 | FOS-L |
| J1404-0130 | 2.522 | 1.719 | > 3.56 | > 17.75 | R1,R2 | STIS |
| J1419-0036 | 0.969 | 0.823 | > 1.32 | > 17.32 | MgII | STIS |
| J1420-0054 | 1.458 | 1.348 | > 3.66 | > 17.76 | MgII | STIS |
| J1423+3252 | 1.905 | 1.491 | 3.46 ± 0.11 | $17.74^{+0.02}_{-0.01}$ | R1,R2 | STIS |
| J1423+3252 | 1.905 | 1.176 | > 2.09 | > 17.52 | R2 | STIS |
| J1426+0051 | 1.333 | 0.844 | > 1.29 | > 17.31 | MgII | STIS |
| J1427-1203 | 0.805 | 0.652 ^b | > 2.76 | > 17.64 | R2 | FOS-L |
| J1431-0050 | 1.188 | 0.858 | > 1.51 | > 17.38 | LQ | STIS |
| B1435+6349 | 2.068 | 1.938 | 1.88 ± 0.07 | $17.48^{+0.01}_{-0.02}$ | R1 | FOS-H |
| B1435+6349 | 2.068 | 1.925 | > 3.03 | > 17.68 | LQ | FOS-H |
| J1436-0051 | 1.273 | 1.264 | 0.98 ± 0.06 | $17.20^{+0.02}_{-0.03}$ | PLLS | STIS |
| J1436-0051 | 1.273 | 0.930 | > 1.78 | > 17.45 | MgII | STIS |
| J1455-0045 | 1.375 | 1.095 | > 3.12 | > 17.69 | MgII | STIS |
| J1501+0019 | 1.930 | 1.486 | > 3.50 | > 17.74 | MgII | STIS |
| J1513+1011 | 1.546 | 1.042 ^b | > 3.71 | > 17.77 | R1,R2 | FOS-L |
| B1517+2356 | 1.903 | 1.887 | 0.53 ± 0.03 | $16.93^{+0.02}_{-0.02}$ | PLLS | FOS-H |
| B1517+2356 | 1.903 | 1.725 | 1.95 ± 0.09 | $17.49^{+0.02}_{-0.01}$ | R1 | FOS-H |
| J1521-0009 | 1.318 | 0.961 | > 1.92 | > 17.48 | MgII | STIS |
| J1525+0026 | 0.801 | 0.797 | > 1.33 | > 17.33 | Prox | STIS |
| J1537+0021 | 1.754 | 1.647 | > 3.41 | > 17.73 | MgII | STIS |
| J1537+3358 | 1.025 | 0.915 | > 3.03 | > 17.68 | DLA | STIS |
| J1539+4735 | 0.772 | 0.730 | 1.21 ± 0.10 | $17.29^{+0.03}_{-0.04}$ | R1 | FOS-L |
| J1601+1714 | 1.952 | 1.581 | 1.87 ± 0.27 | $17.48^{+0.06}_{-0.07}$ | R1 | FOS-L |
| J1614+4704 | 1.860 | 1.867 | 0.47 ± 0.04 | $16.87^{+0.04}_{-0.03}$ | Prox,PLLS | STIS |
| J1614+4704 | 1.860 | 1.735 | 0.54 ± 0.05 | $16.93^{+0.04}_{-0.04}$ | PLLS | STIS |
| J1614+4704 | 1.860 | 1.411 | > 3.98 | > 17.80 | R1,R2 | STIS |
| B1622+2352 | 0.927 | 0.891 | > 2.24 | > 17.55 | MgII | FOS-H |
| J1623+2653 | 2.526 | 1.042 | > 3.08 | > 17.69 | R1,R2 | FOS-L |
| J1629+3808 | 1.461 | 1.110 | 1.60 ± 0.09 | $17.41^{+0.03}_{-0.02}$ | R1 | FOS-L |
| B1630+3744 | 1.478 | 1.096 | 0.29 ± 0.04 | $16.66^{+0.05}_{-0.06}$ | PLLS,IUE | FOS-H |
| J1631+1156 | 1.792 | 0.902 | > 1.51 | > 17.38 | MgII | STIS |
| J1637+2509 | 1.110 | 0.894 | > 1.56 | > 17.39 | DLA | STIS |
| J1649+3046 | 1.123 | 1.078 | > 3.41 | > 17.73 | R1,R2 | STIS |
| J1701+6412 | 2.722 | 2.293 | 0.31 ± 0.05 | $16.69^{+0.07}_{-0.08}$ | PLLS,IUE | STIS |
| J1701+6412 | 2.722 | 2.160 | 0.51 ± 0.05 | $16.92^{+0.04}_{-0.05}$ | PLLS,IUE | STIS |
| J1701+6412 | 2.722 | 1.846 | 0.39 ± 0.06 | $16.80^{+0.06}_{-0.07}$ | PLLS,IUE | STIS |
| J1701+6412 | 2.722 | 1.725 | 0.56 ± 0.07 | $16.95^{+0.05}_{-0.06}$ | PLLS,IUE | STIS |
| J1704+7057 | 2.015 | 1.810 | 2.60 ± 0.13 | $17.62^{+0.02}_{-0.02}$ | R1,R2 | STIS |
| J1704+7057 | 2.015 | 1.101 ^b | > 2.31 | > 17.56 | R2 | STIS |
| J1712+5559 | 1.358 | 1.209 | > 3.00 | > 17.68 | MgII | STIS |
| B1715+5331 | 1.940 | 1.633 | 0.64 ± 0.03 | $17.01^{+0.02}_{-0.02}$ | PLLS | FOS-H |
| J1727+5302 | 1.444 | 1.032 | > 2.49 | > 17.60 | MgII | STIS |
| J1727+5302 | 1.444 | 0.948 | | | MgII,Blue | STIS |
| J1729+5758 | 1.342 | 1.130 | 0.35 ± 0.04 | $16.74^{+0.05}_{-0.05}$ | PLLS | STIS |
| J1733+5533 | 1.072 | 1.000 | > 3.29 | > 17.72 | MgII | STIS |
| J1736+5938 | 1.410 | 1.400 | > 3.50 | > 17.74 | Prox | STIS |
| B1821+1042 | 1.360 | 1.252 | > 3.27 | > 17.71 | MgII | FOS-H |
| J1858+5645 | 1.595 | 1.235 | > 3.65 | > 17.76 | MgII | STIS |
| J2051+1950 | 2.367 | 1.747 ^b | > 2.96 | > 17.67 | R2 | STIS |
| J2144-0754 | 1.811 | 1.802 | > 3.55 | > 17.75 | Prox | STIS |
| J2151+2130 | 1.534 | 1.004 | > 1.87 | > 17.47 | MgII | STIS |
| J2151+2130 | 1.534 | 0.915 | | | MgII,Blue | STIS |
| J2215-2944 | 2.706 | 1.954 | 1.77 ± 0.06 | $17.45^{+0.02}_{-0.01}$ | R1 | STIS |
| J2215-2944 | 2.706 | 1.900 | 0.44 ± 0.08 | $16.85^{+0.07}_{-0.09}$ | PLLS | STIS |
| J2215-2944 | 2.706 | 1.610 | 0.62 ± 0.09 | $16.99^{+0.06}_{-0.06}$ | PLLS | STIS |

TABLE 4 — *Continued*

| Object ^a | z_{em} | $z_{\text{LLS}}^{\text{b}}$ | τ_{LLS} | $\log N_{\text{HI}}$ | Sample ^c | Instrument ^d |
|---------------------|-----------------|-----------------------------|---------------------|-------------------------|---------------------|-------------------------|
| J2233–6033 | 2.238 | 1.929 | 1.53 ± 0.03 | $17.39^{+0.01}_{-0.01}$ | R1 | STIS |
| J2233–6033 | 2.238 | 1.872 | 0.48 ± 0.03 | $16.88^{+0.03}_{-0.02}$ | PLLS | STIS |
| J2331+0038 | 1.486 | 1.143 | > 3.77 | > 17.78 | MgII | STIS |
| J2339–0029 | 1.340 | 0.967 | > 1.98 | > 17.50 | MgII | STIS |
| J2352–0028 | 1.624 | 1.245 | > 2.62 | > 17.62 | MgII | STIS |

^a Objects with a B preface designate objects listed with coordinates from the Besselian epoch (1950). These objects were observed with the FOS high resolution gratings and can be found in Bechtold et al. (2002). Objects with a J preface designate objects listed with coordinates from the Julian epoch (2000). These objects were observed with either the FOS low resolution gratings or the STIS low resolution gratings described in § 3 and listed in Table 1 and Table 2.

^b Redshifts marked b indicate the break of the Lyman limit was used to determine the redshift of the absorber. Unmarked redshifts indicate the Lyman series lines were used to determine the redshift of the absorber.

^c The sample (R1 or R2) where a LLS was discovered. An absorber is marked R1 if $z_{\text{LLS}} \geq z_{\text{min}}$ for that object and $\tau_{\text{LLS}} \geq 1$. An absorber is marked R2 if $z_{\text{LLS}} \geq z_{\text{min}}$ for that object and

$\tau_{\text{LLS}} \geq 2$. The rest of the designations indicate why an absorber was not included in the statistical analysis. Blue, the redshift of the absorber is blueward of z_{min} for that object; DLA, a known DLA prior to observation; GL, part of a gravitationally lensed system (for these systems, we did not include any absorbers associated with the lensing object); MgII, known strong Mg II system prior to observation; PLLS, $\tau_{\text{LLS}} < 1$; LQ, $z_{\text{LLS}} < z_{\text{min}}$ for that object (this occurred in systems where we could identify the Lyman series of a system, but the break occurred outside of our established acceptable redshift path); IUE, objects previously observed with IUE (these objects were targeted with *HST* because of their strong UV flux as measured from IUE observations); 21 cm, known strong 21 cm system prior to observation; and finally, Prox, absorbers where $z_{\text{LLS}} \leq 3000 \text{ km s}^{-1}$ from z_{em} .

^d The instrument used to observe the object (see § 3).

TABLE 5
REDSHIFT DENSITY OF LLSs FOR R1 AND R2.

| z | ΔX | Δz | N | $\langle z_{\text{LLS}} \rangle$ | $l(z)$ | $l(X)$ | $\Delta r_{\text{LLS}} (h_{70}^{-1} \text{ Mpc})$ |
|----------------------------|------------|------------|-----|----------------------------------|-----------------|-----------------|---|
| $\tau_{\text{LLS}} \geq 1$ | | | | | | | |
| [0.255, 2.594] | 195.73 | 79.23 | 61 | 1.434 | 0.77 ± 0.11 | 0.31 ± 0.04 | |
| [0.255, 1.060] | 59.13 | 29.54 | 15 | 0.785 | 0.51 ± 0.14 | 0.25 ± 0.07 | 3047 |
| [1.060, 1.423] | 48.54 | 19.56 | 16 | 1.194 | 0.82 ± 0.22 | 0.33 ± 0.09 | 1213 |
| [1.423, 1.824] | 45.63 | 16.47 | 15 | 1.613 | 0.91 ± 0.25 | 0.33 ± 0.09 | 731 |
| [1.824, 2.594] | 42.44 | 13.66 | 15 | 2.142 | 1.10 ± 0.32 | 0.35 ± 0.10 | 392 |
| $\tau_{\text{LLS}} \geq 2$ | | | | | | | |
| [0.242, 2.594] | 234.70 | 96.14 | 50 | 1.515 | 0.52 ± 0.08 | 0.21 ± 0.03 | |
| [0.242, 1.078] | 80.38 | 40.03 | 15 | 0.895 | 0.37 ± 0.10 | 0.19 ± 0.05 | 3645 |
| [1.078, 1.544] | 73.50 | 29.03 | 15 | 1.157 | 0.52 ± 0.14 | 0.20 ± 0.05 | 1995 |
| [1.544, 1.947] | 44.28 | 15.52 | 10 | 1.751 | 0.64 ± 0.21 | 0.23 ± 0.08 | 917 |
| [1.947, 2.594] | 36.54 | 11.56 | 10 | 2.257 | 0.86 ± 0.30 | 0.27 ± 0.09 | 457 |

TABLE 6
PARAMETERS OF $l(z) = l_0(1+z)^\gamma$.

| Paper | $\tau_{\text{LLS}} \geq$ | z | l_0^a | γ |
|------------------------------|--------------------------|--------------|------------|-----------------|
| Sargent et al. 1989 | 1 | [0.6, 3.6] | 0.76 | 0.68 ± 0.54 |
| Lanzetta 1991 | 1 | [0.35, 2.5] | 1.2 | 0.3 ± 0.9 |
| Storrie-Lombardi et al. 1994 | 1 | [0.4, 4.7] | 0.27 | 1.55 ± 0.45 |
| Stengler-Larrea et al. 1995 | 1 | [0.3, 4.2] | 0.25 | 1.5 ± 0.39 |
| This Paper | 1 | [0.25, 2.59] | 0.28^a | 1.19 ± 0.56 |
| Prochaska et al. 2010 | 2 | [3.5, 4.4] | 0.0006^a | 5.2 ± 1.5 |
| This Paper | 2 | [0.24, 2.59] | 0.17^a | 1.33 ± 0.61 |
| This Paper | 2 | [0.24, 4.9] | 0.30^a | 1.83 ± 0.21 |

^a $l_0 = l_*(1+z_*)^{-\gamma}$

TABLE 7
REDSHIFT DENSITY OF LLSs FOR RP10.

| z | ΔX | Δz | N | $\langle z_{\text{LLS}} \rangle$ | $l(z)$ | $l(X)$ | $\Delta r_{\text{LLS}} (h_{70}^{-1} \text{ Mpc})$ |
|----------------|------------|------------|-----|----------------------------------|-----------------|-----------------|---|
| [0.242, 1.078] | 80.38 | 40.03 | 15 | 0.895 | 0.37 ± 0.10 | 0.19 ± 0.05 | 3645 |
| [1.078, 1.544] | 73.50 | 29.03 | 15 | 1.157 | 0.52 ± 0.14 | 0.20 ± 0.05 | 1995 |
| [1.544, 1.947] | 44.28 | 15.52 | 10 | 1.751 | 0.64 ± 0.21 | 0.23 ± 0.08 | 917 |
| [1.947, 2.594] | 36.54 | 11.56 | 10 | 2.257 | 0.86 ± 0.30 | 0.27 ± 0.09 | 457 |
| [3.500, 3.663] | 119.91 | 31.07 | 56 | 3.593 | 1.80 ± 0.26 | 0.47 ± 0.07 | 94 |
| [3.663, 3.925] | 109.00 | 27.62 | 55 | 3.799 | 1.99 ± 0.29 | 0.50 ± 0.07 | 77 |
| [3.925, 4.907] | 71.98 | 17.50 | 45 | 4.125 | 2.57 ± 0.44 | 0.63 ± 0.11 | 50 |